Universitat de Girona

THEORETICAL STUDY OF REACTIVITY AND DYNAMICS OF HYBRIDE-BRIDGED DIRUTHENIUM COMPLEXES AND SILYLIUM

Samat TUSSUPBAYEV

ISBN: 978-84-692-2300-0
Dipòsit legal: Gi.383-2009
http://hdl.handle.net/10803/8052

Institut de Química Computacional
Departament de Química
Facultat de Ciències
Universitat de Girona

Theoretical study of reactivity and dynamics of hydride-bridged diruthenium complexes and silylium cation

Samat Tussupbayev

Directed by:

Dr. Sergei F. Vyboishchikov

2009

El doctor Sergei F. Vyboishchikov, investigador Ramón y Cajal a l'Institut de Química Computacional de la Universitat de Girona, certifica que:

En Samat Tussupbayev, llicenciat en Química per la Universitat Nacional de Kazakhstan per Al Farabi, ha realitzat sota la meva direcció, a l'Institut de Química Computacional i al Departament de Química de la Universitat de Girona, el treball d'investigació que porta per nom:

"*Theoretical study of reactivity and dynamics of hydride-bridged diruthenium complexes and silylium cation*"

que es presenta en aquesta memòria per optar al Grau de Doctor en Química.

I perquè consti a efectes legals, signo aquest certificat.

Girona, de 2009

Sergei F. Vyboishchikov

List of abbreviations

AO	Atomic orbital
BLYP	Becke-Lee-Yang-Parr functional
BOMD	Born-Oppenheimer MD
DFT	Density functional theory
ECP	Effective core potential
FES	Free energy surface
GEA	Gradient expansion approximation
GGA	Generalized gradient approximation
GTO	Gaussian type orbital
HF	Hartree-Fock
KS	Kohn-Sham
LCAO	Linear combination of AO
LDA	Local density approximation
LSD	Local spin-density
MD	Molecular dynamics
MO	Molecular orbital
PES	Potential energy surface
STO	Slater type orbital
TM	Transition metal
X	Exchange
XC	Exchange-correlation

Preface

The reactivity of multinuclear transition metal polyhydride complexes is of special interest in the area of organometallic chemistry, because of their potential applicability to organic synthesis. A particular example is the multinuclear ruthenium polyhydride complexes, containing only C_5Me_5 (Cp*) as auxiliary ligands, which exhibit diverse reactivity toward a variety of substrates. A deep understanding of the chemical processes is required to control and to develop more efficient ways of synthesis. This can be achieved through the knowledge of the detailed reaction mechanism. On the other hand theoretical (computational) chemistry starts to be of increasing use for a better understanding of chemical processes at the molecular level. In this work the computational chemistry methods have been applied to study the chemistry of a diruthenium tetrahydride complex CpRu(μ-H)$_4$RuCp.

Another subject studied in the thesis is the fluxional behavior of hydride bridged species. Multinuclear transition metal polyhydride complexes reveal a high fluxionality due to the presence of multiple metal centers and mobility of hydrides. It applies to the derivatives of the above mentioned tetrahydride complex, the μ-silylene complexes {Cp*Ru(μ-H)}$_2$(μ-SiPhMe)(μ-SiMe$_2$) and (Cp*Ru)$_2$(μ-SiMe$_2$)(μ-CMe)(μ-H).

The silylium cation $[C_6(SiMe_2)(SiHMe_2)_5]^+$ is another example of hydride bridged species. The hydride bridges stabilize the cation and due to the presence of multiple agostic bonds it demonstrates a unique dynamical behavior. The described fluxional processes have been studied in this work using computational chemistry methods.

In the following seven chapters of this work are briefly highlighted. Chapter 1 reviews the structure and reactivity of transition metal polyhydride complexes. Particular attention is paid to multinuclear cyclopentadienyl-containing metal polyhydride complexes. Moreover, the reactivity of silylium cations, the ways of their stabilization and the dynamic behavior of hydride bridged silylium cations are briefly discussed. Chapter 2 considers the electronic structure calculation methods used in the following chapters. The goals of the thesis are summarized in Chapter 3.

An interesting aspect of the polyhydride complexes is the relation between the mobility of the hydride ligands and the reactivity. Chapter 4 discusses the theoretical study of intermolecular hydrogen exchange between hydride ligands in the diruthenium complex CpRu(μ–H)$_4$RuCp and dihydrogen discovered in the experimental study.

Chapter 5 considers the computational study of the C–H bond activation and hydrogenation of ethylene on diruthenium complex CpRu(μ–H)$_4$RuCp to yield bis(vinyl) complex CpRu(η^2-C_2H_4)(η^1,η^2-C_2H_3)$_2$RuCp. The theoretical study of the mechanism of the subsequent

C–C coupling between coordinated ethylene and μ–vinyl ligands in the latter complex is described in Chapter 6.

The computational study of the fluxional behavior of diruthenium bis(μ-silylene) complexes {CpRu(μ-H)}$_2$(μ-SiPhMe) (μ-SiMe$_2$) and (CpRu)$_2$(μ-SiMe$_2$)(μ-CMe)(μ-H) is discussed in Chapter 7.

The results of a detailed study of the dynamical behavior of the polyagostic cation [C$_6$(SiMe$_2$)(SiHMe$_2$)$_5$]$^+$ are considered in Chapter 8.

Acknowledgements

First and foremost I would like to thank my supervisor Sergei Vyboischikov for sharing his knowledge, taking his time to work with me and having the patience to assist me. Without his expertise and tutelage, this thesis would not be written.

I would like to express my gratitude to all IQC members, namely my compadre Oscar (Aseke), Ferran, Sílvia, Pedro, Dani, Miquel Torrent, Eduard, Mireia, David, Pata, Quim, Juanma, Jordi, Annas, Marcel, Lluís, Cristina, Quansong, Albert, Laia, Eloy for their friendship, welcoming attitude, as well as for introducing me a nightlife of Girona.

I'm also very grateful to the "pillars" of the IQC: Miquel Solà, Miquel Duran, Lluís Blancafort, Annapaola Migani, Sílvia Simon, Josep Maria Luis and Joan Miró for their friendly relation and support.

I would like to thank Emili Besalú for his patience in helping with the "predoctoral stuff". Special thanks to Carme, she is our savior in the bureaucracy chaos.

Bol'shoe spasibo to the russian-speaking members of the IQC: Alexander and Eugeni, a takzhe ogromnoe spasibo Yule i Vike za gostepriimstvo i uyut.

I would like to thank my parents, my brother and all my friends for their support and patience during these four years.

Table of contents

1. Introduction

1.1. Overview of transition metal polyhydride complexes

The discovery of a nearly intact H_2 molecule coordinated to a metal complex by Kubas *et al.*[1] in 1983 was a breakthrough in the historical development of coordination chemistry. Since then, dihydrogen complexes of transition metals have been the subject of large interest because they present models for the metal-induced activation of the hydrogen molecule,[2,3] either through oxidative addition or heterolytic cleavage.[2–5]

Originally, all hydrogen containing transition metal complexes were considered as polyhydrides. After the discovery by Kubas[1] many of them were reattributed as dihydrogen complexes.[3] The H–H distance defines the difference between a *classical polyhydride* (> 1.6 Å), a *non-classical polyhydride* (0.8 ÷ 1.0 Å), and *stretched dihydrogen complexes* with intermediate H–H lengths. Stretched H_2 complexes are described now as complexes containing two hydrogen atoms moving almost freely in a large region within the coordination sphere of the metal.[6,7]

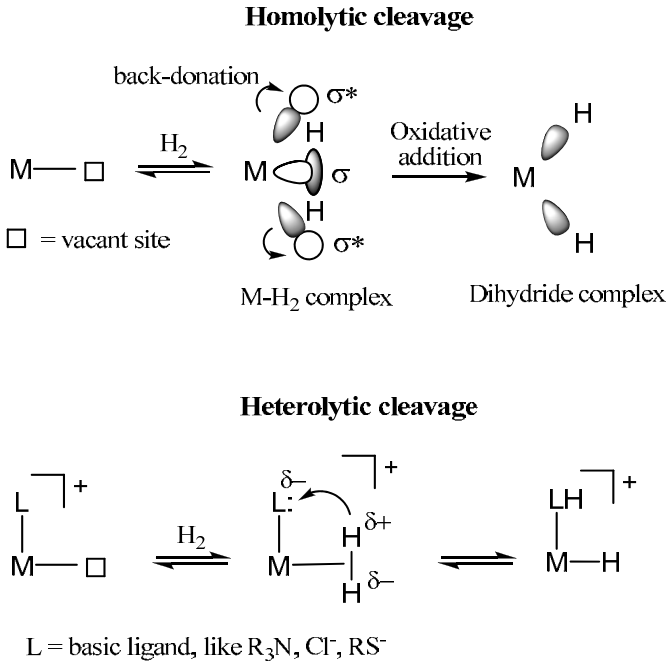

Figure 1. Two ways of splitting the H–H bond on transition metal complexes.

The bonding between transition metal and dihydrogen can be described within the Dewar-Chatt-Duncanson model[8] of donation and back-donation. The σ(H–H) occupied orbital donates electrons to an empty orbital of the metal, while an occupied orbital of the metal donates them back to the σ^*(H–H) empty orbital. Consequently, both contribute to the lengthening of

the H–H bond with respect to free dihydrogen molecule H_2 (where the bond length equals to 0.741 Å)[9] through the loss of electron density from the bonding orbital and a partial occupation of the anti-bonding orbital. The H–H bond can be cleaved and two metal–hydride bonds can be formed, when these two interactions are strong enough.[6,7] It is an example of a *homolytic cleavage* of the H–H bond (Figure 1). The metal center cooperates with a heteroatom of the adjacent ligand during the *heterolytic cleavage* of the H–H bond. This type of cleavage has been observed as a part of the mechanism of Noyori's asymmetric hydrogenation systems[10] and hydrogen activation in hydrogenase enzymes.[11]

A number of quantum chemical studies on the electronic structure and the relative energies of classical and nonclassical isomers have been reported. The role of the central metal was investigated on the complexes $MH_n(PH_3)_m$, $CpMH_nL_{4-n}$, (M = Ru, Os, Rh, Ir), $CpMH_nL_{6-n}$, $MH_n(CO)_mL_p$, and $MH_nCl_mL_p$ (with 4d and 5d metals from groups 6 to 9).[6] It was found that the classical hydrides are preferred for early transition metals with more diffuse d orbitals. Similarly, down a triad, the classical hydrides are more common for the heaviest elements. For the transition metals from the same row, the non-classical structure is preferred for the later metal. For ruthenium, both classical and nonclassical complexes may exist.

The chemistry of ruthenium complexes containing nonclassical hydride ligands was pioneered by Chaudret *et al*. with the synthesis of the hexahydride complex of formula $[Ru(H_2)_2(H)_2(PCy_3)_2]$ (Cy=cyclohexyl).[12] This species was proven to possess a unique structure with two classical hydrides and two molecular dihydrogen ligands in mutually *cis* positions,[12c] as confirmed recently by neutron diffraction for $[Ru(H_2)_2(H)_2(PCyp_3)_2]$ (Cyp = cyclopentyl).

The auxillary ligand can play an important role in the M–H_2 interaction. Systematic calculations on $MH_nL_{4-n}Cp$ (n = 1–4), where M = Ru, Rh, Os, and Ir and L = PH_3 and CO, indicate that most polyhydrides with Cp ligand adopt classical isomers. The strong σ- and π-donating ability of the Cp ligand increases the transfer of metal d electrons to hydrides and stabilizes the classical isomers.[13]

Ziegler and coworkers[14] studied relativistic effects on the relative stabilities of the classical and nonclassical isomers of $M(PH_3)_3H_4$ with M = Fe, Ru, and Os by using nonlocal, quasirelativistic density functional method. The dihydrogen complex is found to be most stable for Fe and Ru while the hydride complex is the isomer of lowest energy for Os, in accordance with experimental observations. Without relativity all three metal centers prefer nonclassical isomer. The observed preference for a dihydride complex in the case of the heavier osmium is explained by a relativistic destabilization of the 5d orbital which makes the metal center more basic.

Occasionally dihydrogen complex can exist in equilibrium with the corresponding dihydride.[3] The classic example is the original system of Kubas,[3a] with $[(PPr^{i}_{3})_2(CO)_3(H_2)]$ displaying a 4:1 mixture of $M(\eta^2\text{-}H_2)$ and $M(H)_2$ isomers at room temperature. The oxidative addition to yield the dihydride complex proceeds with the $\Delta G^{\neq}$ barrier of about 14 kcal/mol. Such a high barrier indicates a deep well for the $M(\eta^2\text{-}H_2)$ precursor, i.e. making it kinetically rather stable. It is consistent with the large number of dihydrogen complexes now known.[6,7]

Quantum chemical calculations together with isotopic substitution studies of the cation $[Cp^*Ru(dppm)(\eta^2\text{-}H_2)]^+$ have showed that the H…H distance in the dihydrogen moiety changes with temperature.[6] MH_2 moieties in stretched dihydrogen systems are characterized by very flat, anharmonic potential surfaces, and thermal population of low-lying excited vibrational states with large amplitude displacements has a significant effect on the H…H distance.

Classical and nonclassical transition metal polyhydride complexes present a great diversity of dynamic processes involving hydrogen atoms coordinated to the metal. Despite the strength of the M-H bonds,[15] hydride ligands show a great mobility, and hydride site exchange is often observed. Because of their intermediate electronegativity, the nondirectionality of the 1s orbital and the absence of steric hindrance, the hydrogen ligands readily switch positions. The nature of these exchange processes and their thermodynamics can be explored with variable-temperature NMR spectroscopy, however their explicit assignment is difficult. Therefore, theoretical calculations have contributed to the understanding of the mechanisms of these dynamic processes. Maseras *et al.*[6] reviewed the theoretical studies of hydride-exchange mechanisms in mononuclear polyhydride complexes, like the pairwise exchange, the polytopal rearrangement, dihydrogen rotation and others.

The polytopal rearrangements take place in the stereochemically nonrigid high-coordinate, usually seven-, eight-, or ninecoordinate polyhydrides. This has been explained by the various geometries available in these complexes.[16]

The hydrogen atoms of a dihydrogen ligand can exchange their positions by a rotation about the $M–H_2$ axis. A small rotation barrier is generally found for H_2 metal complexes. The rotational barrier was shown to be sensitive mainly to the $d_\pi–\sigma^*$ back donation. It is preserved during the rotation, and the d-orbitals that are responsible for the back-donation in the different orientations of H_2 have similar energies and shapes.[6]

The pairwise exchange in addition to the rotation of dihydrogen involves the initial coupling of hydrides. In this mechanism, the formal oxidation state of the metal may change along the exchange pathway.[6]

Thus, in mononuclear complexes hydrogen is found either as a hydride ligand (H) or as dihydrogen (η^2-H_2). In *polynuclear* metal complexes, however, hydrogen may occupy a variety of different positions with respect to the metal centers that are not available to mononuclear complexes, including bridging, face-bridging and interstitial locations (Figure 2).

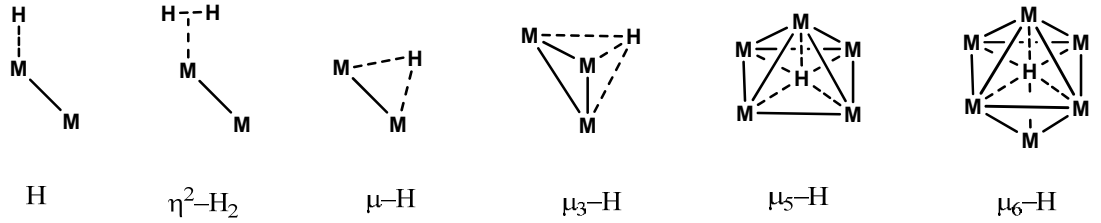

Figure 2. Hydrogen bonding modes observed in polynuclear complexes; terminal hydride (H), dihydrogen complex (η^2-H_2), bridging hydride (μ-H), face-bridging hydride (μ_3-H) and interstitial hydrides (μ_5- and μ_6-H).

The examples of the complexes with μ_n-H binding modes, characterized by neutron diffraction method, are (μ-H)$Ru_3(CO)_9(\mu_3$-η^2-$CCCMe_3)$,[17] (μ_3-H)$_4Co_4(\eta^5$-C_5Me_4-Et)$_4$,[18] [(μ_5-H)$_2Rh_{13}(CO)_{24}]^{3-}$,[19] and [(μ_6-H)Ru_6-$(CO)_{18}]^-$.[20] The terminal hydride and dihydrogen ligands are sufficiently rare in cluster chemistry, and they remain uncharacterized by neutron diffraction.

A bimetallic species with a dihydrogen ligand (η^2-H_2)(isoPFA)Ru(μ-Cl)$_2$(μ-H)RuH-$(PPh_3)_2$ (isoPFA = {η^5-C_5H_5}Fe(η^5-C_5H_3(CHMeNMe$_2$)-P*i*Pr$_2$}) was investigated by X-ray and NMR methods.[21] It should be noted, that it is a rare case of the structure with three different binding modes of H. The NMR spectroscopic data for this compound revealed fast exchange between the η^2-H_2 and the μ-H at 20 °C and a slower exchange of these three hydrogen atoms with the terminal hydride.

The complex Cp*Ru(μ-H)$_4$RuCp*, synthesized by treatment of (Cp*$RuCl_2$)$_2$ with $LiAlH_4$ and ethanol,[22] is a rare example of the tetrahydride bridged complex M(μ-H)$_4$M. The molecular structure of tetrahydride complex **1** determined on the basis of the X-ray and NMR method is shown in Figures 3 and 4. The core of the molecule consists of four bridging hydrogen atoms tightly clustered around the ruthenium-ruthenium vector, and four hydride ligands are essentially arrayed at the vertices of an approximate square put perpendicularly to the Ru-Ru bond (Figures 3 and 4). The average H–H distance of 1.46 Å strongly indicates that there are no bonding interactions among the hydride ligands in **1**. It was therefore concluded that complex **1** is a η^2-H_2 complex rather than a classical σ-bonded metal hydride complex.[22]

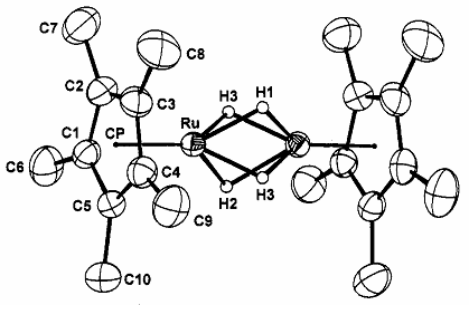

Figure 3. Molecular structure of **1**.[22]

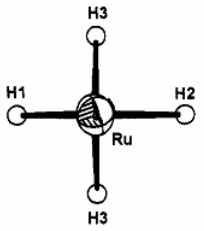

Figure 4. View of the Ru_2H_4 core of the molecule along the Ru-Ru axis, showing the approximate square formed by four bridged hydrides.[22]

The Fe and Os analogues, Cp*Fe(μ–H)$_4$FeCp*[23] and Cp*Os(μ–H)$_4$OsCp*,[24] as well as the related heteronuclear complex Cp*Ru(μ-H)$_4$OsCp*[24a] have similar structure. The Os–Os bond distance of 2.4567(6) Å[24] is nearly identical to the 2.463(1) Å Ru–Ru distance found for Cp*Ru(μ–H)$_4$RuCp*[22] and the 2.4663(5) Å distance seen in the mixed–metal compound Cp*Ru(μ–H)$_4$OsCp*,[24a] but longer than the 2.202(2) Å distance seen in the iron compound Cp*Fe(μ–H)$_4$FeCp*.[23]

The dinuclear complex **1** is the 30 electron complex (Ru(III), d^5, 8 electrons are donated by four μ–H and 12 electrons – by two Cp* rings). Therefore, according to the 18-electron rule **1** should have a triple bond between Ru atoms. However, the theoretical study performed by Morokuma *et al.*[25] of the model complex CpRu(μ–H)$_4$RuCp showed the absence of a direct metal–metal bond. The calculations were performed at the RHF//MP2 level using effective core potential together with the corresponding double-ζ basis set for Ru,[26] 3-21G basis set for hydrides[27] and STO-3G[28] for Cp. The Ru atoms do not have enough orbitals to form so many bonds as suggested by the 18-electron rule.

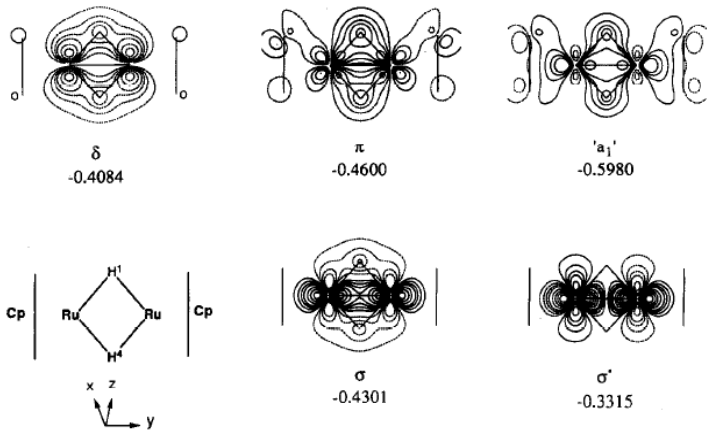

Figure 5. Ab initio canonical orbitals of CpRu(μ–H)$_4$RuCp. Orbital energies are given in atomic units.[25]

The σ and σ* orbitals, which are bonding and antibonding combinations of the Ru d_{y^2} orbital, respectively, are shown in Figure 5. These orbitals are occupied and therefore there is no direct net bonding interaction between the Ru d_{y^2} orbitals. Thus, there are four hydride-bridged, 3c–2e bonds (Ru–H–Ru) between the two Ru atoms in **1**. The direct Ru–Ru interaction is repulsive and the four hydrides work as glue to connect the repulsive fragments.

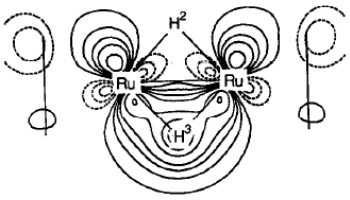

Figure 6. The localized MO representing a hydride-bridged Ru–H–Ru bond of **1**.[25]

The H_2 dissociation reaction to give $CpRu(\mu\text{-}H)_2Cp$ is endothermic by 57 kcal/mol at the HF//MP2 level. The high endothermicity of the reaction was explained by the loss of the strong metal-hydride bonding. The Ru–H–Ru bond energy was estimated using Eq. 1

D(Ru–H–Ru) = [E(CpRu(μ–H)$_2$Cp + 2 × E(H) – E(CpRu(μ–H)$_4$Cp)] (1)

as 74 kcal/mol at the HF//MP2 level.

Fowe *et al.*[29] came to the similar conclusion after studying the nature of the metal-metal bonding interaction in the cationic dinuclear arene ruthenium complexes $[\eta^6\text{-}C_6Me_6)_2Ru_2(\mu\text{-}H)_3]^+$, $[\eta^6\text{-}C_6Me_6)_2Ru_2(\mu\text{-}H)_2(\mu\text{-}1,4\text{-}SC_6H_4Br)]^+$, $[\eta^6\text{-}C_6Me_6)_2Ru_2(\mu\text{-}H)(\mu\text{-}1,4\text{-}SC_6H_4Br)_2]^+$ and $[\eta^6\text{-}C_6Me_6)_2Ru_2(\mu\text{-}1,4\text{-}SC_6H_4Br)_3]^+$. The study was performed at the density functional theory level employing different bond analysis techniques, such as, molecular orbital (MO) theory, bond order (BO) analysis, bond decomposition energy (BDE), electron localization function (ELF) and Laplacian of the density methods. The results show that there is no direct bond between the two ruthenium atoms in these complexes, the MO interaction within the diruthenium backbone being stabilized by the bridging ligands. For complex $[\eta^6\text{-}C_6Me_6)_2Ru_2(\mu\text{-}H)_3]^+$, the ELF clearly shows that the bond within the diruthenium backbone is through the three bridging hydride ligands, which act as a sort of glue by forming three-center two-electron bonds characterized by (Ru, H, Ru) basins with 1.8*e* mostly located in the H atomic basin.

As an extension of bimetallic activation, the trimetallic polyhydride cluster has attracted a notable attention. A cationic triruthenim hexahydride cluster $[\{(Cp^*)Ru(\mu\text{-}H)_2\}_3](X)$ (**2**) was obtained by the reaction of **1** with an acid HX.

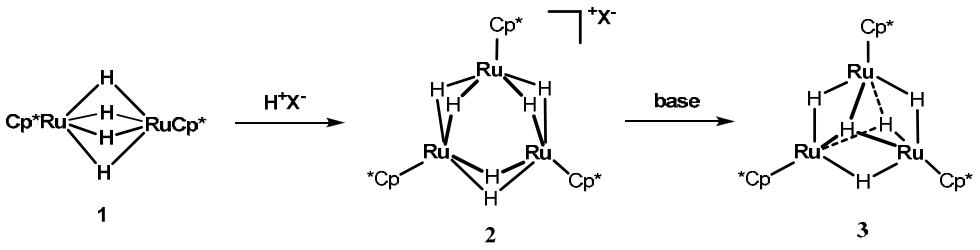

1 2 3

The complex **2** was characterized as a classical hydride complex by the NMR and X-ray methods. Treatment of the cationic cluster **2** with a base afforded a neutral pentahydride cluster *trinuclear* pentahydrido complex $[\{Ru(C_5Me_5)\}_3(\mu\text{–}H)_3(\mu_3\text{–}H)_2]$ (**3**).

The complex **3** contains two different types of bridged hydrides.[30] Three doubly bridging hydrogen atoms and two triply bridging ones bond three ruthenium atoms, which occupy the vertices of a nearly equilateral triangle (Figure 7). The average interatomic distance between μ_3–H and μ–H atoms in **3** is 2.07 A, indicating that **3** is a typical classical hydrido complex.

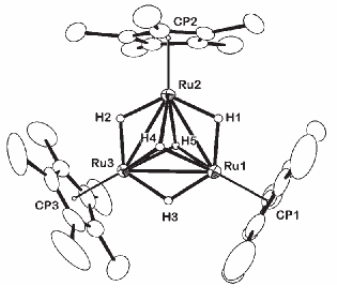

Figure 7. Molecular structure of **3**.[30]

Very recently the synthesis of the Os analogs of the complexes **2** and **3** was reported.[31]

The series of *tetranuclear* complexes having several combinations of the auxiliary cyclopentadienyl ligands, $[(CpRu)_4H_6]$ (**4a**), $[\{(C_5H_4Me)Ru\}_4H_6]$ (**4b**), $[\{(1,3\text{-}Me_2C_5H_3)Ru\}_4H_6]$ (**4c**), $[(Cp_3Cp^*Ru_4H_6]$ (**5**), $[(Cp_2Cp^*_2Ru_4H_6]$ (**6**) and $[(CpCp^*_3Ru_4H_6]$ (**7**) were studied by using X-ray diffraction technique.[32] The clusters **4a–c**, **6** and **7** adopt a pseudo-tetrahedral structure. The corresponding bonds within each of the clusters have similar lengths. Four of the six hydride ligands in **4a–c** triply bridge (μ_3–H) each of the Ru_3 faces, the other two hydride ligands bridge the two (μ–H) short Ru–Ru bonds (Figure 8).

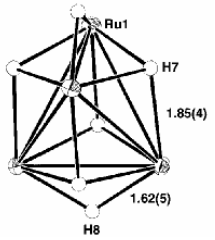

Figure 8. The Ru_4H_6 core of **4b**. C_5H_4Me groups are omitted for clarity.[32]

The pentaruthenium heptahydride clusters $Cp_5Ru_5H_7$ (**8a**) and $Cp_4Cp^*Ru_5H_7$ (**8b**), according to the X-ray study, have a trigonal-bipyramidal geometry.[33] However, the location of the seven hydrogen atoms directly bound to the ruthenium atom was not found.

Complex **8a** exhibits a new type of fluxional behavior that involves exchange of the CpRu groups among the axial sites and the equatorial sites. The site exchange requires the cleavage and the formation of the Ru–Ru bond. The most probable pathway that accounts for this process (Scheme 1) is an intramolecular Ru–Ru bond cleavage and re-formation that closely resembles the *Berry pseudorotation*.

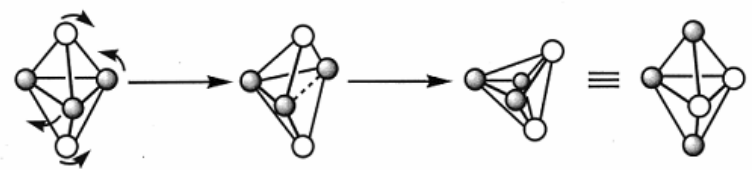

Scheme 1. The mechanism of the exchange of CpRu groups among the axial and equatorial sites in **8a**.[33]

The heterobimetallic complex $Cp^*Ru(\mu\text{–}H)_3IrCp^*$ is an example of the trihydride bridged complex with different metal centers $M(\mu\text{–}H)_3M'$. It was characterized as a classical trihydride complex by the NMR method.[34]

The binuclear *heterometallic* pentahydride complex $Cp^*Ru(\mu\text{–}H)_3Re(H)_2Cp^*$ has both terminal and bridged hydrides.[52] Their exchange, as well as the site exchange among the bridged hydrides was observed for this complex by the NMR methods.

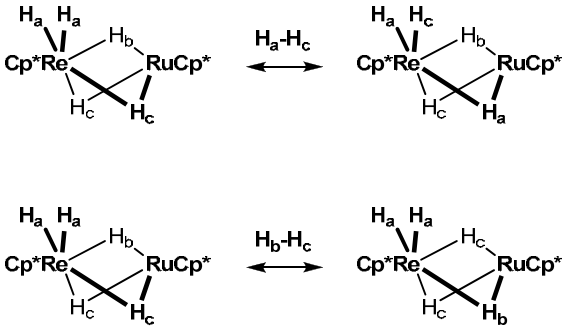

The exchange of terminal (H_a) and bridged (H_b and H_c) hydrides proceeds with a moderate energy barrier ($\Delta H^{\neq}_{298}$ = 15.5 kcal/mol, $\Delta S^{\neq}_{298}$ = 11.5 cal/mol·K and $\Delta G^{\neq}_{298}$ = 12.1 kcal/mol). It was proposed that both processes occur through the intermediate $\eta^2\text{–}H_2$ complex, formed as a result of a coupling between the corresponding hydride ligands.[52]

The terminal or bridging hydride in polyhydride complexes can undergo site exchange with hydrogen in a ligand. For example, the exchange between the bridged hydride and the methylidene hydrogen has been observed in the trimetallic nonacarbonyl complex

$M_3(CO)_9(\mu–H)_3(\mu_3–CH)$, where M = Fe, Ru, Os.[35] The computational study[36] of this process for the Os and Ru complexes carried out at the RHF//MP2 level of theory revealed that the reaction can proceed in two distinct pathways. Both pathways include the following steps: the initial migration of the bridged hydride to an equatorial position to form a seven-coordinated intermediate; the rearrangement of three carbonyls and the hydride; and the insertion of the hydride to M–C bond. The activation barrier for the Os compound is about 22 kcal/mol, while for Ru analog it is lower by about 4 kcal/mol.

Thus, transition metal polyhydride complexes present a variety of coordination modes of hydride ligands. These complexes exhibit diverse fluxionality, which, in particular, provides their high reactivity discussed in the next section.

1.2. Reactivity of multinuclear transition metal polyhydride complexes

The reactivity of transition metal cluster complexes has been of special interest recently, in the area of organometallic chemistry, because of their potential applicability to organic synthesis.[37] Polynuclear transition metal complexes often exhibit unusual reactivities that are not found in mononuclear complexes.[38] The diverse reactivity of multinuclear ruthenium polyhydride complexes, containing pentamethylcyclopentadienyl C_5Me_5 (Cp*) as auxiliary ligands, toward a variety of substrates, developed and reviewed by Suzuki *et al.*[39] has attracted a significant interest. The synthesis of di-,[22] tri-,[30] tetra-,[32] and pentanuclear[33] ruthenium polyhydride clusters having several kinds of cyclopentadienyl groups as auxiliary ligands was reported. The multiruthenium polyhydride complexes, containing pentamethylcyclopentadienyl C_5Me_5 (Cp*) as auxiliary ligands, have been found to be efficient in bond activation reactions, such as those leading to H–H,[40] C–H,[41] Si–H and Si–C,[42] C–C,[43] P–C[44], C–S,[45] C–N,[46] and N–N[47] bond cleavages. Also, these complexes have been shown to favor reactions affording new C–H,[48] C–Si,[49] C–C,[41a,50] and C–O bonds.[51] Subsequently synthesized multinuclear heterometallic polyhydride complexes have also shown a high reactivity in these processes.[34,52]

Many unsaturated multimetallic complexes coordinate H_2 to give hydride species. It is often a reversible process, and after the removal of the H_2 atmosphere the starting complex is regenerated. Therefore many of these complexes undergo rapid H/D exchange, when placed under a D_2 atmosphere.

Suzuki and co-workers have found that the hydride ligands of the dinuclear tetrahydride-bridged complex $Cp^*Ru(\mu–H)_4RuCp^*$ (**1**) exhibit intermolecular hydride exchange with dihydrogen under mild conditions. Exposure of a toluene solution of $Cp^*Ru(\mu–D)_4RuCp^*$ (**1-d_4**) to dihydrogen results in the exchange of the deuteride ligands for hydride:

$$Cp^*Ru(\mu\text{–}D)_4RuCp^* + 2H_2 = Cp^*Ru(\mu\text{–}H)_4RuCp^* + 2D_2.$$

The proposed mechanism of this process is discussed in details in the Chapter 4.

The heterodinuclear polyhydride complexes have been found reactive towards the H/D exchange as well.[34,52]

In the course of a study of the reaction of **1** with a number of *olefins*, Suzuki and coworkers found that a C–H bond of ethylene was cleaved under mild conditions to produce a dinuclear divinyl complex $Cp^*Ru(\eta^2\text{-}C_2H_4)(\mu\text{–}CH{=}CH_2)_2RuCp^*$ (**9**).[41b]

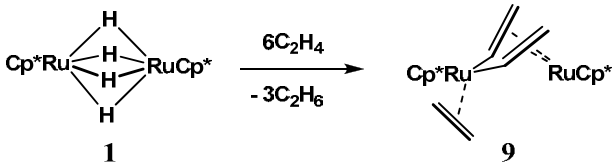

1 **9**

The release of ethane molecules suggests that the coordinatively unsaturated sites are generated on **1** by way of a hydride transfer from the ruthenium center to the ethylene ligand, i.e., hydrogenation of ethylene.

The more intriguing reaction discovered by Suzuki and coworkers is the subsequent C–C coupling reaction between coordinated ethylene and two vinyl ligands in **9** to yield a ruthenacyclopentadiene complex $Cp^*Ru(\eta^2\text{-}C_2H_4)(CMe{=}CH\text{–}CH{=}CMe)RuCp^*$ (**10**).[41b]

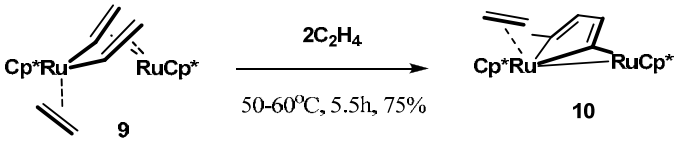

9 **10**

It is a rare example of the functionalization of alkenyl groups formed as a result of C–H bond activation in alkenes by transition metal complex. The proposed mechanisms of the C–H bond activation and the C–C coupling reactions are discussed in details in the Chapters 5 and 6.

Ruthenacycle **10** was further converted into a $\mu\text{-}\eta^2\text{:}\eta^2\text{:}\eta^2$-5-methylhepta-2, 4, 6-trien-2-yl complex **11** upon heating.[41b] The formation of **11** was interpreted by the mechanism involving an insertion of the coordinated ethylene ligand into one of the Ru–C σ bonds of **10**. Subsequent β-H elimination from the resulting intermediary ruthenacycloheptadiene yields **11**.

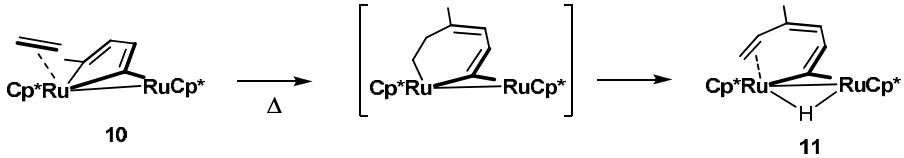

10 **11**

The reaction of **1** with various *organosilanes* provided evidence for the concerted activation of the Si–C and Si–H bonds, in which the two ruthenium atoms cooperatively affect the silane molecule. The stepwise transformation from the μ-silane complex to the μ-silyl complex and further μ-silylene complex was observed in the reaction of **1** with *secondary silanes*. Each metal center mutually took the role of a binding and an activation site.[39]

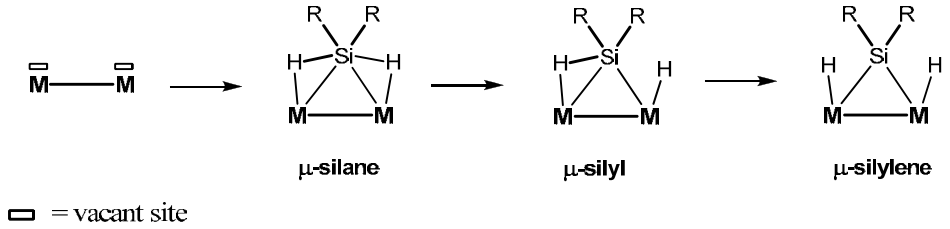

For instance, the reaction of **1** with a *secondary silane* R_2SiH_2 afforded bis(μ-silyl) complexes $\{Cp^*Ru(\mu\text{-}\eta^2\text{-}HSiR_2)\}_2(\mu\text{-}H)(H)$ (**12a**, R = Ph; **12b**, R = Et)[42a] and a μ-silane complex $\{Cp^*Ru(\mu\text{-}H)\}_2(\mu\text{-}\eta^2\text{:}\eta^2\text{-}H_2SiR_2)$ (**13**, R = ^{t}Bu).[42b]

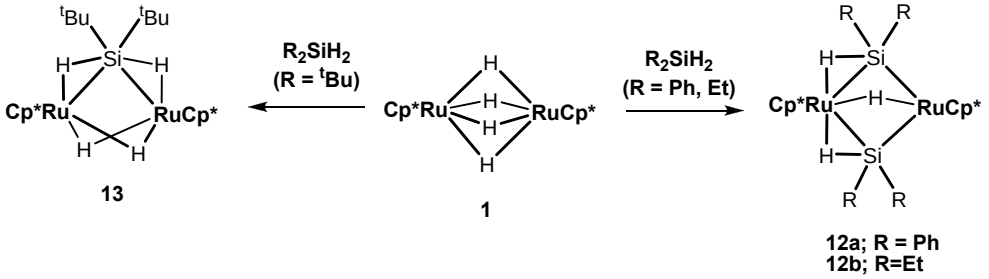

The complexes are characterized by the 3c-2e interactions involving metal center, silicon and hydride ligand. These agostic interactions can be cleaved upon heating to form Ru-Si σ bonds.

Further treatment of **13** with phenylsilane resulted in the formation bis(μ-silyl) complex $(Cp^*Ru)_2(\mu\text{-}\eta^2\text{-}HSi^tBu_2)(\mu\text{-}\eta^2\text{-}HSiPhH)(\mu\text{-}H)(H)$ (**12c**) through oxidative addition of η^2-coordinated Si-H bond.[42b]

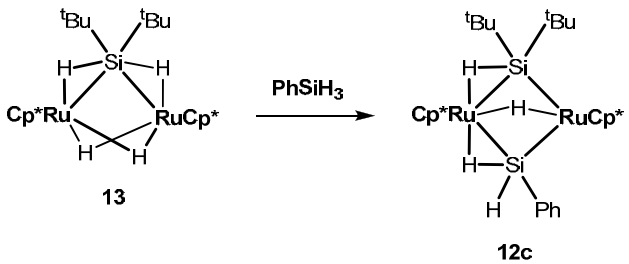

The two η^2-coordinated Si-H bonds of the bis(μ-silyl) complex **12a** were cleaved upon heating to produce a bis(μ-silylene) complex $\{Cp^*Ru(\mu\text{-}SiPh_2)(\mu\text{-}H)\}_2$ (**14**).

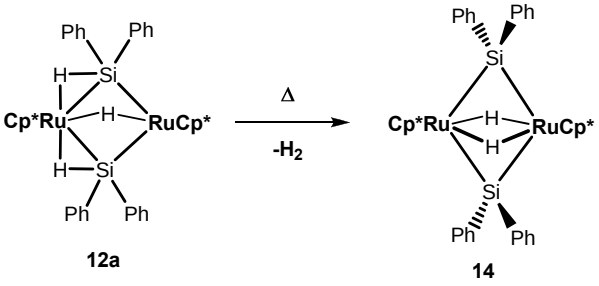

Reaction of **1** with a *tertiary silane*, dimethylvinylsilane resulted in formation of the μ-dimethylvinylsilane complex, $\{Cp^*Ru(\mu\text{–}H)\}_2\{\mu\text{-}\eta^2\text{:}\eta^2\text{-}HSiMe_2(CH{=}CH_2)\}$ (**15**) (Scheme 2), as a result of coordination through both the Si–H and C–C bonds.[42d] One of the hydride ligands in **15**, according to X-ray crystallography, is bridged between Ru and Si, forming the 3c-2e interaction.[42d] The Si–H distance, 1.68(6) Å, is reasonably longer than those reported for organosilicon compounds (1.48 Å).[53]

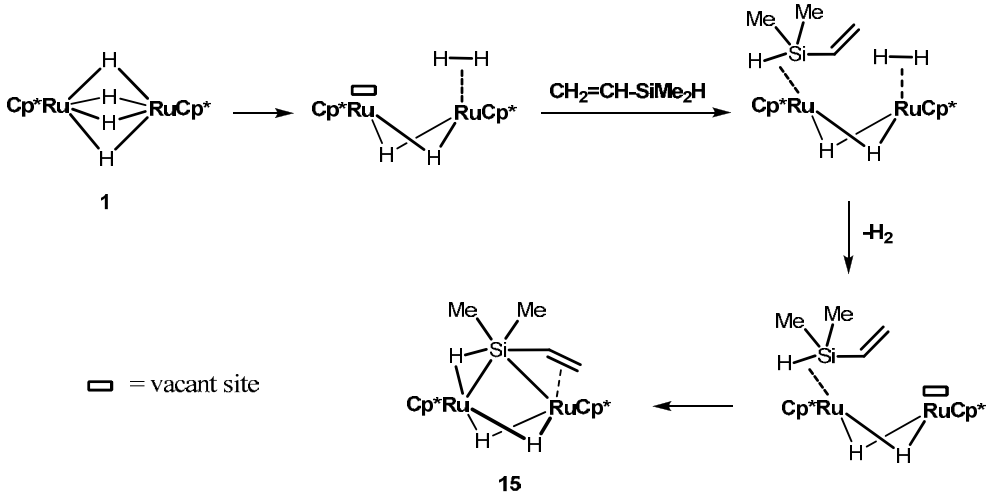

Scheme 2. The proposed mechanism of the reaction of $Cp^*Ru(\mu\text{-}H)_4RuCp^*$ (**1**) with dimethylvinylsilane.

The ^{1}H NMR studies of this process revealed that the coordination of the Si–H bond of dimethylvinylsilane precedes the coordination of the vinyl group.[42d] The elimination of two hydride ligands as dihydrogen takes place after the coordination of the Si–H bond of dimethylvinylsilane. The vacant space generated is then occupied by the vinyl group. In this reaction dimethylvinylsilane plays the role of a trapping reagent for the dinuclear coordinatively unsaturated species.

Further thermolysis of complex **15** afforded a μ-silylene, μ-ethylidyne complex $(Cp^*Ru)_2(\mu\text{–}SiMe_2)(\mu\text{–}CCH_3)(\mu\text{–}H)$ (**16**).

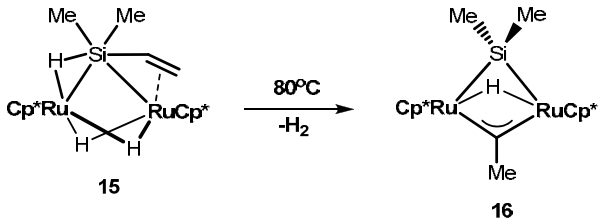

The dinuclear complex **16** is formed as a result of Si–C(sp^2) bond cleavage followed by insertion of the C=C double bond into one of the Ru-H bonds. The site-exchange of methyl groups at the bridging silicon in **16** was monitored by the NMR technique.[42d] The mechanism of the fluxional process is considered in the Chapter 7.

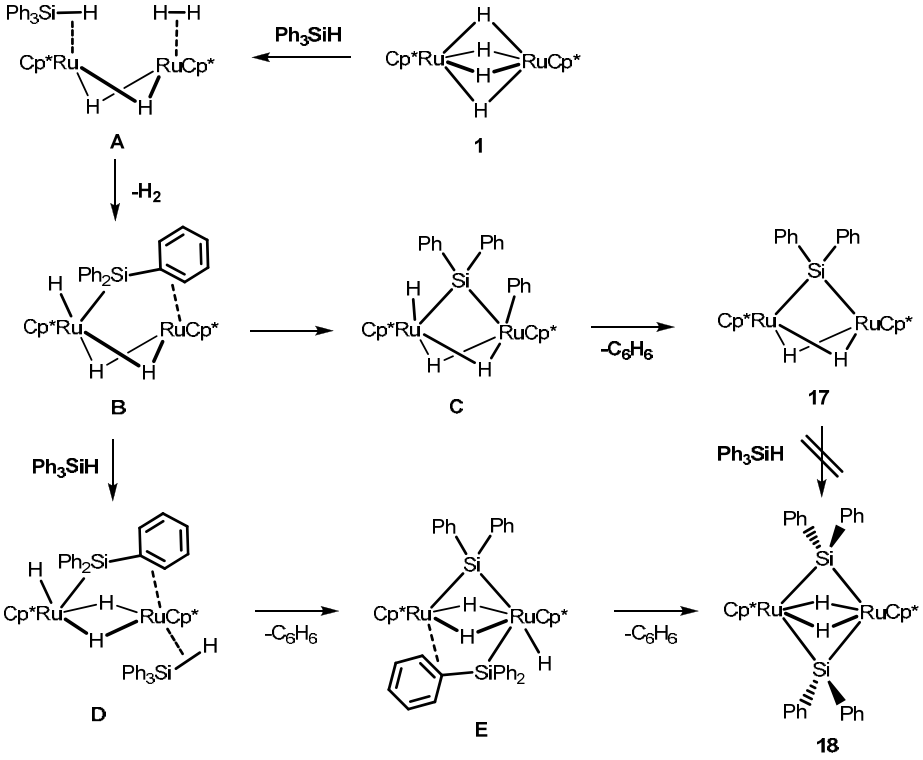

Scheme 3. The proposed mechanism of the reaction of $Cp^*Ru(\mu\text{-}H)_4RuCp^*$ (**1**) with Ph_3SiH.

Reaction of the diruthenium complex **1** with triphenylsilane occurs in a similar way to vinylsilane to yield a mixture of the bis(μ-diphenylsilylene) complex $\{Cp^*Ru\text{-}(\mu\text{–}SiPh_2)(\mu\text{–}H)\}_2$ (**17**) and the mono(μ-diphenylsilylene) complex $\{Cp^*Ru(\mu\text{–}H)\}_2(\mu\text{–}SiPh_2)$ (**18**).[42e] This reaction demonstrates a successful activation of Si–C(aryl) bond of Ph_3SiH. The cleavage is most likely to proceed through the formation of the μ-triphenylsilane intermediates **B** and **E** shown in Scheme 3.

Triruthenium pentahydride $[\{Ru(C_5Me_5)\}_3(\mu\text{–}H)_3(\mu_3\text{–}H)_2]$ (**3**) is an unsaturated 44-electron cluster and is able to capture a weakly coordinating substrate such as dihydrogen or benzene in a triangular reaction site. As a result, **3** readily underwent an H/D exchange reaction between the hydride ligands and D_2 or hydrogen atoms of aromatic rings, benzene-d_6, toluene-d_8, or o-xylene-d_{10} to produce **3-d$_5$**.[30] The latter process proceeds as the result of the C–H bond activation in η^2-arene intermediate complex.

The reactions of complex **3** with substituted alkynes, acetylene, dienes,[54] cyclic dienes,[43b,55] 1,1-disubstituted alkenes,[56] and *n*-alkanes[57] result in the formation various hydrocarbyl ligands. Some of these hydrocarbyl ligands underwent skeletal rearrangement reactions in a different manner from those of monometallic complexes. For instance, the regioselective C–C bond cleavage of 1,1-disubstituted alkenes and cleavage of one of the three Ru–Ru bonds yields a *closo*-ruthenacyclopentadiene complex. Another example is the reaction of **3** with acetylene.[58] The C_2 moiety underwent transformation on the cluster to form μ-vinyl, μ-ethylidene, μ_3-ethylidyne, μ-vinylidene, and μ_3-(||)-ethyne ligands sequentially.

Heating a solution of **3** in various alkanes resulted in the formation of novel trinuclear *closo*-ruthenacyclopentadiene complex **19a–f**.[57]

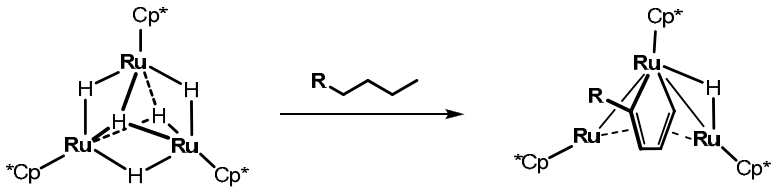

3

19a; R = Me
19b; R = Et
19c; R = Pr
19d; R = Bu
19e; R = Am
19f; R = Hx

In this reaction, six C–H bonds of the alkanes were successively cleaved on the trimetallic site. The *n*-alkane molecule is probably incorporated into the complex from one of the methyl termini at the initial stage of the reaction. These skeletal rearrangement reactions occur due to the cooperative action of the neighboring metal centers, but details of the reactions are still uncertain.

The triruthenium hydride cluster **3** can effectively activate benzothiophene and dibenzothiophene under relatively mild conditions to cleave their C–S bonds selectively due to the cooperative action of the metal centers.[45] Cleavage of the C–S bond of thiophenes by transition metal complexes has attracted the attention of many inorganic and organometallic chemists in connection with hydrodesulfurization from petroleum feedstock. The reaction of **3** with

benzothiophene in toluene afforded a (μ_3–phenethylidyne)(μ_3–sulfido) complex {Cp*Ru}$_3$(μ–H)$_2$(μ_3–S)(μ_3–CCH$_2$Ph) (**20**) as a result of the successive cleavage of two C–S bonds.[45]

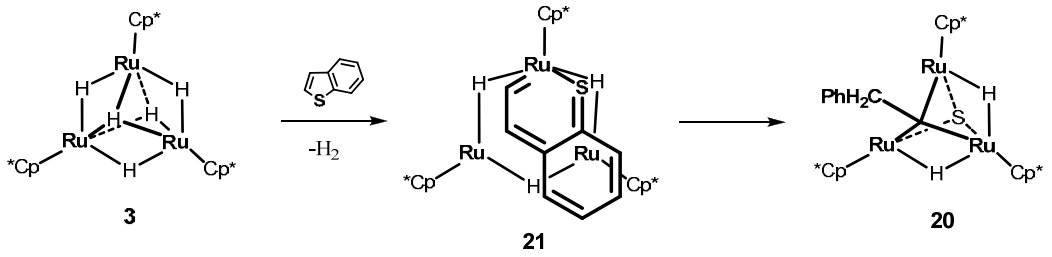

The reaction proceeds through an intermediary triruthenacyclohexadiene complex **21**, which was isolated from the resulting mixture.

The reaction of **3** with dibenzothiophene produced **22** and biphenyl.[45]

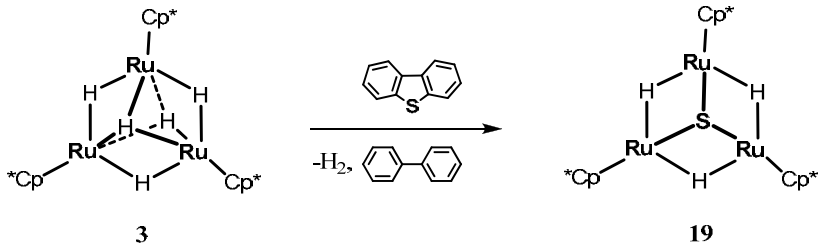

Steric bulk around the sulfur atom in dibenzothiophene is much greater than that in benzothiophene. The mechanism of this reaction, therefore, is expected to be quite different from the previous one. However, no intermediates have been isolated and the mechanism of this reaction still remains unclear.

The triruthenium hydride cluster **3** effectively activates the nitrogen-nitrogen bond of monosubstituted hydrazines, such as MeNHNH$_2$ and PhNHNH$_2$, to form a nonsymmetrically capped bis(μ_3-imido) complex, (Cp*Ru)$_3$(μ_3-NR)(μ_3-NH)(μ-H) (**20a**, R = Me; **20b**, R = Ph).[47a] The reaction of **3** with more bulky ligand, as 1,2-diphenylhydrazine predominantly yielded a monocapped imido complex, (Cp*Ru)$_3$(μ_3-NPh)(μ_3-H)$_3$ (**21**).[47a] More recently Suzuki *et al*. have shown that the complex **3** can effectively cleave a nitrogen-nitrogen double bond of azobenzene to produce (Cp*Ru)$_3$(μ_3-NPh)(μ-H)$_3$ (**22**) and (Cp*Ru)$_3$(μ_3-NPh)$_2$(μ-H) (**23**) via independent routes.[47c] Moreover, it was found that the polyhydride complex **3** can catalyze the hydrogenation of both azobenzene and 1,2-diphenylhydrazine to yield aniline.

The reaction of **3** with cyclopentadiene leading to formation of the trinuclear 2-methylruthenacyclopentadiene at ambient temperature has attracted substantial attention (Scheme 4).[43b] It is the first example of selective C–C bond activation by three cooperating metal centers. This unprecedented reaction was studied computationally by Khoroshun *et al*.[59]

Contrary to Suzuki *et al.*'s original hypothesis, it was found that the reaction proceeds through an associative mechanism with a large number of intermediates. In this mechanism, many processes known in organometallic chemistry, such as oxidative addition, hydride-dihydrogen ligand isomerism, agostic interactions play an important role. The calculated reaction mechanism[59] is summarized in the Scheme 4.

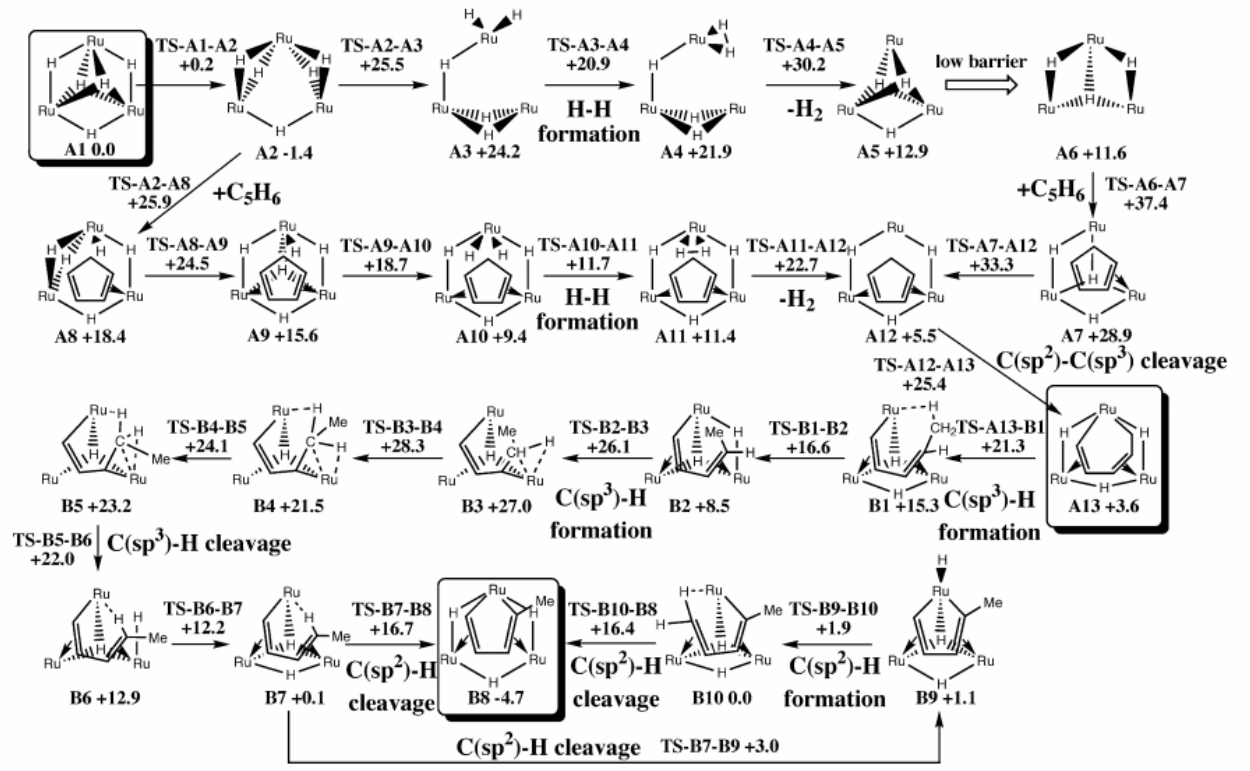

Scheme 4. The Gibbs free energy profile (kcal/mol, 298 K, 1 atm) along the proposed mechanism for the reaction $[\{Ru(C_5Me_5)\}_3(\mu\text{–}H)_3(\mu_3\text{–}H)_2] + C_5H_6$.[59] The spectator Cp ligands are omitted. The models of the experimentally observed species are outlined: reactant, **A1**, intermediate, **A13**, product, **B8**. The B3LYP Gibbs free energies are in kcal/mol, relative to separated **A1** and C_5H_6.

The reactivity of triruthenium species $[cyclo\text{-}Ru_3(\mu_2\text{–}X)_3]^{0,3+}$ (X = H, BH, CH_2, NH_2, OH, Cl, NH, CO, O, PH_2, CF_2, CCl_2, CNH, N_3) was very recently studied theoretically in terms of aromaticity.[60] All $[cyclo\text{-}Ru_3(\mu_2\text{–}X)_3]^{0,3+}$ species, except $[cyclo\text{-}Ru_3(\mu_2\text{–}H)_3]^{3+}$, were predicted to be aromatic molecules. In contrast, the $[cyclo\text{-}Ru_3(\mu_2\text{–}H)_3]^{3+}$ species exhibits a high antiaromatic character. The versatile reactivity of the isocycle $[cyclo\text{-}Ru_3(\mu_2\text{–}H)_3]^{3+}$ is related to a strong antiaromaticity of this species. The aromaticity or antiaromaticity of the isocycles was verified by the nucleus-independent chemical shift, NICS(0), NICS(1), NICS(-1), $NICS_{zz}(1)$, and $NICS_{zz}(-1)$, along with the NICS scan profiles.

Thus, multinuclear polyhydride complexes exhibit diverse reactivity towards a variety of substrates. They are even capable to activate the inert C–H bond of *n*-alkanes and C–C bond of cyclopentadiene. Their reactivity is attributed to the cooperativity of multiple metal centers, as well as the mobility of hydride ligands. Hydride ligands play important roles in the activation of a substrate, especially in the stage of generating a coordinatively unsaturated site on the cluster. When the substrate is coordinated to one ruthenium center, hydrides can be readily removed from the cluster as dihydrogen or by hydrogenation of an unsaturated molecule, such as alkenes.

Another example of a highly reactive species is a silylium cation $[C_6(SiMe_2)(SiHMe_2)_5]^+$. The role the hydrides play in case of the silylium cation is discussed below.

1.3. Hydride mobility in silylium ions

Carbenium and silylium cations are species of a high Lewis acidity, though the silylium cations are much more reactive. It is provided by a larger size and a lower electronegativity of silicon atom.[61,62] The electrophilicity of silylium cations is so high that they readily react even with very weak nucleophiles.[63–69] For example, silylium cation Et_3Si^+ is capable to activate the aliphatic carbon–fluorine bonds of perfluoroalkyl groups, the C–F bond is converted to the C–H bond under mild conditions.[70] The overall process can be considered as a Si–H/C–F metathesis. Later a new class of carborane-supported, silylium compounds acting as catalysts for hydrodefluorination of trifluoromethyl and nonafluorobutyl groups was reported.[71] The trialkylsilylium carboranes $[R_3Si(CHB_{11}Cl_{11})]^-$ and $[R_3Si(CHB_{11}R_5Br_6)]^-$, R = H, Me dramatically lower the temperature of the ring-opening polymerization of chlorophosphazene trimer $[N_3P_3Cl_6]$.[72]

However, the tricoordinate silylium requires a severe sterical protection to benefit its high reactivity.[73,74] In the very recent studies[71,72,75] the silylium cations are protected by *closo*-carboranes $[RCB_{11}X_{11}]^-$ and $[(HCB_{11}R_5Y_6)]^-$ with R = H, alkyl; X = F, Cl, Br and Y = Cl, Br chemically robust, weakly coordinating anions. These are often termed as "innocent" counterions.

Another way of stabilizing silylium ions is provided by formation of a 3c-2e bridging bond $(R_3Si–H–SiR_3)^+$, usually within a ring structure.[76–79] Müller and coworkers have synthesized and characterized the disilyl cation **24** with a symmetric SiHSi bridge.[76] Later, Sekiguchi *et al*. have characterized the silyl cation **25** using NMR spectroscopy.[77] Reed and colleagues obtained the carborane salts of simple hydrogen-bridged disilyl cations **26** in crystalline form.[78]

Although disilyl cation **24** is stable at room temperature, the high reactivity prevented a thorough study of its chemistry.[76] More recently, Müller *et al*. have synthesized disilyl cation **27** with an 1,8-naphthalenediyl backbone, which was found to be more stable than **24**.[79] The SiHSi linkage is symmetrical, corresponding to a single minimum potential.

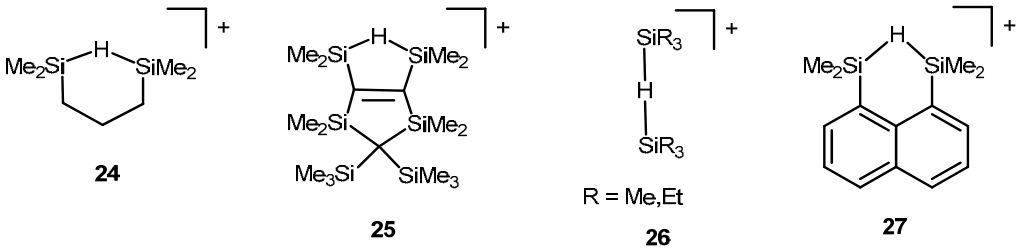

Nikonov *et al*. recently reported[80] the synthesis and characterization of cations $[C_6(SiMe_2)(SiHMe_2)_5]^+$ (**28**) and $[1,4\text{-}C_6(SiMe_2)(Me)(SiHMe_2)_4]^+$ (**29**). These are obtained by the hydride abstraction from the neutral species, $C_6(SiHMe_2)_6$ and $C_6(Me)(SiHMe_2)_5$, correspondingly.

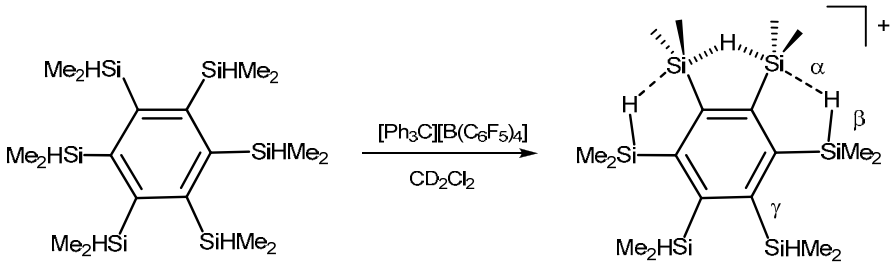

28

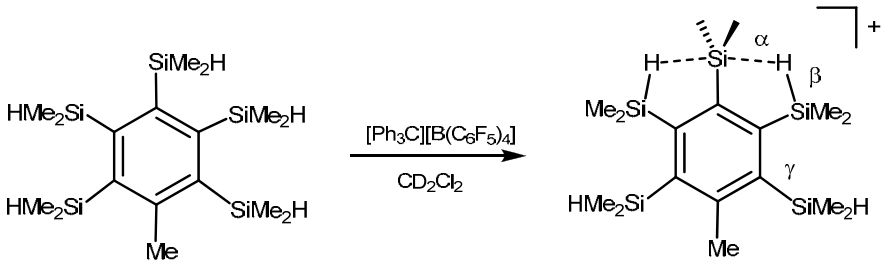

29

The cations were characterized using the IR and NMR spectra as well as by the DFT calculations.[80] Cation **28** has a symmetric Si–H–Si bridge with two equivalent strongly elongated α-Si–H bonds. This α-Si–H–Si bridge is supported by agostic $Si^{\alpha}\cdots H^{\beta}$ interactions, which contribute to electronic saturation of the α-silicon atoms. The $Si–H^{\beta}$ bonds are also lengthened, but to a lesser extent than the $Si–H^{\alpha}$ bonds. In contrast, the $Si–H^{\gamma}$ bonds are only

slightly stretched, with a $Si^{\beta}\cdots H^{\gamma}$ separation being too large for a significant interaction. The NMR study of the cation **28** revealed its fluxional character.[80] It was proposed that the hydride bridge in **28** can migrate throughout the ring. However, the detailed mechanism of this process remains unclear. The possibility that it occurs through a simple shift of one or several hydrogens was rejected, since then a nonequivalent structure with a different conformation of β- and γ-silyls would arise.[80]

The analogous cation $[1,4\text{-}C_6(SiMe_2)(Me)(SiHMe_2)_4]^+$ (**29**) has a completely different structure. It has a single silicon cationic center supported by two strong agostic Si–H bonds. Such a diagostic bonding is unprecedented in the silicon cation chemistry. Two Si^{β}–H–Si^{α} bridges are equivalent to each other, but asymmetric with respect to the hydrogen position. The NMR study indicated the absence of fluxionality in the cation **29**.[80]

Two important observations can be done from comparison of the cations **27** and **28**. First, the replacement of a $SiMe_2H$ group by a methyl changes the coordinational motif of the cationic fragment from a symmetric Si–H–Si bridge in **27** to the agostic coordination in **28**. It suggests that intrinsically the bridges are very labile. On the other hand, the lack of fluxionality in **6** implies that the methyl acts as an "insulator", while cation **27** presents a "conducting" medium with a relatively free motion of the cationic "hole" position. The cation **27** can serve as model for future ionic conductors based on the Si–H chains.

2. Electronic structure calculations

This chapter reviews the computational methods used in the following chapters. Section §2.1 introducing the DFT method consists of six paragraphs. The first one discusses the Hohenberg-Kohn theorems that provide the justification for using the electron density as the central quantity in electronic structure calculations. The next paragraph considers the Kohn-Sham equations giving a route to practical calculations in DFT. The different approaches to the implementation of the Kohn-Sham scheme are given in §2.1.3–2.1.6.

The modern quantum chemical calculations are typically performed within a finite set of basis functions, particularly, within most commonly used Gaussian-type functions and these are viewed in §2.2. The calculations of the species containing heavy elements are usually performed using effective core potentials, which are briefly discussed in §2.3. Sections §2.4 and §2.5 summarize molecular dynamics methods utilized in the following chapters.

2.1. Density functional theory

The aim of an electronic structure calculation is to calculate properties of a system from only the knowledge of the constituent atoms. When done without explicit recourse to experimental data (with the exception of the use of fundamental constants and comparison with experimental results), these can be termed *ab initio* calculations.

Traditionally electronic structure calculations have found the energy of a system by solving the time-independent Schrödinger equation[81]

$$\hat{H}(\mathbf{r}_1,..,\mathbf{r}_N)\ \Psi(\mathbf{r}_1,..,\mathbf{r}_N) = E\Psi(\mathbf{r}_1,..,\mathbf{r}_N) \qquad (2)$$

where $\Psi(\mathbf{r}_1,..,\mathbf{r}_N)$ is the electronic wave function and $\hat{H}(\mathbf{r}_1,..,\mathbf{r}_N)$ is the electronic Hamiltonian describing the motion of *N* electrons in the field of *M* point charges,

$$\hat{H} = \left[\sum_{i=1}^{N} -\frac{1}{2}\nabla_i^2 - \sum_{i=1}^{N}\sum_{a=1}^{M}\frac{Z_a}{R_{ia}} + \sum_{i=1}^{N}\sum_{j>i}^{N}\frac{1}{r_{ij}}\right] \qquad (3)$$

where ∇_i^2 is the Laplacian operator, R_{ia} is the distance between *a*th nucleus and *i*th electron, r_{ij} is the distance between *i*th nucleus and *j*th electron, Z_a is the atomic number of nucleus *a*. The first term in the Eq. (3) is the operator of the kinetic energy of the electrons, the second term represents the coulomb attraction between electrons and nuclei and the last term stands for the electron-electron repulsion.

Electronic structure calculations have proved useful in many areas chemistry and physics, especially with the rapid growth in computer power. An alternative to wavefunction based methods, density functional theory (DFT) has become widely used over the past 20 years.[82] The DFT provides an (in principle) exact method for calculating the energy of a system of interacting electrons in terms of a set of single electron equations. In certain cases the accuracy of DFT calculations is equal to those of more computationally demanding quantum chemical calculations.[82b]

The motivation of the DFT is that the ground state properties of a system can be described by considering the ground state electron density. The density can be found from the electronic wavefunction $\Psi(\mathbf{r}_1, \mathbf{r}_2, .., \mathbf{r}_n)$ by

$$\rho(\mathbf{r}_1) = N \int \Psi^*(\mathbf{r}_1, \mathbf{r}_2, .., \mathbf{r}_n)\Psi(\mathbf{r}_1, \mathbf{r}_2, .., \mathbf{r}_n) d\mathbf{r}_2 .. d\mathbf{r}_n \,. \qquad (4)$$

This has an obvious advantage over the wavefunction approach; for *N* electron system, the wavefunction is a complex function of 3*N* variables or 4*N*, if spin is included, while the charge density is a function of 3 or 4 variables, respectively. The usefulness of the DFT arises as the ground state properties of a system are determined by the ground state density, which is a unique function of the potential for a given number of electrons.

The earliest work in this spirit was that of Thomas and Fermi.[83,84] Here the energy was given by the kinetic energy of a uniform electron gas and the classical electrostatic interaction between the electrons and nuclei for an electron gas of a given energy. It was extended by adding the exchange energy of the electrons from the work of Dirac.[85] The Thomas-Fermi (TF) theory gave poor results due to the crude approximations for the kinetic energy.[86] It was the work of Kohn, Hohenberg, and Sham[87,88] that provided a route to useful calculations, which will be discussed in the following sections. Whereas the TF approach involves the electron density only, the Kohn-Sham (KS) approach reintroduced one-electron orbitals. These can be found from solving one-electron equations involving an orbital-dependent kinetic energy functional and a local effective potential.

2.1.1. The Hohenberg–Kohn Theorems

The approach of Hohenberg and Kohn is to formulate density functional theory as an exact theory of many-body systems. Density functional theory is based upon two theorems first proved by Hohenberg and Kohn.[87]

Theorem 1. *Every observable of a stationary quantum mechanical system (including energy), can be calculated, in principle exactly, from the ground-state density alone, i.e., every observable can be written as a functional of the ground-state density.*

Thus, the ground state energy of a system of electrons is a unique functional of the ground state density, i.e. $E_0 = E[\rho_0(\mathbf{r})]$.

Theorem 2. *The ground state density can be calculated, in principle exactly, using the variational method involving only density.*

So, the Hohenberg-Kohn theorem states that the ground state electron density minimizes the energy functional

$$E[\rho] = F_{HK}[\rho] + \int v_{ext}(\mathbf{r})\rho(\mathbf{r})d\mathbf{r} \tag{5}$$

where v_{ext} is the external potential, which represents the electron-nuclear attraction

$$v_{ext} = \sum_{a=1}^{M} \frac{-Z_a}{|\,\mathbf{R_a} - \mathbf{r}\,|} \tag{6}$$

Z_a is the charge of an *a*-th nucleus (atomic number), $|\,\mathbf{R_a} - \mathbf{r}\,|$ is the distance between a given electron and the nucleus *a*.

F_{HK} is a universal functional of the electron density:

$$F_{HK}[\rho] = T[\rho] + J[\rho] + E_{NC}[\rho] \tag{7}$$

here $T[\rho]$ is the kinetic energy, $J[\rho]$ is the classical Coulomb energy

$$J[\rho] = \frac{1}{2}\iint \frac{\rho(\mathbf{r})\rho(\mathbf{r}')}{|\,\mathbf{r} - \mathbf{r}'\,|}\, d\mathbf{r}\, d\mathbf{r}' \tag{8}$$

and $E_{NC}[\rho]$ is the non-classical electron-electron interaction energy.

Furthermore the minimum value of *E* is E_0, the ground state electronic energy. This introduces the concept of electron density as a fundamental variable. If the functional $E[\rho]$ can be minimized with respect to the electron density, this will yield the ground state electronic energy and density of the system.

2.1.2. Kohn-Sham Equations

The Hohenberg-Kohn theorems show that it is possible to use the ground state density to calculate properties of the system. The Kohn-Sham equations provide a route of finding the ground state density. A main advantage of this scheme is that it allows a straightforward determination of a large part of the kinetic energy in a simple way.

Central to the Kohn-Sham method[88] is the introduction of a fictitious system, which mimics in some way the true many-electron system. This fictitious system differs from the real one by the electron-electron repulsive interaction switched off. This is often called a system of *non-interacting* electrons. The ground state wavefunction of this system is far less complicated due to the absence of interactions between the particles. In fact, one can write the ground state wavefunction explicitly in terms of simple one-electron orbitals. The only complication is that the full wavefunction, Ψ_S, must still satisfy exchange anti-symmetry. This is achieved by placing one-electron wavefunction ψ_i in a *Slater determinant*,[89] as follows:

$$\Psi_S = \frac{1}{\sqrt{N!}} \det\{\psi_i(\mathbf{x}_1)\psi_j(\mathbf{x}_2)\cdots\psi_k(\mathbf{x}_N)\} \tag{9}$$

Kohn and Sham repartitioned[88] the total energy functional into following parts:

$$E[\rho] = T_s[\rho] + \int \rho(\mathbf{r}) v_{ext}(\mathbf{r}) d\mathbf{r} + J[\rho] + E_{xc}[\rho] \tag{10}$$

where $T_s[\rho]$ is the kinetic energy of *non-interacting* electrons. However, electrons still interact with nuclei, which is represented by the second term of the right-hand side of the Eq. (10). $J[\rho]$ is the classical Coulomb energy, which is given by the Eq. (8). The last term, $E_{xc}[\rho]$, is called the exchange-correlation energy. It includes the non-classical electron-electron interaction energy and the part of the kinetic energy corresponding to the fully interacting system $T[\rho]$.

Representing the electron density by a set of occupied one-electron orbitals $\{\psi_i\}$ gives

$$\rho(\mathbf{r}) = \sum_{i=1}^{occ.} \psi_i^*(\mathbf{r})\psi_i(\mathbf{r}), \tag{11}$$

$$T_s[\rho] = -\frac{1}{2}\sum_{i}^{N} \left\langle \psi_i^* \middle| \nabla_i^2 \middle| \psi_i \right\rangle. \tag{12}$$

If the orbitals are required to be orthonormal, i.e.

$$\int \psi_i^*(\mathbf{r})\psi_j(\mathbf{r})d\mathbf{r} = \delta_{ij}\,, \tag{13}$$

then a functional of the orbitals can be defined

$$\Omega[\psi_i] = E[\rho] - \sum_i \sum_j \varepsilon_{ij} \int \psi_i^*(\mathbf{r})\psi_j(\mathbf{r})d\mathbf{r}\,, \tag{14}$$

where ε_{ij} are Lagrange multipliers to ensure the orbitals are orthonormal. Minimization of $\Omega[\psi_i]$ with respect to $\psi_i^*(\mathbf{r})$ gives the Kohn-Sham equations

$$\left[-\frac{1}{2}\nabla_i^2 + v_{eff}(\mathbf{r})\right]\psi_i(\mathbf{r}) = \varepsilon_i\psi_i(\mathbf{r})\,, \tag{15}$$

where $v_{eff}(\mathbf{r})$ is the Kohn-Sham potential defined as

$$v_{eff}(\mathbf{r}) = v_{ext}(\mathbf{r}) + \int \frac{\rho(\mathbf{r}')}{|\,\mathbf{r}-\mathbf{r}'\,|}d\mathbf{r}' + v_{xc}(\mathbf{r})\,, \tag{16}$$

The second term in the Eq. (16) is often termed as Hartree potential v_{H}. The last term is the exchange-correlation potential

$$v_{xc}(\mathbf{r}) = \frac{\delta E_{xc}}{\delta\rho(\mathbf{r})}\,. \tag{17}$$

On going from the Eq. (14) to (15) a unitary transformation is performed to obtain the canonical form of the Kohn–Sham equations.[88] As can be seen the Eq. (15) is of the same form as the single particle Schrödinger equation with an effective local potential v_{eff} defined in the Eq. (16). This is in contrast to the Hartree-Fock equations,[81] which contain a non-local potential in the one-electron equations.

The third term in the effective potential Eq. (16) is the exchange-correlation potential. This is of central importance for the accuracy of DFT calculations, and there has been much work in finding accurate approximations of v_{xc}.[82]

The Kohn-Sham equations derived in this section are summarized in the flow chart in Figure 9. An actual calculation employs a numerical procedure that successively changes v_{eff} and ρ to approach the self-consistent solution.

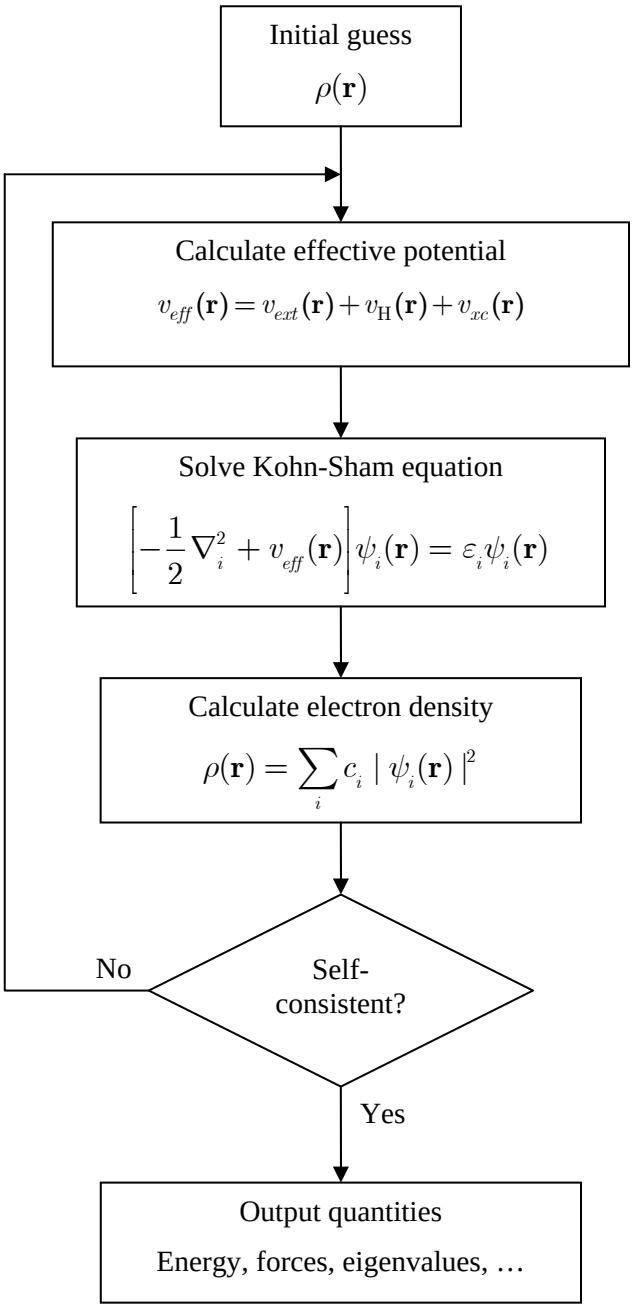

Figure 9. Schematic representation of the self-consistent loop for solution of Kohn-Sham equations.

2.1.3. Local Density Approximation

First implementations of the Kohn-Sham method were using the local approximations to the exchange correlation energy. The density is treated locally as a uniform electron gas in

this simplest approximation. The exchange correlation energy at each point in the system is the same as that of a uniform electron gas of the same density. This approximation was originally introduced by Kohn and Sham[88] and holds for a slowly varying density. The exchange-correlation energy for a density $\rho(\mathbf{r})$ is given by

$$E_{xc}^{LDA} = \int \rho(\mathbf{r})\varepsilon_{xc}^{\mathrm{hom}}(\mathbf{r})d\mathbf{r}\,, \tag{18}$$

where $\varepsilon_{xc}^{\mathrm{hom}}$ is the exchange-correlation energy per particle of an uniform electron gas of density ρ. The exchange-correlation potential is then given by

$$V_{xc}^{LDA}[\rho] = \frac{\delta E_{xc}^{LDA}}{\delta\rho} = \varepsilon_{xc}^{\mathrm{hom}}[\rho] + \rho\frac{\delta\varepsilon_{xc}^{\mathrm{hom}}[\rho]}{\delta\rho}\,. \tag{19}$$

This can then be inserted into the Eq. (18) for use in calculations. However, for practical utilization of the LDA it is necessary to determine the exchange-correlation energy for the uniform electron gas of a given density. It is common to split $\varepsilon_{xc}^{\mathrm{hom}}$ into exchange and correlation potentials $\varepsilon_{xc}^{\mathrm{hom}} = \varepsilon_{x}^{\mathrm{hom}} + \varepsilon_{c}^{\mathrm{hom}}$. The simplest form of the exchange potential is given by the Dirac functional[85]

$$\varepsilon_{x}^{\mathrm{hom}}[\rho] = -\frac{3}{4}\left(\frac{3}{\pi}\right)^{\frac{1}{3}}\rho\,. \tag{20}$$

Accurate values for $\varepsilon_{c}^{\mathrm{hom}}$ have been determined from Quantum Monte Carlo (QMC) calculations.[90]

2.1.4. Generalized Gradient Approximations

As the LDA approximates the energy of the true density by the energy of a local constant density, it fails when the density undergoes rapid changes such as in molecules. An improvement to this can be made by considering the gradient of the electron density. The first step beyond the local approximation is a functional of the magnitude of the gradient of the density $|\nabla\rho|$ as well as the value ρ at each point. Such a Gradient Expansion Approximation (GEA) was suggested in the original paper of Kohn and Sham[88], and carried out by Herman *et al.*[91] However the GEA does not lead to consistent improvement over the LDA. It violates the sum

rules and other relevant conditions[91] and, indeed, leads to worse results. The basic problem is that gradients in chemical systems are so large that the GEA breaks down.

The term Generalized Gradient Approximation (GGA) stands for a variety of ways proposed for functions that modify the behavior at large gradients, while preserving the desired properties.

Symbolically this can be written as

$$E_{xc}^{GGA} = \int \rho(\mathbf{r}) \varepsilon_{xc}^{\mathrm{hom}} F_{xc}[\rho, \nabla\rho] d\mathbf{r} \tag{21}$$

where F_{xc} is dimensionless and $\varepsilon_{xc}^{\mathrm{hom}}$ is the exchange-correlation energy of the uniform electron gas.

In practice, E_{xc}^{GGA} is usually split into its exchange and correlation contributions

$$E_{xc}^{GGA} = E_{x}^{GGA} + E_{c}^{GGA} \tag{22}$$

and two terms are approximated individually.

The exchange part can be written as

$$E_{x}^{GGA} = E_{x}^{LDA} - \int F_{x}(s) \rho^{4/3}(\mathbf{r}) d\mathbf{r} \tag{23}$$

where the argument of the function *F* is the reduced density gradient

$$s(\mathbf{r}) = \frac{|\nabla\rho(\mathbf{r})|}{\rho^{4/3}(\mathbf{r})} \tag{24}$$

s(**r**) can be interpreted as a local inhomogeneity parameter. For example, the values of *s*(**r**) in the region close to nuclei (large density gradients and large densities) are of the range of the *s*(**r**) values in the bonding and tail regions (small density gradients and small densities).

For the function F_x two main approaches were proposed.[92] The first one is based on a GGA exchange functional developed by Becke[93] (abbreviated as B or B88)

$$F_{x}[s(\mathbf{r})] = 2^{-1/3} \beta \frac{s(\mathbf{r})^2}{1 + 6\beta s \sinh^{-1} s(\mathbf{r})} \tag{25}$$

where β optimized using Hartree-Fock exchange energies of noble gas atoms (β = 0.0042).

The functionals utilizing the described approach include among others the PW91 exchange functional[94] and the CAM functionals developed by Handy and coworkers.[95]

The second class of GGA exchange functionals use for *F* a rational function of the reduced density gradient. For example, free of semiempirical parameters *F* function of Perdew's 1986 exchange functional[96] is given below

$$F_x^{86} = \left(1 + 1.296\left(\frac{s}{(24\pi^2)^{1/3}}\right)^2 + 14\left(\frac{s}{(24\pi^2)^{1/3}}\right)^4 + 0.2\left(\frac{s}{(24\pi^2)^{1/3}}\right)^6\right)^{1/15} \qquad (26)$$

The other widely known functionals of this type are the early functionals by Becke (B86)[97], the functional by Lacks and Gordon[98] and PBE by Perdew, Burke and Ernzerhof.[99]

The corresponding gradient-corrected correlation functionals have even more complicated analytical forms. They are discussed briefly here, since they cannot be understood by simple physically motivated reasoning. Among the widely used correlation functionals is the P86 (also termed as P) functional.[96] It is the counterpart of the 1986 Perdew exchange functional. It employs an empirical parameter, which was fitted to the correlation energy of the neon atom. Another popular correlation functional is the LYP functional.[100] It is based on an approximate formula for the correlation energy of the helium atom by Colle and Salvetti[101]. It differs from the other GGA in that it contains some local components. It should be noted that all these correlation functionals are based on systems that only include dynamical correlation effects. Widely used GGAs can now provide accuracy required for density functional theory to be widely adopted by the chemistry community.

2.1.5. Hybrid functionals

The exchange part of the exchange-correlation energy is significantly larger in absolute numbers than the corresponding correlation effects.[82] From the other hand the exchange energy of a Slater determinant can be computed exactly.[81] Therefore hybrid functionals, which combine elements of Hartree-Fock (HF) and Kohn-Sham (KS) methods, have become popular in electronic structure calculations. The starting point of this approach is *the adiabatic connection* formula

$$E_{XC} = \int_0^1 E_{XC}^{\lambda}\, d\lambda \qquad (27)$$

where λ is an electronic coupling-strength parameter that switches on the Coulomb repulsion between electrons. The formula connects the non-interacting KS reference system (λ = 0) to the fully interacting real system (λ = 1), through a continuum of partially interacting systems ($0 \leq \lambda \leq 1$), all sharing a common density ρ. It is not practical to perform this integral analytically and so it must be approximated. The simplest approximation to Eq. (27) is a linear interpolation[102]

$$E_{XC} = \frac{1}{2}(E_{XC}^{0} + E_{XC}^{1}) \tag{28}$$

where E_{XC}^{0} is the exchange-correlation potential energy of the non-interacting reference system. As there are no electronic interactions in this system there is no correlation term and so E_{XC}^{0} corresponds to the pure exchange energy of the Kohn-Sham determinant and can be calculated exactly. E_{XC}^{1} is the exchange-correlation potential energy of the full-interacting real system. It is usually approximated by common density functionals. An application of the Eq. (28) is the so-called half-and-half approach, which is obtained when $E_{XC}^{0} = E_{X}^{HF}$ (Hartree-Fock exchange energy) and $E_{XC}^{1} = E_{XC}^{LSD}$ (the local spin density approximation to exchange and correlation).[102]

A more valuable approach has been obtained by Becke[103] using a three-parameter equation:

$$E_{XC}^{B3} = E_{XC}^{LSD} + a(E_{X}^{HF} - E_{X}^{LSD}) + bE_{X}^{B88} + cE_{C}^{PW91} \tag{29}$$

where E_{X}^{B} and E_{C}^{PW91} are the Becke (B88) exchange functional and the Perdew and Wang's 1991 (PW91)[104] correlation functional, respectively. The three semi-empirical parameters *a*, *b*, and *c* have been determined by fitting the heats of formation of a standard set of molecules.[103]

In B3LYP, one of the most often used hybrid functionals, the PW91 correlation functional is replaced by the LYP functional.

$$E_{XC}^{B3LYP} = (1-a)E_{X}^{LSD} + aE_{X}^{HF} + bE_{X}^{B88} + cE_{C}^{LYP} + (1-c)E_{C}^{LSD} \tag{30}$$

The values for the parameters are *a* = 0.20, *b* = 0.72, and *c* = 0.81.

For some hybrid functionals these parameters were proposed on the basis of theoretical considerations. In particular, Adamo and Barone developed[105] a parameter free hybrid functional PBE0:

$$E_{XC}^{PBE0} = E_{XC}^{PBE} + 0.25(E_X^{HF} - E_X^{PBE}) \tag{31}$$

where the weight 0.25 was determined by the lowest order of Gorling-Levy perturbation theory,[106] which provides an accurate description of the dependence of E_{XC} upon λ.

2.1.6. The basic machinery of DFT programs

The Kohn-Sham orbitals can be expanded in basis functions exactly like the Hartree-Fock orbitals. The Kohn-Sham equations can then be expressed in a matrix form, identical in form to the Roothaan-Hall equations[81]

$$\mathbf{HC} = \mathbf{SCE} \tag{32}$$

In this matrix equation the elements of the Kohn-Sham matrix **H** are given by:

$$H_{\mu\nu} = \int \phi_\mu(\mathbf{r}) \left\{ -\frac{1}{2}\nabla_1^2 - \left(\sum_{a=1}^{M} \frac{Z_a}{\mathbf{R}_a} \right) + \int \frac{\rho(\mathbf{r}')}{|\,\mathbf{r}-\mathbf{r}'\,|} d\mathbf{r}' + v_{xc}[\mathbf{r}] \right\} \phi_\nu(\mathbf{r}) d\mathbf{r} \tag{33}$$

The first two terms are straightforward and are equal to the core contribution, $H_{\mu\nu}^{core}$. The Coulomb repulsion contribution can be expanded in terms of the basis functions and the density matrix, $\mathbf{P}$:

$$\iint \frac{\phi_\mu^*(\mathbf{r})\rho(\mathbf{r}')\phi_\nu(\mathbf{r})}{|\,\mathbf{r}-\mathbf{r}'\,|} d\mathbf{r}\, d\mathbf{r}' = \sum_{\lambda\sigma} P_{\lambda\sigma} \iint \frac{\phi_\mu^*(\mathbf{r})\phi_\nu(\mathbf{r})\phi_\lambda^*(\mathbf{r}')\phi_\sigma(\mathbf{r}')}{|\,\mathbf{r}-\mathbf{r}'\,|} d\mathbf{r}\, d\mathbf{r}' = \sum_{\lambda\sigma} P_{\lambda\sigma}(\mu\nu \mid \lambda\sigma)$$

For a closed-shell system with *N* electrons the elements of the density matrix are given by:

$$P_{\mu\nu} = 2\sum_{i}^{N/2} c_{\mu i} c_{\nu i} \tag{34}$$

This is just the same as for the Roothaan-Hall approach to Hartree-Fock theory. The overlap matrix, *S*, is defined similarly:

$$S_{\mu\nu} = \int \phi_\mu(\mathbf{r})\phi_\nu(\mathbf{r})d\mathbf{r} \tag{35}$$

The overall procedure to achieve self-consistency is very reminiscent of that used in Hartree-Fock theory, involving first an initial guess of the density by superimposing atomic densities, construction of the Kohn-Sham and overlap matrices, and diagonalization to give the eigenfunctions and eigenvectors from which the Kohn-Sham orbitals can be constructed and thus the density for the next iteration. This cycle continues until convergence is achieved.

Thus, density functional programs are built in a similar way to the Hartree–Fock programs. The main difference of the DFT program is that exchange integrals are replaced by integrals with the potential from the XC functionals.[82] In Hartree–Fock program the Fock matrix elements for Coulomb and exchange are calculated together.[81] Computational time is dominated by the calculation of the two-electron integrals.

In DFT calculation only the Coulomb part is needed, except for hybrid functionals. The Coulomb contribution has a special structure that can be used together with further approximations to increase the efficiency of the program. For the calculation of the Coulomb part of the Kohn–Sham matrix all integrals $(\mu\nu,\lambda\sigma)$ over all basis functions are required. This method scales like M^4, where M is the number of basis functions. For this reason other approximate methods for the calculation of the Coulomb energy are used.

Resolution of identity (RI) method. The electron density is defined as

$$\rho(\mathbf{r}) = \sum_{\mu\nu} P_{\mu\nu}\phi_\mu^*(\mathbf{r})\phi_\nu(\mathbf{r}) \tag{36}$$

The product of two atom-centered basis functions is a new function

$$\chi_{(\mu\nu)}(\mathbf{r}) = \phi_\mu^*(\mathbf{r})\phi_\nu(\mathbf{r}) \tag{37}$$

The density is therefore described exactly in a basis of the size M^2.

The basic idea of the method is to use an approximate description of the density instead of the exact one, where the new basis (χ_α) is only slightly larger than the basis used for the orbitals (ϕ_μ).

$$\tilde{\rho}(\mathbf{r}) \approx \sum_\alpha c_\alpha \chi_\alpha(\mathbf{r}) \tag{38}$$

Then the contribution to the Kohn–Sham matrix

$$F^c_{\mu\nu} = \sum_\alpha c_\alpha \iint \frac{\phi^*_\mu(\mathbf{r})\phi_\nu(\mathbf{r})\chi_\alpha(\mathbf{r}')}{|\,\mathbf{r}-\mathbf{r}'\,|} d\mathbf{r}\, d\mathbf{r}' = \sum_\alpha c_\alpha(\mu\nu \mid \alpha) \tag{39}$$

This technique was originally suggested by Baerends *et al.*[107] for STO basis functions and later extended by Sambe *et al.*[108] to contracted GTO basis sets. The method scales like M^3. Special basis sets for the electron density have to be used that match the basis sets for the wavefunctions. Typically these basis sets have three times more functions than the wave function basis. The expansion coefficients c_α can be calculated minimizing the difference to the exact electron density

$$F = \int [\rho(\mathbf{r}) - \tilde{\rho}(\mathbf{r})]^2 d\mathbf{r} \tag{40}$$

or preferentially by minimizing the Coulomb self-repulsion of the residual density,

$$F' = \iint \frac{[\rho(\mathbf{r}) - \tilde{\rho}(\mathbf{r})][\rho(\mathbf{r}') - \tilde{\rho}(\mathbf{r}')]}{|\,\mathbf{r}-\mathbf{r}'\,|} d\mathbf{r}\, d\mathbf{r}' \tag{41}$$

This method is implemented in many quantum chemistry codes, like Turbomole,[109] Gaussian 03,[110] DeMON.[111]

Local expansion of density. The local expansion of density is based on similar ideas as the RI methods, but instead of looking for a global approximation to the density separate approximations to all pair densities are used.

$$\rho_{AB}(\mathbf{r}) = \sum_{\substack{\alpha\beta \\ \alpha\in A,\beta\in B}} P_{\alpha\beta}\Phi_\alpha(\mathbf{r})\Phi_\beta(\mathbf{r}) \tag{42}$$

$$\rho_{AB}(\mathbf{r}) \approx \sum_{\mu\in A} c_\mu \chi^A_\mu(\mathbf{r}) + \sum_{\nu\in B} c_\nu \chi^B_\nu(\mathbf{r}) \tag{43}$$

The pair density of atoms A and B is expanded in a basis located at the atoms A and B. The advantage of this method is that the calculation of the expansion coefficients is done locally and is therefore independent of the size of the molecule. The disadvantage lies in the limitation of the expansion to the functions on the same atoms. To achieve good results large

basis sets (with high angular momenta) have to be used. This method is used in the program ADF.[112]

The exchange-correlation contribution to the Kohn-Sham matrix elements (the final term in Eq. (33)) is invariably evaluated using a grid of points. This is a consequence of the complexity of the functionals employed. For the evaluation of the exchange and correlation contribution, in the spin unpolarized case, the following operations[82] are performed:

1) collocation of $\rho(\mathbf{r}) = \sum_{\mu\nu} P_{\mu\nu}\phi_\mu^*(\mathbf{r})\phi_\nu(\mathbf{r})$;
2) numerical approximation of $\nabla\rho$ based on the values of $\rho(\mathbf{r})$ on the grid;
3) evaluation of ε_{xc} and its derivatives $\frac{\delta\varepsilon_{xc}}{\delta\rho}$ and $\frac{\delta\varepsilon_{xc}}{\delta|\nabla\rho|}$ on each point of the grid;
4) computation of v_{xc} on the grid

$$v_{xc} = \frac{\delta\varepsilon_{xc}}{\delta\rho} - \nabla\cdot\left(\frac{\delta\varepsilon_{xc}}{\delta|\nabla\rho|}\frac{\nabla\rho}{|\nabla\rho|}\right);$$

5) calculation of the matrix element of the sum of v_{xc} and the Hartree potential v_{H} between the Gaussians $\int\left(v_{xc}(\mathbf{r}) + v_{\mathrm{H}}(\mathbf{r})\right)\varphi_\mu(\mathbf{r})\varphi_\nu(\mathbf{r})d\mathbf{r}$.

If a DFT program uses a basis set containing *K* functions and employs either a grid-based integration scheme with *P* points or an auxiliary basis set with *P* functions then the computational complexity of the calculation scales as K^2P. As *P* is often linearly related to *K*, density functional theory is often said to scale as the cube of the number of basis functions, K^3. This contrasts with the fourth-power scaling for conventional Hartree-Fock calculations.

2.2. Basis Sets

The quantum chemical methods aim to compute properties of interest without recourse to experimental data. It requires finding the wavefunction, which is generally unknown. Therefore the latter is usually expanded in terms of a set of known functions. The one-electron orbital can be written as

$$\phi_i = \sum_{j=1}^{\infty} c_{ij}\varphi_j, \qquad (44)$$

where φ_j form a complete set of functions. Obviously it is impossible to use an infinite number of basis functions so the sum in Eq. (44) is taken over a finite number of functions. This

introduces another source of error into the calculations as it is not then possible to describe components of Ψ along the missing functions.

For isolated atoms and molecules the wavefunction exponentially decays to zero at large distances. This implies that the basis functions used for these calculations should behave in a similar way.

The functions correctly describing the radial part of the atomic orbitals and called Slater orbitals were proposed by Zener[113] and Slater[114]

$$r^{n^*-1}\exp\left(-\frac{Z-s}{n^*}r\right) \tag{45}$$

where n^* is the effective quantum number, s is the the screening constant, and Z is the atomic number. n and s parameters are defined by the Slater's rules. The exponential dependence on distance is the same as for the hydrogen atom.

Later, Roothaan and Bagus[115] introduced for the LCAO method the functions called Slater type orbitals (STO). STOs have the following form (in spherical coordinates)

$$\varphi_{STO}^{nlm\zeta}(r,\theta,\varphi) = N_n Y_{lm}(\theta,\varphi) r^{n-1}\exp(-\zeta r), \tag{46}$$

where N_n is a normalization constant, l, m and n are the principal, azimuthal and magnetic quantum numbers, respectively; $Y_{lm}(\theta,\varphi)$ is a spherical harmonic corresponding to l and m, and ζ is the orbital exponent. The ζ parameters were optimized variationally with respect to each total atomic energy.

The Gaussian functions, generally named Gaussian type orbitals (GTO), are the usual alternative functions to the STOs in the molecular calculations. The spherical GTOs were proposed for the first time by Boys[116] and McWeeny[117]. They have the following form

$$\varphi_{GTO}^{nlm\zeta}(r,\theta,\varphi) = N_n Y_{lm}(\theta,\varphi) r^{n-1}\exp(-\zeta r^2). \tag{47}$$

In both cases the angular dependence of the wavefunction is contained in the spherical harmonics, where the l, m values determine the type of the orbital (e.g. $l = 0$ is a s type orbital, $l = 1$ a p orbital, etc).

The main difference between STO and GTO is the power of r in the exponent. The r^2 dependence in the exponent in the GTOs is a poorer representation than that of the STO. GTOs have a zero slope at the nucleus ($r = 0$), whereas STOs have a cusp. These factors suggest that

more GTOs are needed to form a suitable basis set than STOs, roughly three times as many are needed to achieve the same accuracy. However, two-electron integrals can be evaluated analytically by using GTOs. This computational efficiency more than compensates for the additional number of functions needed, so GTOs are more commonly used in calculations.

In practice the electronic structure calculations are performed with the so called contracted GTOs (CGTO), each of them given by a fixed linear combination of primitive GTOs.

$$\varphi_{\tau}^{CGTO} = \sum_{a} d_{a\tau} \varphi_{a}^{GTO} . \tag{48}$$

Molecular orbitals then are a linear combination of the CGTOs and the coefficients $d_{a\tau}$ are obtained in the electronic molecular calculation. However, neither the exponents of the primitive GTOs nor the coefficients $d_{a\tau}$ are changed along the calculation. The main idea behind the contraction of the basis set functions is that the inner atomic shells do not experiment great changes in the chemical bond formation. It is assumed that their description in the molecular environment is similar to their description in the atom.

The use of CGTO allows the saving in storage and computational time in the molecular integral calculations. Taking that *K* and *n* are the number of primitive and contracted GTOs, respectively, the contraction process reduces in $(K/n)^4$ the number of integrals to be calculated and stored.

The accuracy of the calculation strongly depends on the size of the basis set. As a minimum requirement for useful calculations it is necessary to have at least a double-zeta quality for valence orbitals. Additional higher angular momentum (*d*, *f* orbitals) basis functions may also be added to account for polarization effects.

2.3. Treating core electrons

Since ruthenium is a moderately heavy element, it can be beneficial to make use of effective core potentials (ECPs), in which the inner-shell electrons are replaced with a model potential. Typically the ECPs are constructed on a grid using all-electron numerical (relativistic or non-relativistic) wavefunctions. The total pseudopotential is then fit to the analytical form,[118]

$$\hat{U}^{ECP} = \sum_{\alpha=1}^{N'_{NUC}} \sum_{i=1}^{N_{VAL}} \left(U_{l_{\max}+1}^{\alpha}(r_{i\alpha}) + \sum_{l=0}^{l_{\max}} \sum_{m=-l}^{l} \left| Y_{lm}(\Omega_{i\alpha}) \right\rangle U_{l}^{\alpha}(r_{i\alpha}) \left\langle Y_{lm}(\Omega_{i\alpha}) \right| \right), \tag{49}$$

where the sum over α is over only those atoms having a pseudopotential. For atom α, $r_{i\alpha}$ is the distance and $\Omega_{i\alpha}$ is the solid angle of electron i measured from α, $l_{\max}$ is the largest orbital angular momentum among the core orbitals, and U_l^α is a local pseudopotential for atom α that depends only on $r_{i\alpha}$ and the angular momentum l. The spherical harmonics Y_{lm} act as projection operators, imposing orthogonality between the missing core and the valence wave function. The functions U_l^α determine the actual form of the ECP and are obtained on a grid. For molecules they are then fit to a linear combination of Gaussians for ease of integration, i.e.

$$U_l(r) = \frac{1}{r^2}\sum_k d_{kl} r^{n_{kl}} \exp(-b_{kl} r^2), \qquad (50)$$

where d_{kl}, n_{kl} and b_{kl} are fitting parameters.

It is generally recognized that the outermost $(n-1)s^2$ and $(n-1)p^6$ core electrons should not be replaced by an ECP, but should be retained in the calculations. Small-core ECPs are more reliable than large-core ECPs, where only the $(n)s$ and $(n-1)d$ electrons of the transition metals are calculated. Several groups developed valence basis sets in conjunction with small-core ECPs[119 -122] for the transition metals.

An important theoretical aspect for calculating transition metal compounds concerns the effect of relativity. It is well known that relativistic effects must be considered in the calculation in order to obtain reliable geometries and energies of second- and third-transition metal-row molecules.[123] Elements of the first transition metal row are little influenced by relativity, except for copper.[123,124] The most convenient way to include relativistic effects in the calculations is the use of quasi-relativistic ECPs. The techniques of relativistic ECPs for molecules containing transition metals and other heavy atoms have recently been reviewed.[118]

2.4. Ab initio molecular dynamics

The aim of molecular dynamics (MD) is to model the detailed microscopic dynamical behavior of many different types of systems as found in chemistry, physics or biology. The history of molecular dynamics goes back to the mid 1950's when first computer simulations on simple systems were performed.[125]

The nuclear motion of the particles is modeled using the laws of classical mechanics within MD. For a set of nuclei treated as classical masses with an interaction energy $E\left[\{\mathbf{R}_I\}\right]$ dependent on the positions of the particles $\{\mathbf{R}_I\}$, the equations of motion are

$$M_I\ddot{\mathbf{R}}_I = -\frac{\partial E}{\partial \mathbf{R}_I} = \mathbf{F}_I[\{\mathbf{R}_I\}] \tag{51}$$

Such equations can be solved analytically only in the small-amplitude harmonic approximation. In general, they are solved by numerical simulations using discrete time steps based on discrete equations such as the velocity Verlet algorithm.[126] The advantage of this technique is that it uses as basic variables positions and velocities at the same time instant *t*. The velocity Verlet algorithm appears like a Taylor expansion for the coordinates:

$$\mathbf{R}_I(t+\Delta t) = \mathbf{R}_I(t) + \mathbf{V}(t)\Delta t + \frac{\mathbf{F}(t)}{2M_I}\Delta t^2 \tag{52}$$

This equation is combined with the update for the velocities

$$\mathbf{V}(t+\Delta t) = \mathbf{V}(t) + \frac{\mathbf{F}(t+\Delta t) + \mathbf{F}(t)}{2M_I}\Delta t^2 \tag{53}$$

The key property of the velocity Verlet algorithm is that the errors do not accumulate. Despite the fact that the equations are only approximate for any finite Δ*t*, the energy is conserved and the simulations are stable for long runs.

Classical molecular dynamics simulations are well established as a powerful technique to study dynamic and thermodynamic properties of atomic and molecular systems at a finite temperature.[125] Advances in electronic structure calculations have made MD simulations possible with forces derived directly from the electrons with no parameters. These are often termed ″ab initio″ or ″first principles″ MD simulations.[127] Most often the ″electronic part″ is calculated by the DFT method. The length and time scales of typical ab initio molecular dynamics simulations are currently given by approximately 10 to 1000 atoms and 1 to 100 ps.

Born–Oppenheimer (BO) molecular dynamics is a commonly used form of ab initio molecular dynamics simulations. The interaction energy $E\left[\{\mathbf{R}_I\}\right]$ in the molecular dynamics method has the same physical meaning as the Kohn-Sham energy within the Born-Oppenheimer approximation. The Kohn-Sham energy depends only on the nuclear positions

and defines the hypersurface for the movement of the nuclei. The Lagrangian for the BO dynamics is therefore[127]

$$L_{BO} = (\mathbf{R}, \dot{\mathbf{R}}) = \sum_{I=1}^{N} \frac{1}{2} M_I \dot{\mathbf{R}}_I^2 - \min_{\{\psi_i\}} E_{KS}\left(\{\psi_i\}; \mathbf{R}^N\right), \tag{54}$$

and the minimization is constraint to orthogonal sets of $\{\psi_i\}$. The equations of motions are

$$M_I \ddot{\mathbf{R}}_I = -\nabla_{\mathbf{R}}\left[E_{KS}\left(\psi, \mathbf{R}^N\right)\right] = -\frac{d}{d\mathbf{R}_I}\left[\min_{\{\psi_i\}} E_{KS}(\{\psi_i\}; \mathbf{R}^N)\right] \tag{55}$$

The forces in BOMD (with the optimized Kohn–Sham orbitals) are

$$F_{KS}(\mathbf{R}_I) = -\frac{\partial E_{KS}}{\partial \mathbf{R}_I} + \sum_{ij} C_{ij} \frac{\partial}{\partial \mathbf{R}_I} \left\langle \psi_i \middle| \psi_j \right\rangle \tag{56}$$

The accuracy of the forces used in BOMD depends linearly on the accuracy of the minimization of the Kohn–Sham energy.[127]

To perform a computer experiment the initial values for positions and velocities have to be chosen together with an appropriate time step Δ*t*. The initial positions of the atomic coordinates are usually taken from the optimized geometry of the system. For BOMD, the time step used in the propagation of the atomic coordinates is only dependent on the frequency spectrum of the atomic system. The velocities can be assigned randomly selecting from a Maxwell-Boltzmann distribution at the temperature of interest:

$$p(v_{ix}) = \left(\frac{m_i}{2\pi k_B T}\right)^{1/2} \exp\left[-\frac{1}{2}\frac{m_i v_{ix}^2}{k_B T}\right] \tag{57}$$

The Maxwell-Boltzmann equation provides the probability that an atom i of mass m, has a velocity v_x in the x direction at a temperature T. A Maxwell-Boltzmann distribution is a Gaussian distribution, which can be obtained using a random number generator. The initial velocities are often adjusted so that the total momentum of the system is zero. Having set up the system and assigned the initial velocities, the simulation can start. At each step the force on each atom must be calculated by differentiating the potential function.

The first part of the simulation is the equilibration phase in which strong fluctuation may occur. Once all important quantities are sufficiently equilibrated, the actual (″production″) simulation is performed. Finally, observables are calculated from the trajectory.

The parameters that are used to characterize whether equilibrium has been reached depend to some extent on the system being simulated. The kinetic and potential energies would be expected to fluctuate in a simulation in the microcanonical ensemble (constant *NVE*), but the total energy should remain constant. The components of the velocities should describe a Maxwell-Boltzmann distribution (in all three directions *x*, *y* and *z*) and the kinetic energy should be equally distributed among the three directions *x*, *y* and *z*. It is usually desired to perform a simulation at a specified temperature and so it is common practice to adjust the temperature of the system by scaling the velocities during the equilibration phase. During the production phase the temperature is a variable of the system.

2.5. Metadynamics method

One of the main advantages of molecular dynamics is the ability to simulate complex chemical reactions. However, a straightforward application of MD techniques is frustrated by the timescale problem, since typical reaction rates far exceed the affordable simulation times. This is the well-known rare event problem for which many solutions have been proposed.[128]

The classical approach of quantum chemistry to this problem is to determine local minima and saddle points on the potential energy surface (PES). The minima determine the possible equilibrium configuration, while saddle points determine reaction pathways. The classical approach is powerful, but fails when the PES is complex or when entropy effects play an important role.

These intricacies can be overcome using the recently developed metadynamics method.[129] It is based on the ideas of the extended Lagrangian[130] and coarse-grained non-Markovian dynamics.[131] The first crucial step in the method is to choose a set of collective variables (CV) *S*, which are functions of the ionic coordinates R_I. The CVs must include all the relevant modes that cannot be sampled in the time scale of the simulation, as well as be able to distinguish between reactants and products. The method will not sample motions along slow modes that are not included in the collective variables. Examples of collective variables are distances between atoms, dihedral angles, coordination numbers, or any other function of the ionic coordinates R_I. The aim of the method is to explore the FES $F(\mathbf{s})$ of a limited set of collective variables s_α. The extended Lagrangian within the Born–Oppenheimer molecular dynamics is given by

$$L = L_{BO} + \sum_\alpha \frac{1}{2} M_\alpha \dot{s}_\alpha^2 - \sum_\alpha \frac{1}{2} k_\alpha [S_\alpha(\mathbf{R}_I) - s_\alpha]^2 + V(t,s) \qquad (58)$$

The second term on the right-hand side is the total kinetic energy of the fictitious particles, which for large enough masses are adiabatically separated from the ionic and electronic degrees of freedom. Each fictitious particle s_α is connected to its actual collective variable $S_\alpha(\mathbf{R_I})$ by a harmonic spring. For large enough force constants k_α, the springs restrain the molecular configuration close to the slowly moving particles s_α. The total potential energy of the harmonic springs gives rise to the third right hand-side term in Eq. (56). The last term, the history-dependent biasing potential is written in the discrete form as

$$\mathrm{V}(t,s) = \sum_{t_i<t} h \exp\left[-\frac{(s-s_i)^2}{2(\Delta s_i^{\perp})^2}\right] \exp\left[-\frac{((s^{i+1}-s^i)(s-s^i))^2}{2(\Delta s_i^{||})^4}\right] \tag{59}$$

Here *t* indicates the actual simulation time, *i* counts the metadynamics steps, the first exponential gives the hill's shape in the direction perpendicular to the trajectory, whereas the second exponential tunes the shape along the trajectory. In this form, the width of the hill along the trajectory is determined by the displacement in the space of collective variables, walked between two consecutive metadynamics steps, $\Delta s_i^{||} = f_b\left[\sum_\alpha (s_\alpha^{i+1}-s_\alpha^i)^2\right]^{1/2}$. The factor f_b, the hill height *h* and the width of hill in perpendicular to the trajectory direction $\Delta s_i^{\perp}$ are input parameters.

$\mathrm{V}(t,s)$ describes a slowly growing multidimensional Gaussian tube, with its axis along the trajectory. This biasing potential is a sum of repulsive Gaussian-shaped potential hills, each with height *h*. The history-dependent potential builds up until it counterbalances the underlying free energy well, allowing the system to escape via a saddle point to a nearby local minimum, where the procedure is repeated. When all minima are “filled” with Gaussian potential hills, the system moves barrier-free among the different states. The FES is obtained as[129]

$$V(t,s)_{t\to\infty} = -F(s) \tag{60}$$

to arbitrary accuracy, depending on hill size *h* and time interval Δ*t*.

3. Objectives

The five chapters (Chapters 4–8) of the thesis, where the main results are presented, can be grouped into two parts.

The first part deals with the chemistry of the diruthenium tetrahydride complex CpRu(μ-H)$_4$RuCp (**1**). It includes the next reactions: the intermolecular exchange of hydrides in the complex **1** with dihydrogen (Chapter 4); the C–H bond activation in ethylene on the complex **1** to give the bis(vinyl) complex CpRu(C_2H_4)(μ-η^1:η^2-$CHCH_2$)$_2$RuCp (**10**) (Chapter 5); the subsequent coupling reaction in the bis(vinyl) complex **10** among coordinated ethylene and two vinyl ligands to yield ruthenacyclopentadiene complex CpRu(η^2-C_2H_4)(CMe=CH–CH=CMe)RuCp (Chapter 6). The main aim is to establish a detailed mechanism of these reactions, taking into account Suzuki's suggestion, by locating possible intermediates and the transition states. A special attention will be paid to the characteristic features of the reactions, such as the cooperativity of multiple metal centers in activation of C–H bond in ethylene and C–C bond formation on binuclear ruthenium complex.

The second part includes the study of the fluxional behavior of two μ-silylene complexes (Chapter 7) and a silylium cation (Chapter 8). The site-exchange of hydride ligands and methyl groups of μ–$SiMe_2$ bridge was observed for the complex μ-silylene complexes {Cp*Ru(μ-H)}$_2$(μ-SiPhMe)(μ-$SiMe_2$), while only the latter process was monitored for the complex (Cp*Ru)$_2$(μ-$SiMe_2$)(μ-CMe)(μ-H). In this work the main aim is to establish which pathway is responsible for the site-exchange of hydride ligands and methyl groups of μ-$SiMe_2$ bridge in these complexes.

The work presented in Chapter 8 is a joint experimental and theoretical study of the dynamics of hydrogen bridges in cation $[C_6(SiMe_2)(SiHMe_2)_5]^+$ (**28**). The temperature-dependent NMR studies performed by Dr. G. Nikonov demonstrated that cation **28** exhibits an intriguing dynamics that deserves a special examination. There are two processes taking place, both resulting in a shift of the Si–H–Si bridge position. From our side the DFT calculations of the energetics of this cation have been performed to elucidate the detailed mechanism of the hydride transfer. The static DFT studies have been complemented by the ab initio molecular dynamics simulations.

4. DFT study of hydride exchange in binuclear ruthenium complex

ARTICLE 1

S. Tussupbayev, S.F. Vyboishchikov. "DFT Study of Hydride Exchange in a Binuclear Ruthenium Complex". *Organometallics.* 26, 1 (1 january 2007) : p. 56-64.

http://dx.doi.org/10.1021/om060700y

Institut de Química Computacional, Campus de Montilivi, Universitat de Girona, 17071 Girona, Catalonia, Spain

Received 2 august 2006; published Issue 1 january 2007.

ABSTRACT

This paper presents a DFT study of hydrogen exchange in the binuclear polyhydride complex $CpRu(\mu\text{-}H)_4RuCp$ (1) with molecular hydrogen. Both dissociative (through the $CpRu(\mu\text{-}H)_2RuCp$ intermediate) and associative mechanisms (through hydrogen coordination to yield intermediates $Cp_2Ru_2H_6$ and subsequent hydrogen dissociation) are considered. The calculations show that the dissociative pathway has a prohibitively high barrier for hydrogen dissociation, with $\Delta G^{\ddagger}_{298}$ about 34 kcal·mol^{-1}. The associative mechanism is much more favorable. There are, in turn, two possible pathways, going through either *cis*-$Cp(H)_2Ru(\mu\text{-}H)_2Ru(H)_2Cp$ (2a) or *trans*-$Cp(H)_2Ru(\mu\text{-}H)_2Ru(H)_2Cp$ (2b). The *cis* pathway is more favorable, with $\Delta G^{\ddagger}_{298}$ barriers for the rate-determining step of 24 kcal·mol^{-1}. The intermediate 2a can either dissociate directly or undergo isomerization processes involving interchanging of bridging and terminal hydrides. Overall, the calculations support the associative pathway for the hydrogen exchange, but show that the details of the mechanism are rather complicated.

5. Computational study of the C–H bond activation in ethylene on a binuclear ruthenium complex

ARTICLE 2

S. Tussupbayev, S.F. Vyboishchikov. "Computational Study of the C−H Bond Activation in Ethylene on a Binuclear Ruthenium Complex". *Organometallics.* 27, 15 (11 august 2008) : p. 3681-3692.

http://dx.doi.org/10.1021/om7012309

Institut de Química Computacional, Campus de Montilivi, Universitat de Girona, 17071 Girona, Catalonia, Spain.

Received 7 December 2007; Article ASAP 8 july 2008. Published in Issue 11 August 2008.

ABSTRACT

The reaction is substantially exothermic the calculated total reaction enthalpy ΔH_{298}° between $1 + 6C_2H_4$ and $26 + 3C_2H_6$ is about −90 kcal·mol^{-1}. The reaction occurs through a number of stages, each including ethylene coordination, at least two hydride migrations, and ethane elimination. The rate-determining step of the mechanism is the initial coordination of the first ethylene molecule to the reactant 1 to give the ethylene π complex $(H)_2CpRu(\mu\text{-}H)_2RuCp(\eta^2\text{-}C_2H_4)$ (2). The free energy barrier is about 27 kcal·mol^{-1} according to the static DFT calculations. Metadynamic simulations of the coordination process yield a ΔG_{298} barrier of about 20 kcal·mol^{-1}.

Another high-barrier step is the ethylene coordination to $CpRu(\eta^2{:}\eta^1\text{-}CH CH_2)_2RuCp$ (25) to give the final product 26. In total, the title reaction is a sophisticated multistep reaction with a large number of possible pathways. The mechanism of the reaction is largely determined by the flexibility of hydride ligands and by cooperation between both Ru centers.

6. Computational study of C–C coupling on diruthenium bis(*μ*-vinyl) ethylene π–complex

ARTICLE 3

S. Tussupbayev. S.F. Vyboishchikov. “Computational study of C–C coupling on diruthenium bis(μ-vinyl) ethylene π-complex”. En premsa.

Institut de Química Computacional, Campus de Montilivi, Universitat de Girona, 17071 Girona, Catalonia, Spain

ABSTRACT

We have performed a computational study of the C–C coupling reaction between coordinated ethylene and two vinyl ligands in the binuclear bis(vinyl)-ethylene complex CpRu(η2-C2H4)(μ-η1:η2-CHCH2)2RuCp (1) to yield the ruthenacyclopentadiene complex CpRu(η2-C2H4)(CMe=CH–CH=CMe)RuCp (28), described by Takao et al. This reaction is a sophisticated multistep process with a large number of possible pathways. Agostic interactions and the cooperativity of both Ru centers play a crucial role in the mechanism of the reaction. Our calculations provide support for Takao et al.’s proposal that the conversion of the reactant 1 to the final product 28 proceeds through the intermediate Cp(H)Ru(μ-H)(CMe=CH–CH=CMe)RuCp (20). However, the pathway originally proposed by Takao et al. leading to the intermediate 20 is unfavorable (Δ≠G°298 = 33 kcal·mol–1). We found a new, more favorable pathway with a Δ≠G°298 of 20 kcal·mol–1. The rate-determining step of the mechanism is ethylene coordination to the intermediate CpRu(μ-H)(CHMe=CH–CH=CMe)RuCp (22). The free energy barrier is about 29 kcal·mol–1 and 24 kcal·mol–1 at BP86 and MPWLYP1M level, correspond-ingly.

KEYWORDS

Density-functional calculation - Reaction mechanisms - C–C coupling reactions – Metallacycles - Hydrides.

7. DFT study of fluxional behavior of diruthenium *μ*-silylene complexes

ARTICLE 4

S. Tussupbayev. “DFT study of fluxional behavior of diruthenium μ-silylene complexes”. En premsa.

Institut de Química Computacional, Campus de Montilivi, Universitat de Girona, 17071 Girona, Catalonia, Spain.

ABSTRACT

The paper presents a computational study of the fluxional behavior of diruthenium bis(μ-silylene) complexes {CpRu(μ-H)}2(μ-SiPhMe) (μ-SiMe2) (1) and (CpRu)2(μ-SiMe2)(μ-CMe)(μ-H) (2). Two new pathways have been discovered for the site-exchange of hydrides in 1. The exchange of methyls in 1 proceeds as a result of the 1,2-shift of the μ–SiMe2 (Path 2) in accordance with the Suzuki et al.’s original proposal. The Path 1 involving the isomerization to the terminal silylene was rejected for both complexes, 1 and 2.

The exchange of methyls in 2 occurs by the hydride transfer through the μ–SiMe2 ligand (Path 2) with the free energy barrier of 17.2 kcal/mol. It is in a reasonable agreement with the experimentally determined value (ΔG≠333 = 15 kcal/mol). The migration of the hydride through the μ–CMe2 requires a significantly higher ΔG≠333 barrier of 26 kcal/mol.

KEYWORDS

DFT calculation - Reaction mechanism - Fluxional behavior - Bridged silylene complex - Hydride ligands - Binuclear – Ruthenium.

8. Dynamics of Si–H–Si bridges in agostically stabilized silylium ions

ARTICLE 5

S. Tussupbayev. G.I. Nikonov. S.F. Vyboishchikov. “Dynamics of Si–H–Si bridges in agostically stabilized silylium ions”. En premsa.

Institut de Química Computacional, Campus de Montilivi, Universitat de Girona, 17071 Girona, Catalonia, Spain.
Chemistry Department, Brock University, 500 Glenridge Ave., St. Catharines, ON, L2S 3A1, Canada.

ABSTRACT

The silylium ion [C6(SiMe2)(SiHMe2)5]+ offers an amazing example of multiple Si···H interactions. It exhibits a symmetric Siα–H–Siα motif supported by two additional Siβ–H···Siα agostic interactions. This cation is highly fluctional in NMR spectra at room temperature due to shift of the hydride bridge. The DFT calculations show that the hydride shift is related to internal rotation of silyl groups. We performed NMR, static DFT, and dynamics studies of this process and found two possible mechanisms of this process, associated with internal rota-tion of either β- or γ-silyls. The energy barrier is largely caused by the silyl internal rotation, whereas the hydride transfer itself is intrinsically quite easy. The γ-silyl rotation is somewhat more favorable than the β-silyl rotation. Vibrational dynamics of the cation is also discussed.

9. Results and discussion

This section briefly summarizes all the results reported in the Chapters 4–8.

9.1. DFT study of hydride exchange in binuclear ruthenium complex

The associative pathway. The hydrogen exchange in **1** occurs via formation of hexahydride complexes **2a** and **2b** with $\Delta G^{\neq}_{298}$ barriers of 25 and 28 kcal/mol, respectively. The hydrogen association is strongly affected by the entropy effects. Further elimination of dihydrogen from **2a** and **2b** is an exothermic process with $\Delta G^{\neq}_{298}$ barriers of 8 and 12 kcal/mol, correspondingly. This mechanism is mainly in accord with that suggested by Suzuki.[41b]

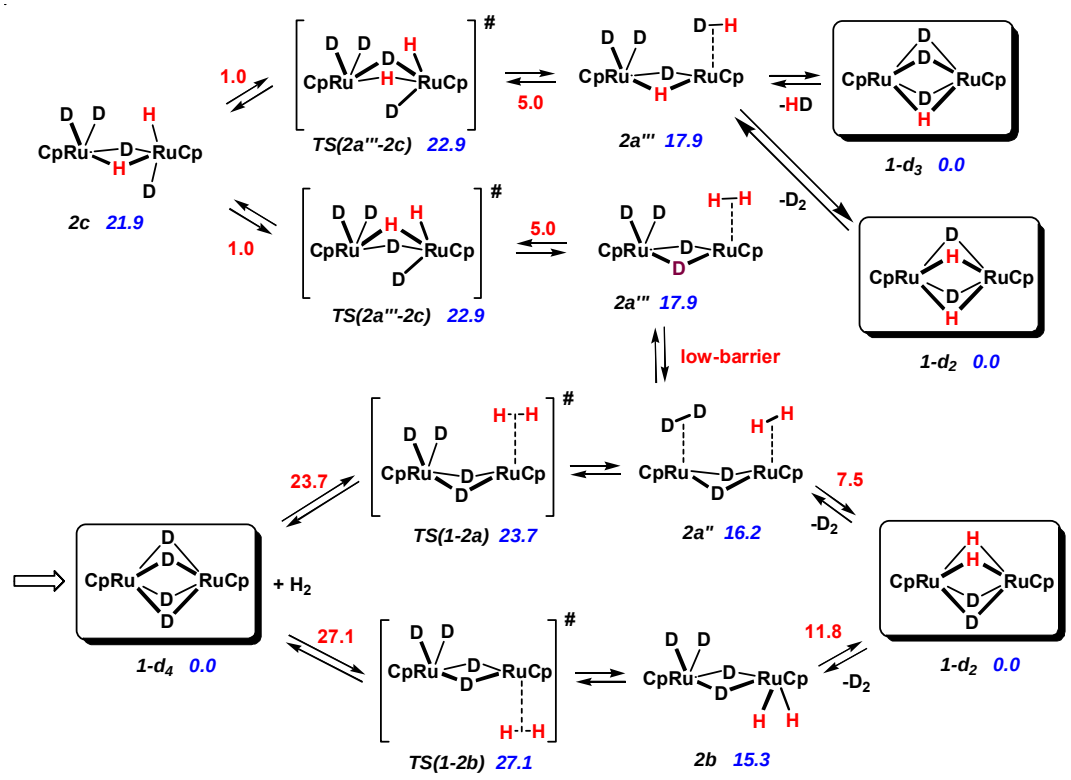

Scheme 5. The calculated steps of the hydrogen exchange reaction. Relative Gibbs free energies are in kcal·mol^{-1}. The numbers above arrows are $\Delta G^{\neq}_{298}$ values in kcal·mol^{-1}.The ΔG°_{298} values were calculated using the ^{1}H isotope of hydrogen. The relative Gibbs free energies were calculated at BP86/BS1 level, where BS1 corresponds to the effective core potential + double-ζ valence basis set for Ru, 6-311G(d,p) for C, H and 6-31G(d,p) for Cp.

Both **2a** and **2b** are classical hydride complexes. We found that along with them there exist the corresponding dihydrogen complexes **2a′–2a‴** and **2b′–2b‴**. The H_2 ligand in **2a‴** and

2b‴ is collinear to the Ru–Ru vector. Our calculations predict fast dihydrogen–bis(hydride) exchange for the hexahydride complexes.

Alternatively, in the *cis* route the hydrogen exchange can proceed through an additional isomerization of **2a‴** to **2c** with $\Delta G^{\neq}_{298}$ = 5 kcal/mol. All these steps are summarized in the Scheme 5.

The dissociative pathway. The Gibbs free energy ΔG°_{298} for the dissociation of **1** to give CpRu(μ-H)$_2$RuCp is 27.3 kcal·mol^{-1}, while ΔE_e is even about 37 kcal·mol^{-1}. The dissociation occurs asymmetrically, with two of the bridging hydrides of **1** moving toward one of the ruthenium atoms and finally eliminating dihydrogen. The $\Delta G^{\neq}_{298}$ barrier is 33.2 kcal·mol^{-1}. The ΔG°_{298} and $\Delta G^{\neq}_{298}$ for the hydrogen dissociation are by far less favorable than the corresponding values for the associative mechanism. Therefore, the dissociative mechanism should be discarded, in agreement with Suzuki's suggestion.[41b]

9.2. Computational study of the C–H bond activation in ethylene on binuclear ruthenium complex

The whole mechanism was divided into four parts (Schemes 6–9). The Part 1 connects the reactant **1** and the intermediate **7**, Parts 2A and 2B describe two alternative pathways of the consequent conversion of **7** into **13a**, corresponding to the experimentally observed intermediate **B**, and in the Part 4 the conversion of the latter into the final product **26a** is considered.

Part 1. The first step of the associative mechanism is the coordination of ethylene to complex **1** to yield ethylene π-complexes **2a–c** through the corresponding transition states **TS(1-2a), TS(1-2b)**, and **TS(1-2c)**. The coordination requires substantial $\Delta G^{\neq}_{298}$ barriers of +26.6, +29.6, and +26.9 kcal·mol^{-1}, correspondingly. Nevertheless, they are lower than the free energy barrier for the H_2 dissociation from **1** to give CpRu(μ–H)$_2$RuCp ($\Delta G^{\neq}_{298}$ = +34.2 kcal·mol^{-1}; see Scheme 6).

There is a direct pathway from the ethylene π-complexes **2a** and **2b** to **7**, as a result of reductive coupling of terminal hydrides and the subsequent dihydrogen elimination ($\Delta G^{\neq}_{298}$ = 10.4 and 11.5 kcal·mol^{-1}, correspondingly). However, the experimental data indicate that the direct H_2 elimination does not occur.[41b]

The insertion of ethylene into the Ru–H bond in **2a**–**c** to produce ethyl complexes **4a** and **4b** occurs through the β-agostic complexes **3a**–**c**. The free energy barriers of these transformations are +13.8, +14.4, and +11.8 kcal·mol^{-1}, respectively.

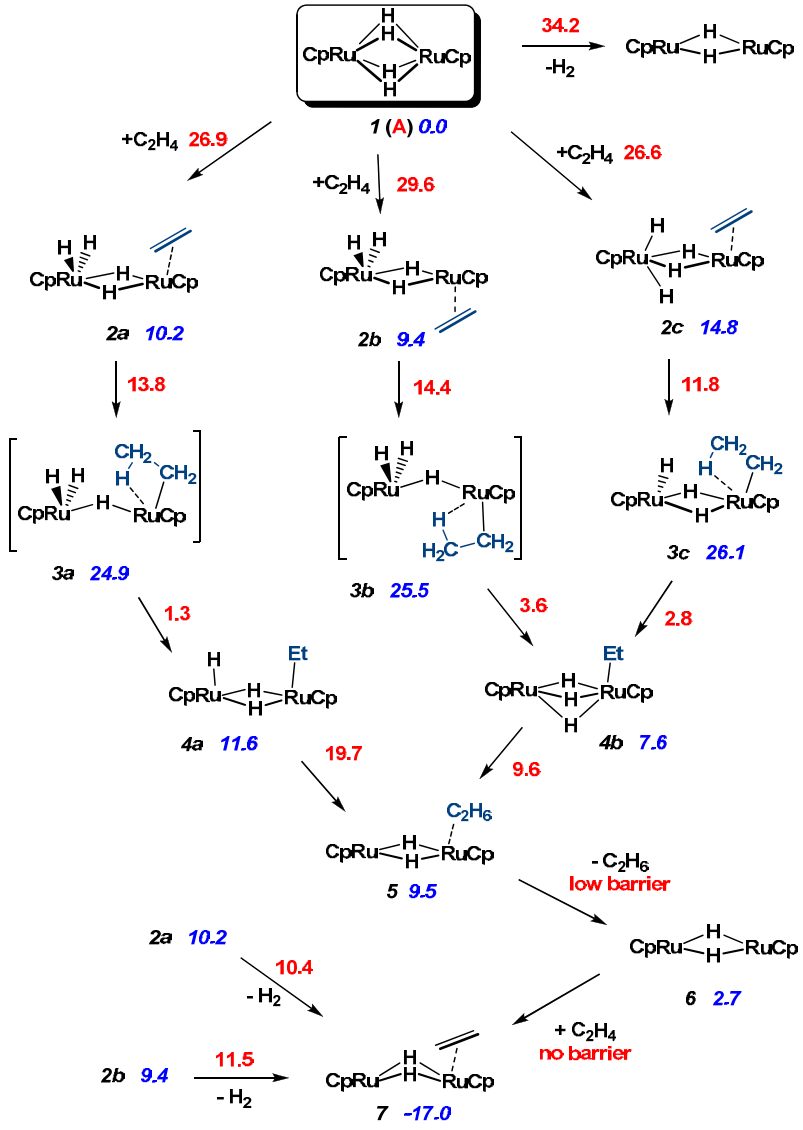

Scheme 6. The calculated steps of the first part of the C–H bond activation reaction mechanism. Relative Gibbs free energies are in kcal·mol^{-1}. The numbers above arrows are $\Delta G^{\neq}_{298}$ values in kcal·mol^{-1}. Here and further the relative Gibbs free energies were calculated at BP86/BS1 level, where BS1 corresponds to the effective core potential + double-ζ valence basis set for Ru, 6-311G(d,p) for C, H and 6-31G(d,p) for Cp.

The migration of a bridging hydride to ethyl ligand in **4a** and **4b** yields an ethane σ-complex **5** (Scheme 6). The migration of hydride through **TS(4b-5)** is more preferable ($\Delta G^{\neq}_{298}$ = +9.6 kcal·mol^{-1}).

The elimination of ethane yields the unsaturated dihydride complex CpRu(μ-H)$_2$RuCp (**6**) (Scheme 6). Therefore, the following coordination of the second ethylene molecule to **6** to give **7** proceeds without a barrier. The ethylene π-complex **7** has an isomer **7′** with asymmetrically bridged ethylene. The free energy barrier of the conversion of **7** to **7′** is 3.4 kcal·mol^{-1}. The geometry of **7′** suggests that this is an intermediate on the way of the transformation from

the ethylene complex to the vinyl-hydrido one. Thus, the conversion of **7** to **7′** should facilitate the C–H bond activation in ethylene.

Part 2. For the further stages of the reaction mechanism, two pathways are possible, as shown in Schemes 7 and 8. The first one starts from the intramolecular C–H bond activation in ethylene in **7′** to give the monovinyl complex **8** with the energy barrier of +10.4 kcal·mol^{-1} (Scheme 7).

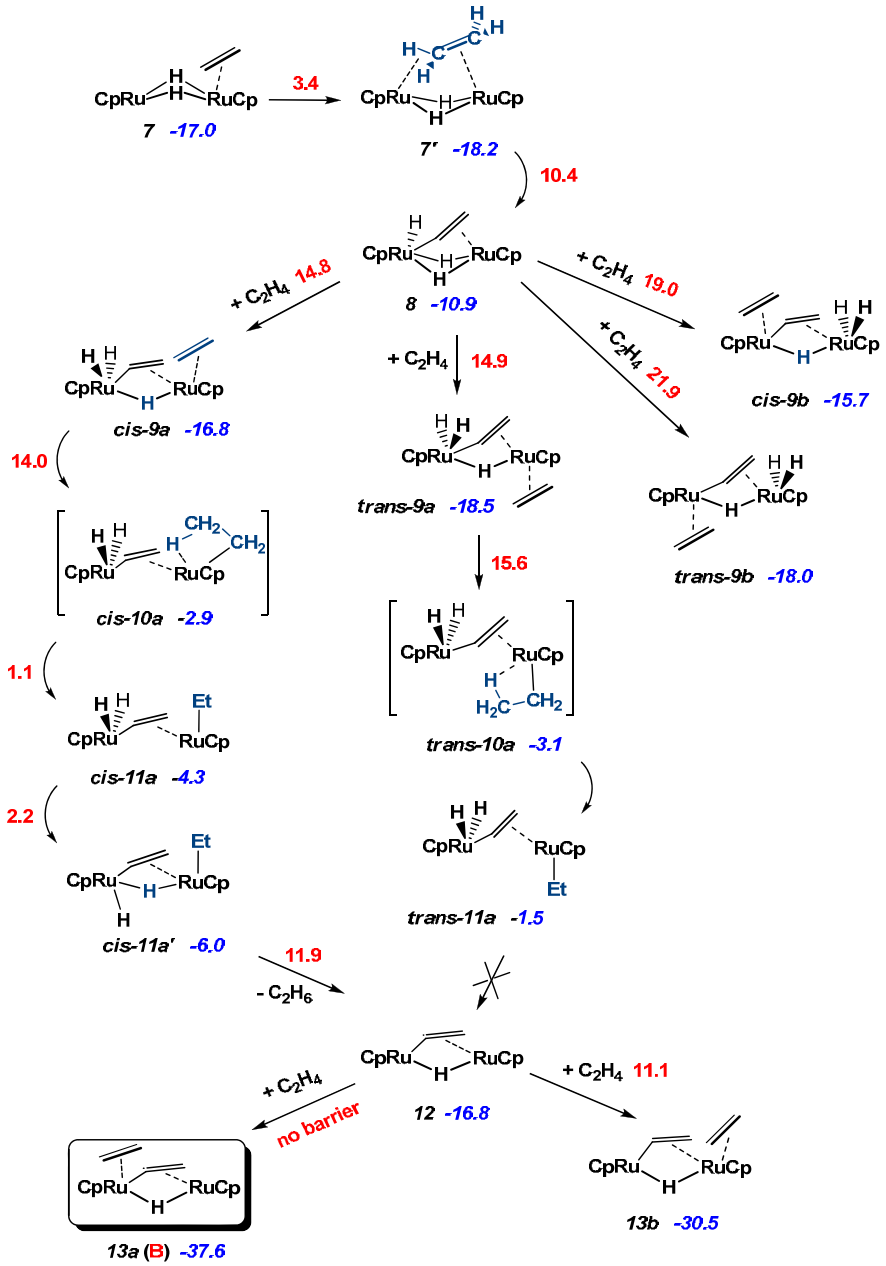

Scheme 7. The calculated steps of the second part of the C–H bond activation reaction mechanism. Relative Gibbs free energies are in kcal·mol^{-1}. The numbers above arrows are $\Delta G^{\neq}_{298}$ values in kcal·mol^{-1}.

The coordination of the third ethylene molecule to **8** can proceed in a number of ways. Four resulting structures are possible: ***cis*-9a**, ***trans*-9a**, ***cis*-9b**, and ***trans*-9b** (Scheme 7). The formation of ***cis*-9a** and ***trans*-9a** is somewhat more preferable than of ***cis*-9b** and ***trans*-9b**. Therefore, from here on, only ***cis*-9a** and ***trans*-9a** are considered.

The ethylene coordination to **8** to yield ***cis*-9a** and ***trans*-9a** proceeds with moderate energy barriers ($\Delta G^{\neq}_{298}$ = +14.8 and +14.9 kcal·mol^{-1}, correspondingly). Ethylene attack is accompanied by the rearrangement of hydrides in **TS(8–*cis*-9a)** and **TS(8–*trans*-9a)**.

The π-complexes ***cis*-9a** and ***trans*-9a** undergo ethylene insertion into Ru–H bond to yield the ethyl complexes ***cis*-11a** and ***trans*-11a** through the agostic complexes ***cis*-10a** and ***trans*-10a**, correspondingly (Scheme 7).

The two terminal hydrides in ***cis*-11a** readily collapse to give the structure ***cis*-11a′** ($\Delta G^{\neq}_{298}$ = +2.2 kcal·mol^{-1}). For ***trans*-11a** such a rearrangement of terminal hydrides is complicated sterically by the adjacent Cp ring. The bridging hydride in ***cis*-11a′** further migrates to the ethyl ligand to directly produce the vinyl-hydride complex **12** (Scheme 7). The migration proceeds through the transition state **TS(*cis*-11a′–12)** with the free energy barrier of +11.9 kcal·mol^{-1}. Our calculations show that the ethane σ-complex is not formed and ethane leaves immediately.

The coordination of the fourth ethylene molecule to **12** to yield **13a** (Scheme 7) proceeds without a barrier. This is in line with a high exothermicity of the coordination process (ΔH°_{298} = –33.4 kcal·mol^{-1}, ΔG°_{298} = –20.8 kcal·mol^{-1}). We have also examined the possibility of ethylene coordination to the other ruthenium atom in **12** to yield **13b**. This way of coordination is less exothermic (ΔG°_{298} = –13.7 kcal·mol^{-1}) and proceeds with a significant barrier ($\Delta G^{\neq}_{298}$ = +11.1 kcal·mol^{-1}).

Part 3. Alternatively to the C–H bond activation in **7**, the coordination of the third ethylene molecule can occur. The incoming ethylene can attack either in the *cis* or *trans* position with respect to the coordinated ethylene ligand in **7** to yield the bis(ethylene) complexes ***cis*-14** or ***trans*-14** (Scheme 8). The energy barriers of the coordination are significant ($\Delta H^{\neq}_{298}$ = +8.3 and +6.9 kcal·mol^{-1}; $\Delta G^{\neq}_{298}$ = +18.3 and +16.4 kcal·mol^{-1}, respectively).

The insertion of ethylene into the Ru–H bond in bis(ethylene) complexes ***cis*-14** and ***trans*-14** to yield ethyl complexes ***cis*-16** and ***trans*-16** occurs through the agostic complexes ***cis*-15** and ***trans*-15** (Scheme 8). The formation of ***cis*-15** and ***trans*-15** proceeds with significant energy barriers ($\Delta G^{\neq}_{298}$ = +15.5 and +17.1 kcal·mol^{-1}) through transition states **TS(*cis*-14-*cis*-15)**

and **TS(*trans*-14-*trans*-15)**, correspondingly. The conversion of ***cis*-15** and ***trans*-15** into respective ***cis*-16** and ***trans*-16** proceeds without a $\Delta G^{\neq}_{298}$ barrier.

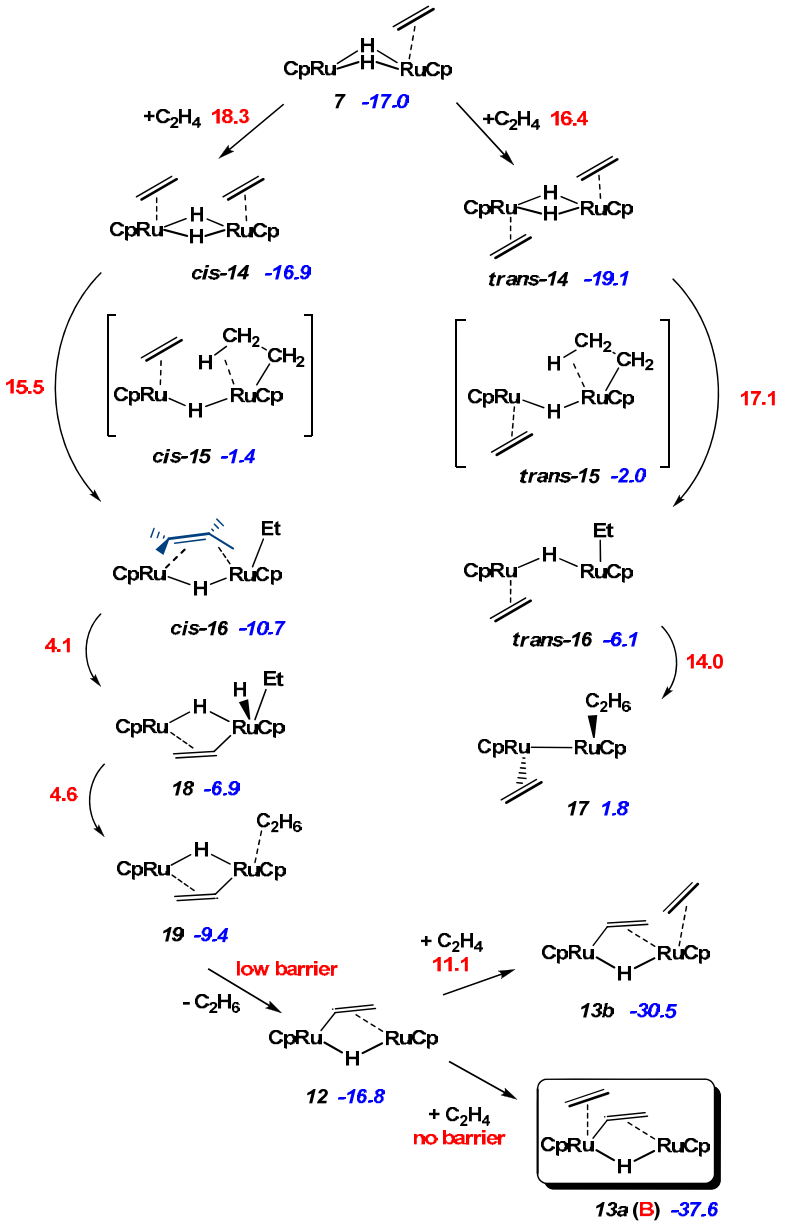

Scheme 8. The calculated steps of the third part of the C–H bond activation reaction mechanism. Relative Gibbs free energies are in kcal·mol^{-1}. The numbers above arrows are $\Delta G^{\neq}_{298}$ values in kcal·mol^{-1}.

The next step is the cleavage of the C–H bond in ethylene in ***cis*-16** to give vinyl-hydride complex **18**. The activation proceeds through the transition state **TS(*cis*-16–18)**. The free energy barrier of this process is $\Delta G^{\neq}_{298}$ = +4.1 kcal·mol^{-1}. Further the resulting terminal hydride migrates to the ethyl ligand in **18** to yield ethane σ-complex **19** via transition state **TS(*cis*-18–19)** ($\Delta G^{\neq}_{298}$ = +4.6 kcal·mol^{-1}).

Part 4. The final part of the mechanism (Scheme 9) starts from the coordination of the fifth ethylene molecule to **13a** or **13b** to produce a bis(ethylene) complex **20**. The coordination proceeds with a lower barrier ($\Delta G^{\neq}_{298}$ = 11.8 kcal·mol^{-1}) for the less stable **13b** compared to **13a** ($\Delta G^{\neq}_{298}$ = 14.2 kcal·mol^{-1}).

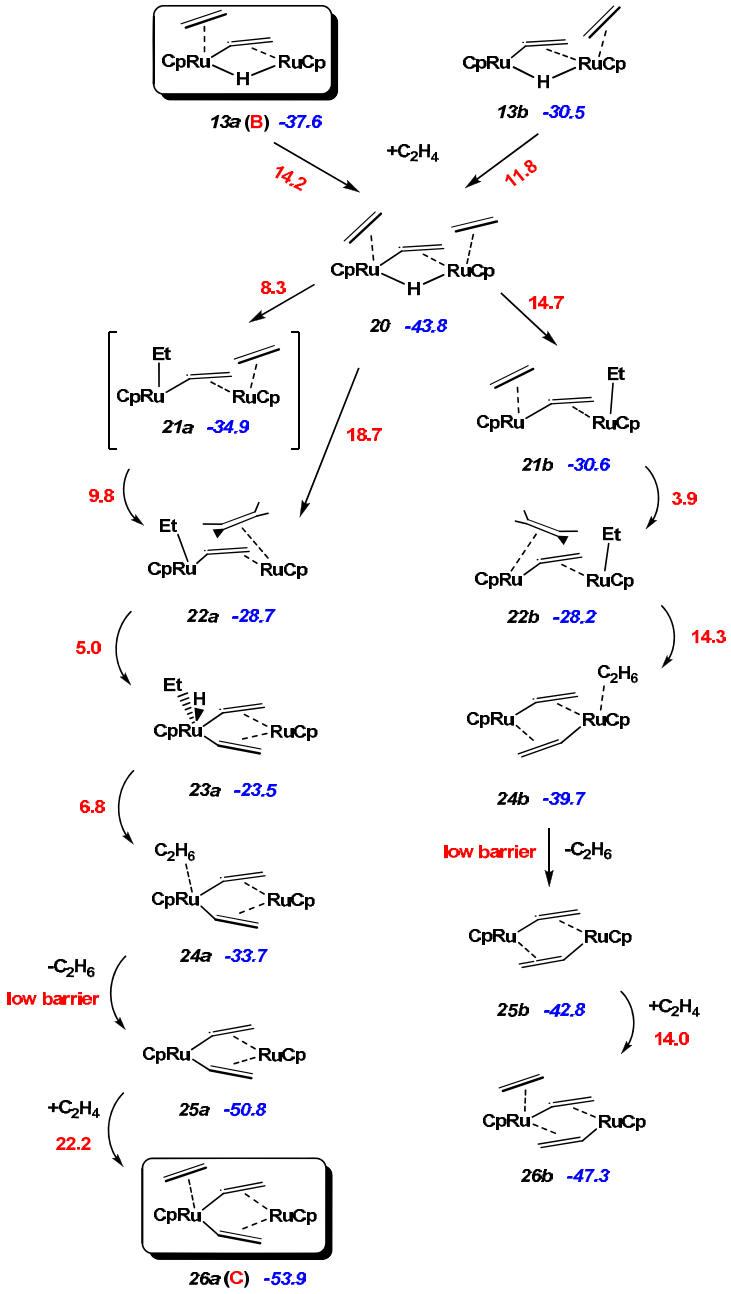

Scheme 9. The calculated steps of the fourth part of the C–H bond activation reaction mechanism. Relative Gibbs free energies are in kcal·mol^{-1}. The numbers above arrows are $\Delta G^{\neq}_{298}$ values in kcal·mol^{-1}.

Two subroutes, denoted "**a**" and "**b**", are possible from here on (Scheme 9). The subroute "**a**" eventually leads to the product **26a**, while "**b**" yields the alternative complex **26b**. The

insertion of ethylene in both pathways to yield ethyl complexes **22a** and **22b** occurs through agostic complexes **21a** and **21b**, correspondingly. Since **21a** is a very shallow minimum, in the ethylene insertion should be considered as one-step process leading directly from **20** to **22a** with considerable energy barrier ($\Delta G^{\neq}_{298}$ = 18.7 kcal·mol^{-1}). The formation of **22b** proceeds with lower barriers $\Delta G^{\neq}_{298}$ = 14.7 and 3.9 kcal·mol^{-1} through transition states **TS(20-21b)** and **TS(21b-22b)**, correspondingly.

The C–H bond cleavage in **22a** to give vinyl-hydride complex **23a** is a low barrier step ($\Delta G^{\neq}_{298}$ = 5.0 kcal·mol^{-1}). Further, the ethane σ-complex **24a** is formed through the transition state **TS(23a–24a)** with a $\Delta G^{\neq}_{298}$ barrier of 6.8 kcal·mol^{-1}. In **22b** both processes occur in a concerted manner through the transition state **TS(22b–24b)** with the $\Delta G^{\neq}_{298}$ barrier 14.3 kcal·mol^{-1}.

The reductive elimination of ethane from **24a** and **24b** yields bis(vinyl) complexes **25a** and **25b**, correspondingly. The coordination of ethylene to **25a** proceeds with a rather high energy barrier ($\Delta H^{\neq}_{298}$ = 13.3 kcal·mol^{-1}, $\Delta G^{\neq}_{298}$ = 22.2 kcal·mol^{-1}). It can be attributed to loss of the α-agostic interaction in **25a** in the course of the coordination. The formation of **26b** proceeds easier ($\Delta H^{\neq}_{298}$ = 2.6 kcal·mol^{-1}, $\Delta G^{\neq}_{298}$ = 14.0 kcal·mol^{-1}, respectively). Thus, the pathway leading to the final product **26a** is in general harder to overcome than that leading to **26b**. However, the former is more exothermic.

Metadynamics results. As seen, the highest energy barrier step of the mechanism is the coordination of the first ethylene molecule to the reactant **1** to yield ethylene π-complexes **2a**–**c** ($\Delta G^{\neq}_{298}$ is about 27–29 kcal·mol^{-1}). The metadynamics simulation yields an estimate of the Gibbs free energy difference ΔG°_{300} between **1** + C_2H_4 and **2a**–**2c** of about –8 kcal·mol^{-1}. This compares reasonably with the static DFT value of –9.4 kcal·mol^{-1}. The activation free energy obtained from the metadynamics is about 20 kcal·mol^{-1}.

9.3. Computational study of C–C coupling in diruthenium bis(*μ*-vinyl) ethylene π–complex

The proposed mechanism is divided into three parts. The Part 1 (Scheme 10) describes the initial two steps leading to the intermediate **3**. The Part 2A and Part 2B (Schemes 11 and 12) represent possible pathways of the formation of the intermediate ruthenacycle **18**. The final conversion of the latter to the product complex **26** is described in the Part 3 (Scheme 13).

Part 1. According to the mechanism proposed by Suzuki and coworkers the first step is the activation of a $C^{\alpha}(sp^2)$–H bond of the vinyl group in **1** to form the μ-vinylidene species **2** (Scheme 10). The following insertion of the remaining vinyl group into a newly formed Ru–H bond produces the μ-ethylidene-μ-vinylidene intermediate **3**. From here on several pathways are possible (see Schemes 11 and 12).

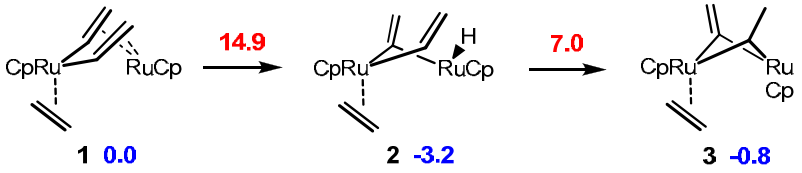

Scheme 10. Part 1 of the mechanism of the C–C coupling reaction. Relative Gibbs free energies are in kcal·mol^{-1}. The numbers above arrows are $\Delta G^{\neq}_{298}$ values in kcal·mol^{-1}. Here and further the relative Gibbs free energies were calculated at BP86/BS1 level, where BS1 corresponds to the effective core potential + double-ζ valence basis set for Ru, 6-311G(d,p) for C, H and 6-31G(d,p) for Cp.

Part 2A. The routes starting with the C–H bond activation in ethylene in **3**, as proposed by Suzuki *et al*.,[41b] are described in this part (Scheme 11). Subject to which of the carbon atoms is involved in the C–H bond cleavage two isomeric vinyl-hydrido intermediates **4** and **4'** are possible.

Route 2A.1. The transition state **TS(3–4)** is only 0.6 kcal/mol higher in energy than **4** on the ΔG°_{298} scale. Thus, **4** is a very shallow minimum and the reverse step (**4**→**3**) virtually proceeds without a barrier. The subsequent step is the C–C coupling between the C^{α} atoms of the vinyl and vinylidene group in **4** to yield **5**. The coupling proceeds with a moderate energy barrier of 14.5 kcal/mol. However, taking into account that the energy barrier of the conversion **4**→**3** is very low, the energy difference of 32.6 kcal/mol between **TS(4-5)** and **3** should be taken as the activation barrier $\Delta G^{\neq}_{298}$ of the reaction from **3** to **5**. It is a rather high energy barrier and therefore this route was rejected.

We have examined the possibility of ethane formation in **4** by the way of hydrogenation of μ-ethylidene. The hydride migration to the C^{α} atom of the ethylidene group in **4** yields ethyl species **6**. The insertion of the μ-ethylidene into the Ru–H bond is facile ($\Delta G^{\neq}_{298}$ = 4.3 kcal/mol). Further C–H bond activation at C^{α} atom of the vinyl ligand in **6** can yield a hydride ligand. However, the extensive potential energy scans revealed, that the C–H bond cleavage is sterically hindered by the neighboring Cp ring in **6**.

Route 2A.2. The isomeric to **4** vinyl-hydrido species **4'** is higher in energy than the corresponding transition state **TS(3–4')** by 0.2 kcal/mol on the ΔG°_{298} scale. However, it can be eas-

ily ($\Delta G^{\neq}_{298}$ = 1.2 kcal/mol) converted to the more stable by 3.0 kcal/mol positional isomer **4''** via the internal rearrangement. The subsequent C–C coupling in **4''** can proceed in two ways (Scheme 11). The first possibility is the coupling between C^{α} atoms of μ-vinyl and μ-ethylidene ligands to yield **7**. The conversion is thermodynamically favorable (ΔG°_{298} = -11.5 kcal/mol), however there is a high energy barrier to overcome ($\Delta G^{\neq}_{298}$ = 36.7 kcal/mol). Otherwise, the coupling can take place between C^{β} atom of μ-vinyl and C^{α} atom of μ-vinylidene to produce **8**. In contrast, this step is endothermic (ΔG°_{298} = 8.4 kcal/mol), but it also proceeds with a high energy barrier ($\Delta G^{\neq}_{298}$ = 32.6 kcal/mol).

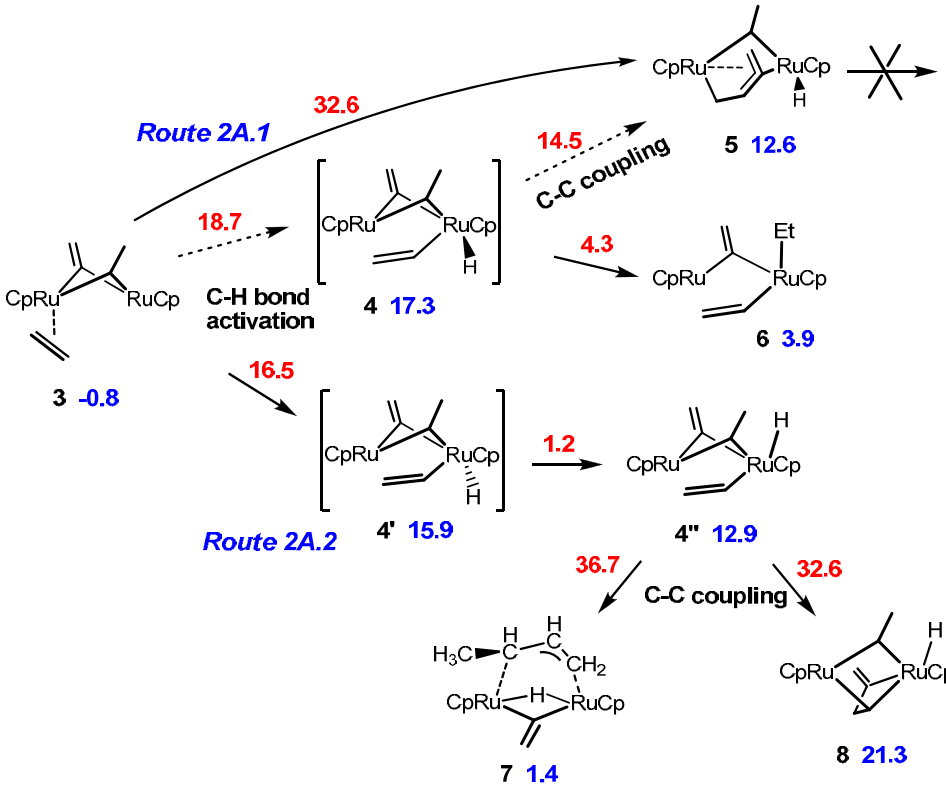

Scheme 11. Part 2A of the mechanism of the C–C coupling reaction. Relative Gibbs free energies are in kcal·mol^{-1}. The numbers above arrows are $\Delta G^{\neq}_{298}$ values in kcal·mol^{-1}.

Thus, the pathways, proposed by Suzuki *et al.*,[41b] proceed with prohibitively high energy barriers. The new pathways discovered in this work are described in the next part.

Part 2B. In principle, the direct C–C coupling can occur in **3**. Two alternative pathways are possible here.

Route 2B.1. The coupling between μ-vinylidene and the coordinated ethylene yields methylene ruthenacyclobutane species **9** (Scheme 12). The latter is only 4.6 kcal/mol less stable

than **3** on the ΔG°_{298} scale. The coupling proceeds with a substantial energy barrier $\Delta G^{\neq}_{298}$ of 24.2 kcal/mol. The next step is the C–H bond cleavage at C^{α} of the μ-ethylidene ligand in **9** with the perspective of the following C–C coupling between the ruthenacyclobutane and μ-CCH_3 ligand. The C–H bond cleavage proceeds with the energy barrier $\Delta G^{\neq}_{298}$ of 7.6 kcal/mol. than with the less saturated μ-vinylidene group.

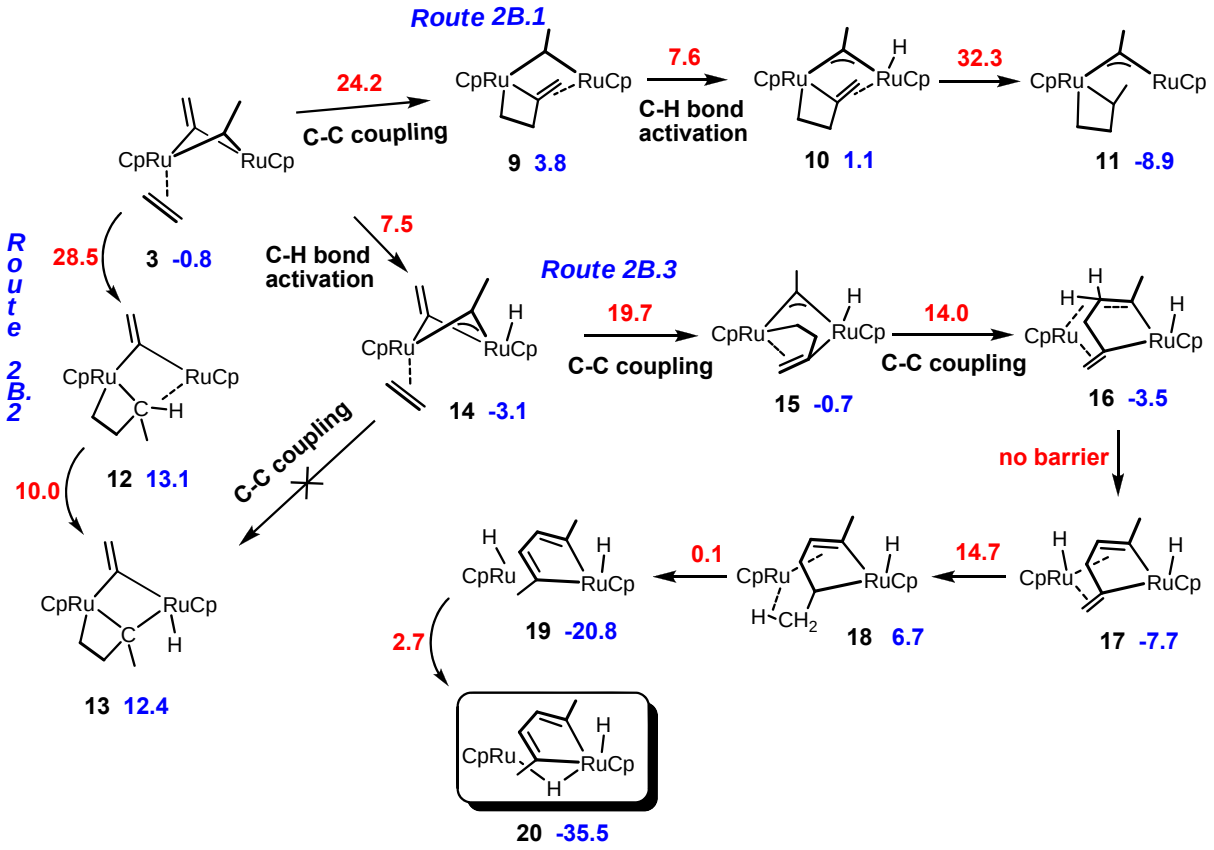

Scheme 12. Part 2B of the mechanism of the C–C coupling reaction. The new pathways discovered in this work are presented. Relative Gibbs free energies are in kcal·mol^{-1}. The numbers above arrows are $\Delta G^{\neq}_{298}$ values in kcal·mol^{-1}.

Route 2B.2. Alternatively the coupling between the μ-ethylidene and the coordinated ethylene yields methyl ruthenacyclobutane species **12**. The resulting complex **12** is 13.9 kcal/mol less stable than **3** on the ΔG°_{298} scale. This step proceeds with substantial $\Delta G^{\neq}_{298}$ barrier of 28.5 kcal/mol. Therefore it is relatively easily ($\Delta G^{\neq}_{298}$ = 10.0 kcal/mol) cleaved to produce **13**.

Additional routes arise if one considers the possibility of the C^{α}–H bond activation in the μ-ethylidene in **3** taking place before the corresponding C–C coupling step (Scheme 12). The C–H bond activation at C^{α} atom of the μ-ethylidene ligand in **3** produces **14** with the energy barrier $\Delta G^{\neq}_{298}$ of 7.5 kcal/mol. It is very close to the value of the energy barrier of the C–H bond cleavage in **9**.

Route 2B.3. The C–C coupling in **14** yields a different from **10** product, μ-but-1-ene-2,4-diyl species **15**. Thus, the change in the order of two steps: C–H bond cleavage and C–C coupling leads to the different products, **10** and **15** (Scheme 12). The reason for this is that the terminal hydride in **14** hinders the η^2-coordination of the methylene part of the C^4 species. As a consequence the energy barrier of the C–C coupling in **14** ($\Delta G^{\neq}_{298}$ = 19.6 kcal/mol) is lower by 4.6 kcal/mol than that in **3**. The following step is the C–C coupling step between μ-but-1-ene-2,4-diyl and μ-CCH_3 ligand to produce **16**. It is converted into **17** without a barrier as a result of C–H bond cleavage. The next step is the insertion of the methylene group into the newly formed Ru–H bond to give agostic ethyl complex **18**. The energy barrier of this process is 14.7 kcal/mol. The agostic ethyl complex **18** is a shallow minimum lying close to the corresponding transition state on the PES. It is only 0.3 kcal/mol below the transition state **TS(17–18)** on the ΔG°_{298} scale. It is readily converted to the much more stable (ΔG°_{298} = -27.5 kcal/mol) non-agostic ethyl complex **19**. There is virtually no barrier for this process ($\Delta G^{\neq}_{298}$ = 0.1 kcal/mol). The internal rearrangement, enclosing the rotation of the latter in the direction perpendicular to the Ru–Ru vector, yields **20**.

Route 2B.4. The coupling between the coordinated ethylene and μ-CCH_3 in **14** was examined. However, the extensive PES scans revealed that there is no minimum energy path for this transformation. The expected coupling product, **10**, is, probably, formed indirectly in the course of the *route 1* described above.

Part 3. The conversion of the experimentally obtained intermediate **20** into the final product **28** is described in this part.

Route 3.1. The direct ethylene coordination to the (bis)hydrido-ruthenacycle **20** to yield ethylene π-complex **21** is a largely endothermic step (ΔG°_{298} = +43.1 kcal/mol) with a very high energy barrier ($\Delta G^{\neq}_{298}$ = 63.1 kcal/mol). The coordination of the upcoming ethylene is hindered by the terminal hydride.

Route 3.2. In the alternative pathway the terminal hydride migration to the C^{α} atom of the ruthenacycle in **20** takes place before the ethylene coordination step. The insertion of ruthenacycle into Ru–H bond yields **22** through the transition state **TS(20-22)** at a low energy barrier ($\Delta G^{\neq}_{298}$ = 2.9 kcal/mol). The subsequent coordination of ethylene to **22** proceeds with the free energy barrier of 28.6 kcal/mol, which is lower than the energy barrier of the direct coordination by 34.5 kcal/mol.

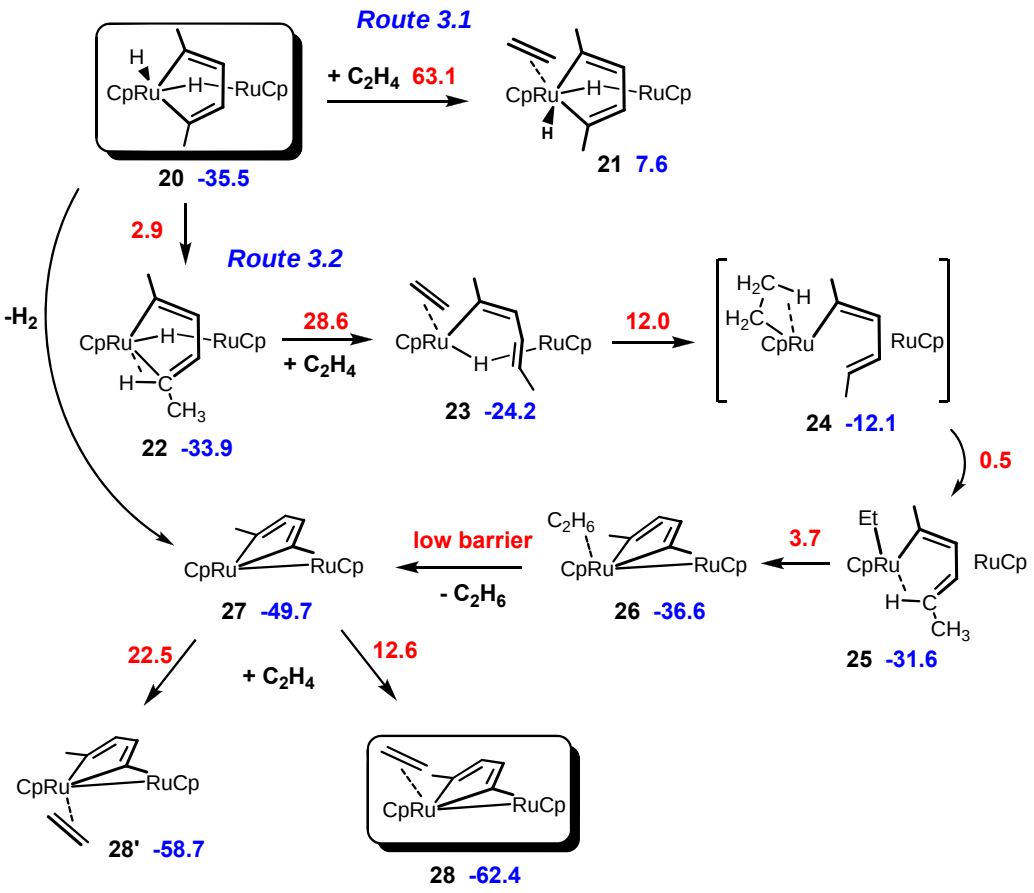

Scheme 13. The final part of the mechanism of the C–C coupling reaction. Relative Gibbs free energies are in kcal·mol^{-1}. The numbers above arrows are $\Delta G^{\neq}_{298}$ values in kcal·mol^{-1}.

At the following steps the coordinated ethylene is hydrogenated and eliminated as ethane. The insertion of the coordinated ethylene into the Ru–H bond yields agostic ethyl species **23**. The insertion proceeds through the transition state **TS(23–24)** with the energy barrier $\Delta G^{\neq}_{298}$ of 12.0 kcal/mol. The agostic ethyl complex **24** is readily converted to the much more stable (ΔG°_{298} = -19.6 kcal/mol) non-agostic ethyl complex **25**. There is virtually no barrier for this process ($\Delta G^{\neq}_{298}$ = 0.5 kcal/mol). The subsequent migration of hydrogen to the ethyl ligand produces an ethane σ-complex **26**. The elimination of ethane from **26** yields the ruthenacycle **27**. It is a favorable step mostly due to the entropy effects (ΔH°_{298}= -2.4 kcal/mol, ΔG°_{298}= -13.1 kcal/mol).

The final step, the coordination of the second ethylene molecule to **27** can proceed in two ways (Scheme 13). The incoming ethylene can attack either in the *cis* or *trans* position with respect to the ruthenacycle to produce the final product **28** or its isomer **28'**. The formation of **28** proceeds via the transition state **TS(27-28)** with much less effort ($\Delta H^{\neq}_{298}$= 2.7 kcal/mol, $\Delta G^{\neq}_{298}$= 12.6 kcal/mol), than of **28'** via the transition state **TS(27-28')** ($\Delta H^{\neq}_{298}$= 12.2

kcal/mol, $\Delta G^{\neq}_{298}$= 22.5 kcal/mol). In both cases the entropy effects are of importance for the energy barrier.

9.4. DFT study of fluxional behavior of diruthenium *μ*-silylene complexes

Exchange of hydride ligands in 1. The first step is the formation of the non-classical intermediate with η^2-coordinated Si–H bond. This intermediate is formed whether through the bridge μ-$SiMe_2$ or μ-SiPhMe to afford, correspondingly, **h1** or **h3**.

Path 1. **h1** and **h3** are formed through the transition states **TS(1–h1)** and **TS(1–h3)** with $\Delta G^{\neq}_{300}$ barriers of 7.4 and 7.9 kcal/mol, respectively. These data indicate that the nature of the substituent on the silylene bridge (μ-$SiMe_2$ and μ-SiPhMe) has a little effect on the $\Delta G^{\neq}_{300}$ value.

Further the hydride migrates through the transition states **TS(h1–h2)** and **TS(h3–h2)**. The calculations show that the rotation of the silyl group does not occur. The intermediates **h1** and **h3** are readily converted into **h2** with $\Delta G^{\neq}_{298}$ barrier of 1.2 and 1.1 kcal/mol, correspondingly.

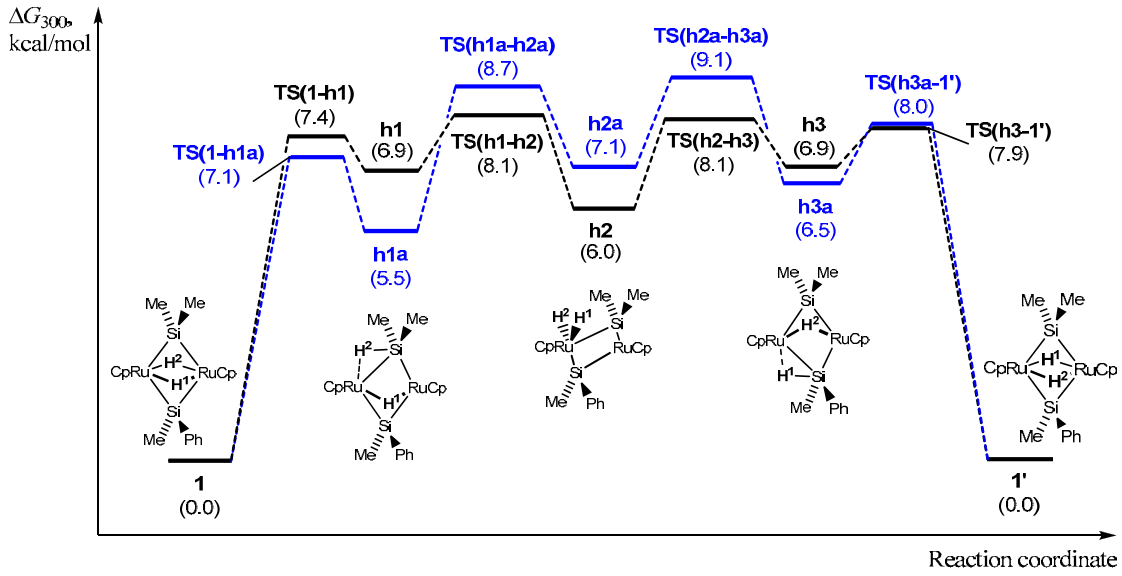

Chart 1. Free energy profile of the site-exchange of hydrides in **1**: two subroutes of the Path 1. Here and further the relative Gibbs free energies were calculated at BP86/BS2 level, where BS2 corresponds to the effective core potential + double-ζ valence basis set for Ru, 6-31G(d,p) for C, H and 6-31G(d) for Cp.

The intermediate **h2** has a geometrical isomer **h2a**. They differ by the relative position of the terminal hydrides with respect to the substituents at the μ-silylene. Due to existence of two intermediates **h2** and **h2a** the additional subroute, Path 1a, arises. The free energy profile of both subroutes is summarized in the Chart 1. The difference in the energy barriers of formation of the non-classical complexes formed through the bridge μ–$SiMe_2$ (**h1** or **h1a**) and μ–SiPhMe (**h3** or **h3a**) is rather small. Hence, the reaction can proceed in both directions.

Two subroutes have quite similar free energy profiles. Though, the minima **h1a** and **h3a** are somewhat deeper than those **h1** and **h3**, correspondingly. Still all the intermediates are rather shallow minima, which makes difficult the assignment of the rate-limiting-step. Taking all this into account, one can conclude that the activation barrier should be the average value within 7–9 kcal/mol. The energy barrier is somewhat underestimated, when compared to the experimental $\Delta G^{\neq}_{300}$ value of 11.8 kcal/mol.

Path 2. The second pathway includes additionally the direct hydride exchange in **h2** and **h2a** through the transition states **TS(h2–h2')** and **TS(h2a–h2a')**. The $\Delta G^{\neq}_{300}$ barriers of this step are 7.7 and 7.8 kcal/mol, correspondingly.

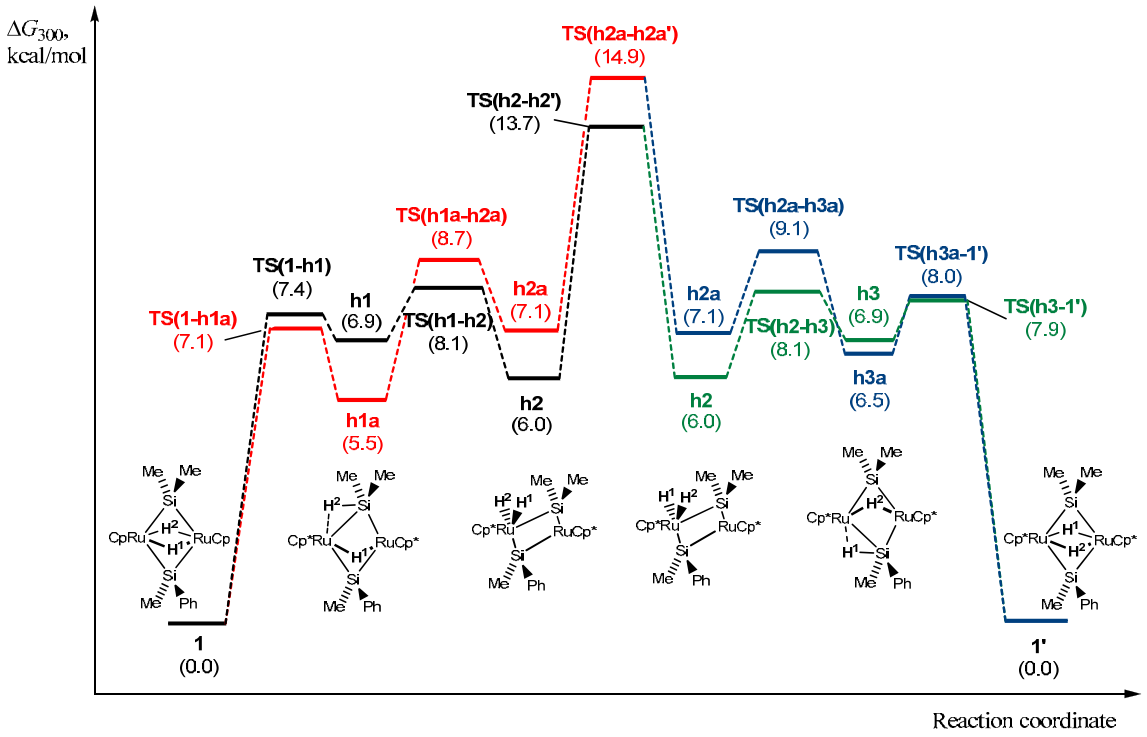

Chart 2. Free energy profile of the site-exchange of hydrides in **1**: four subroutes of the Path 2

The free energy profile of the Path 2 is summarized in the Chart 2. There are four subroutes in this pathway. The Chart 2 presents only the first half of each subroute, since they are symmetric with respect to the transition state **TS(h2–h2')**.

Two alternative conclusions can be made about the rate-determining step, as well as about the whole mechanism of hydride exchange from the analysis of the Chart 2. First, if one takes that all the intermediates are shallow minima, then the activation barrier of the Path 2 should be within 13–14 kcal/mol. In this case the described above Path 1 with the activation barrier of 7–9 kcal/mol is preferable.

From the other hand, one can consider at least those minima lying 2 kcal/mol below the corresponding transition state as deep enough. Then the activation barrier would be within 7–9

kcal/mol, like of Path 1, and both pathways become equivalent. This paradigm can be resolved by means of molecular dynamics simulations, which are planned to be performed in near future.

Exchange of methyl groups in 1. The Path 1 was rejected, since no stationary point was located on this pathway.

The Path 2 starts with the formation of the non-classical complex **h1** or **h1a**. The latter is converted into the classical complex **m1** or **m1a** via the transition state **TS(h1–m1)** or **TS(h1a–m1a)**, respectively, as a result of loss of the agostic Ru–η^2-Si–H interaction. The $\Delta G^{\neq}_{300}$ barrier of this step is 4.0 and 4.5 kcal/mol, correspondingly.

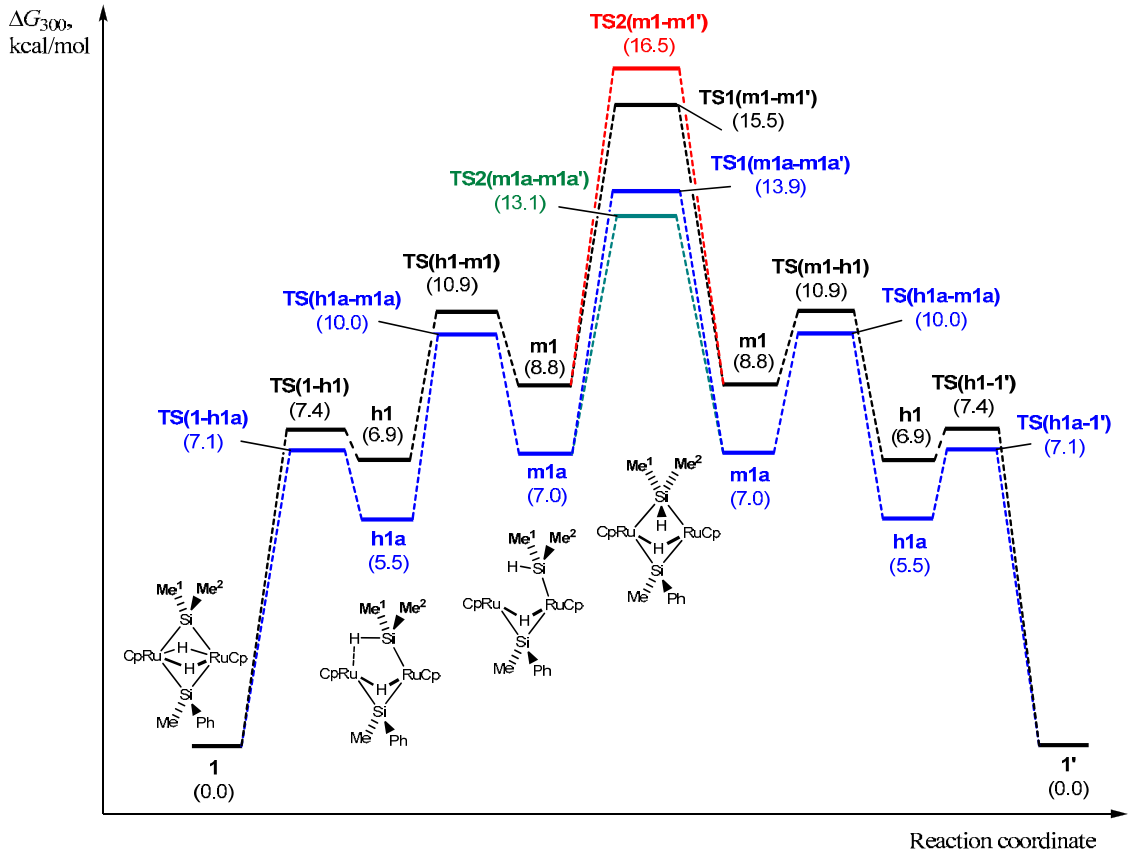

Chart 3. Free energy profile of the site-exchange of methyl groups in 1: four subroutes of the Path 2

The key step, 1,2-shift of the μ-$SiMe_2$ bridge, can take place in two ways in **m1** and **m1a** through four transition states **TS1(m1–m1')**, **TS2(m1–m1')**, **TS1(m1a–m1a')** and **TS2(m1a–m1a')**. The corresponding $\Delta G^{\neq}_{300}$ barrier values are 6.7, 7.7, 6.1 and 6.9 kcal/mol, respectively.

The free energy profiles of the four subroutes of the Path 2 are summarized in the Chart 3. The intermediates **h1** and **m1** do not play a significant role in the estimation of the energy barrier of the exchange of methyls. It is estimated as the difference between the transition state **TS1(m1–m1')**, **TS2(m1–m1')**, **TS1(m1a–m1a')** or **TS2(m1a–m1a')** and the starting

complex **1** to give, respectively, 15.5, 16.5, 13.1 or 13.9 kcal/mol. The experimentally determined $\Delta S^{\neq}_{300}$ value of -7.8 cal/mol·K also agrees reasonably with the calculated ones -7.7, -11.8, -6.2 and -5.7 cal/mol·K.

Exchange of methyl groups in 2. Three pathways have been proposed for the site-exchange of methyl groups in **2**. The Path 1 was rejected, since no stationary point was located on this pathway. The exchange of methyl groups in **2** proceeds in two steps in the Path 2: initial cleavage of the bridging Ru–H bond and the following transfer of the hydride to the other side of the RuCRuSi plane. Taking into account the flatness of the minimum **b1**, the $\Delta G^{\neq}_{333}$ barrier has to be calculated as the difference in ΔG°_{333} of **TS(b1–b1')** and **1**, i.e. 17.2 kcal/mol.

The Path 3 is quite similar to the described above Path 2. The exchange of methyls on the Path 3 proceeds with the free energy barrier of 25.5 kcal/mol.

Thus, the exchange of methyls in **2** occurs by way of more preferable Path 2 with the free energy barrier of 17.2 kcal/mol. This value is in a reasonable agreement with the experimentally determined $\Delta G^{\neq}_{333}$ barrier of 15 kcal/mol.

9.5. Dynamics of Si–H–Si bridges in agostically stabilized silylium ions

This work was done in the collaboration with the group of Dr. G. I. Nikonov from the Chemistry Department of Brock University, where all the NMR studies of the dynamical behavior of the cation $[C_6(SiMe_2)(SiHMe_2)_5]^+$ have been carried out. Our contribution to this work is the computational study of this system using static DFT and molecular dynamics methods.

The DFT calculations show that the dynamic processes are only possible when an internal rotation of a silyl group takes place. We found two possible mechanisms of this process, associated with internal rotation of either β- or γ-silyl groups. The general picture of the hydride transfer obtained from the calculations is as follows. Rotating a β-silyl group forces the Si^{α}–H^{β} distances increase, which increases the electrophilicity of the corresponding α-silyl. The bridging H^{α} then moves toward the Si^{α}, which in turn makes the other α-silyl more electrophilic. As a consequence, the β-hydride moves too, turning to the bridging one. In the first mechanism, the complete shift of the bridging position occurs by a full 180° rotation of the β-silyl group. In the second mechanism, a full rotation of the γ-silyl group takes place, which due to steric effects causes some internal rotation of the β-silyl. Thus, two mechanisms with two different barriers can take place, which is in line with experiment. The static DFT calcula-

tions yield ΔG_{298} barriers of 7.9 kcal·mol^{-1} for γ-silyl rotation and about and 11.5 kcal·mol^{-1} for β-silyl rotation, the latter value is in good accord with experimental result.

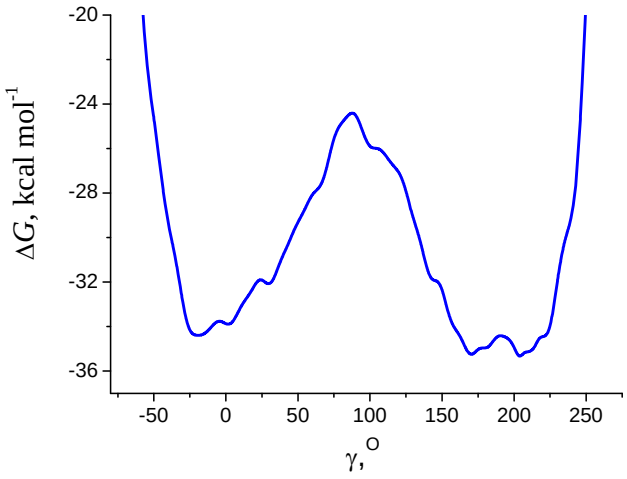

Figure 10. Free energy profile of the γ-silyl rotation from the metadynamics simulation

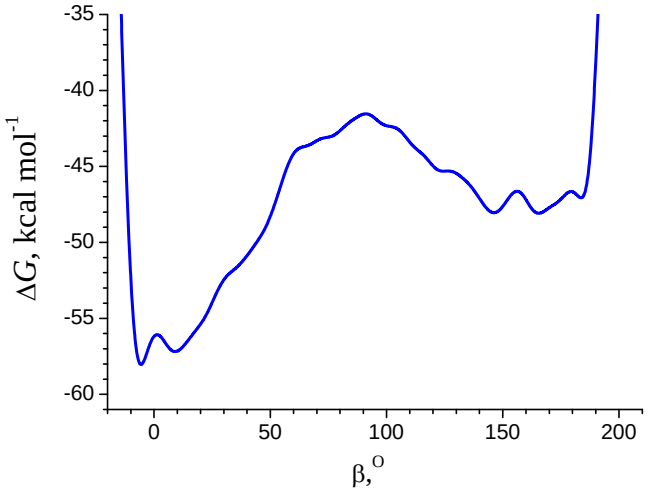

Figure 11. Free energy profile of the β-silyl rotation from the metadynamics simulation

A more complete description of the hydride transfer process was obtained from a metadynamics study, with respective γ- and β-rotation dihedral angles taken as collective variables. These calculations yield the γ-silyl and β-silyl rotation barriers of 10 and 16 kcal·mol^{-1}, respectively, in acceptable agreement with the static DFT results (Figures 10 and 11).

We also tried to estimate what proportion of the barrier is due to silyl internal rotation (which is of sterical nature) and what is due to hydride transfer. The first estimation based on the comparation of the rotation barriers of the cation **1a** and the neutral system $C_6(SiHMe_2)_6$ gives the value of the intrinsic hydrogen transfer barrier of about 2.5 kcal·mol^{-1}. The statisti-

cal analysis of the relevant internal coordinates in the course of dynamics predicts notably lower barrier of approximately 0.5 kcal·mol^{-1}.

The analytic harmonic frequency analysis as well as vibrational dynamics reveals a clear difference between α-, β, and γ-vibrations. According to the vibrational dynamics results, the Si–H bond exhibits moderate anharmonicity. At 15 K the vibrations are rather localized, whereas at 161 K and 304 K there is a substantial, though incomplete, mixing of Si–H bonds, such that the β-silyls partly get an α-bridge character and vice versa.

10. Conclusions

1. We have considered both dissociative and associative mechanism for the hydrogen exchange in ($CpRu(\mu\text{-}H)_4RuCp$) (**1**). The former proceeds through the dissociation of dihydrogen to afford $CpRu(\mu\text{-}H)_2RuCp$. The barrier for this process, with $\Delta G^{\neq}_{298}$ about 33.2 kcal·mol^{-1}, is prohibitively high.

Much more affordable is the associative mechanism, which occurs through hexahydride intermediates $Cp_2Ru_2(H)_6$. The reaction steps of the associative mechanism with their respective intermediates and transition states are summarized in Scheme 2. There are in turn two possible pathways, going either through the *cis* complex **2a″** or *trans* complex **2b**. The $\Delta G^{\neq}_{298}$ barriers are 23.7 and 27.1 kcal·mol^{-1}, respectively. This turns out to be the rate-determining step. Therefore, the *cis* pathway is preferred. The subsequent hydrogen elimination from **2a″** to yield **1** (denoted as **1-d$_2$** in Scheme 2) has a $\Delta G^{\neq}_{298}$ barrier of 7.5 kcal·mol^{-1}. Alternatively, the intermediate **2a″** can transform via **2a‴** and **TS(2a‴-2c)** to **2c** with the total $\Delta G^{\neq}_{298}$ barrier of 6.7 kcal·mol^{-1}. Thus, the direct dihydrogen elimination competes with the isomerization processes involving interchanging of bridging and terminal hydrides.

In the reverse step, which is a low-barrier process, terminal hydride in **2c** can be exchanged by a bridging hydride. The intermediate **2a‴** can also undergo dihydrogen elimination to eventually afford **1**.

Note that the initial hydrogen coordination to give **2a″** or **2b** is strongly affected by entropy effects. As seen from the rightmost column of Table 1, the entropy contributes to about 6–8 kcal·mol^{-1} to the ΔG°_{298} (and $\Delta G^{\neq}_{298}$) of this process in the gas phase. However, in solution the entropy effect is typically halved. On the other hand, the barrier calculated at B3LYP level, which is presumable superior, is about 3 kcal·mol^{-1} lower than the BP86 value. Thus, the actual barrier for the rate-determining step is expected to be below 20 kcal·mol^{-1}.

By and large, our calculations support Suzuki's conclusion that the associative mechanism for the hydrogen exchange is more favorable than the dissociative one. On the other hand, our study demonstrates that the actual mechanism is by far more complicated that a simple hydrogen coordination and elimination, with many intermediates found. These intermediates can interchange bridging and terminal hydrides, thus contributing to the hydrogen exchange.

2. We have presented a scheme of the whole mechanism of the conversion of the diruthenium tetrahydride complex **1** into ethylene bis(vinyl) complex **31** involving the C–H bond activation in ethylene with participation of both metal centers. The reaction is substantially exo-

thermic – the calculated enthalpy difference ΔH°_{298} between **1** (**A**) + $6C_2H_4$ and **31a** (**K**) + $3C_2H_6$ is about 90 kcal·mol^{-1}. The rate-determining step of the mechanism is the initial coordination of the first ethylene molecule to the reactant **1** to give the ethylene π-complexes **2a**–**c**. The free energy barrier is about 27–29 kcal·mol^{-1} according to the static DFT calculations, while metadynamic calculations of the coordination process yield a slightly lower ΔG°_{298} barrier of about 21 kcal·mol^{-1}. Another high-barrier step is the ethylene coordination to **30a** to produce the final product **31a**. The corresponding free energy barrier is 22 kcal·mol^{-1} according to the static DFT calculations.

The results obtained indicate that the C–H bond activation of ethylene on dinuclear ruthenium species is a sophisticated multistep reaction with a large number of possible pathways. The mechanism of the reaction is largely determined by the flexibility of hydride ligands. The hydride ligands easily change from the bridging coordination to the terminal one. For instance, the initial ethylene coordination to **1** is accompanied by the conversion of two bridged hydrides into terminal ones. Further, in the course of the ethylene insertion into Ru–H bond they collapse occupying a generated vacant space in **4**. This change between bridging and terminal coordination of hydrides is also inherent to the ethylene coordination to **8** and the following insertion step described in Part 3 (Scheme 3). Essentially, the bridging hydrides play a role of an electron-mediating “buffer” facilitating the coordination of the incoming ethylene on the adjacent metal center and its further transformations.

The presented computational results provide further support for the concept of cooperation between two Ru centers in a multistep transformation. The cooperative involvement of the two Ru centers in the C–H bond activation, as well as in the agostic interaction with the C_2H_5 fragment at various stages of our mechanism, is evident from Schemes 2–5. For instance, the C–H bond cleavage in ethylene π-complex **7** occurs through the structure **7′** (Fig. 6) with an asymmetric coordination of ethylene, π-bonded to one Ru atom, while through agostic bond to the other. The existence of **7′** should facilitate the C–H bond activation in ethylene.

Another example of the unusual reactivity of the binuclear complex attributed to the cooperativity of the metal centers is the C–H bond cleavage in ethylene in the complexes **22a** and **22b**. The cleavage proceeds simultaneously with the migration of the resulting hydride to ethyl ligand stipulated by the closeness of the latter and asymmetrically bridged ethylene in **22a** and **22b**.

The role of the hydride mobility can be best seen in the initial stages of the reaction (Scheme 2). First, a migration of the bridging hydride in **1** opens a vacant coordinaton site suitable to accept the incoming ethylene. Subsequently, the ethylene captures one of the remaining bridging hydrides to form an ethyl ligand. Simultaneously, a terminal hydride from

the other ruthenium center turns to a bridging one, thus optimizing the coordination environment of the ruthenium. This bridging/terminal hydride interconversion is a major source of flexibility of the studied diruthenium hydride complexes, contributing essentially to the richness of their chemistry.

3. We present the computational study of the C–C coupling reaction between coordinated ethylene and two vinyl ligands on a binuclear bis(vinyl)-ethylene complex **1** to yield a ruthenacyclopentadiene complex **28**.

The rate-determining step of the mechanism is the coordination of the first ethylene molecule to the intermediate **22** to give the ethylene π-complex **23**. The enthalpy barrier $\Delta^{\neq}H^{\circ}_{298}$ is 18 kcal·mol^{-1}, and $\Delta^{\neq}G^{\circ}_{298}$ barrier is about 29 kcal·mol^{-1} at BP86 level. On the other hand, the barrier calculated at MPWLYP1M level is about 5 kcal·mol^{-1} lower than the BP86 value. Thus, the actual barrier for the rate-determining step is expected to be below 24 kcal·mol^{-1}. It should be also borne in mind that the actual $\Delta^{\neq}S^{\circ}$ of a coordination reaction in solution is much less negative than in the gas phase. Thus, the actual ethylene coordination barrier in solution is expected to be about 20 kcal·mol^{-1}. Another high-barrier step is the C–C coupling between the coordinated ethylene and μ-vinylidene in **14** to yield **15**. The corresponding free energy barrier is 20 kcal·mol^{-1}.

The calculations show that, in general, the C–C coupling occurs more readily between less saturated carbon atoms. For instance, the C–C coupling between μ-vinyl and μ-vinylidene ligands in **4** has a much lower energy barrier ($\Delta^{\neq}G^{\circ}_{298}$ = 14 kcal·mol^{-1}) than the C–C coupling between μ-vinyl and μ-ethylidene in **4″** ($\Delta^{\neq}G^{\circ}_{298}$ = 37 kcal·mol^{-1}). The coordination environment of both ruthenium atoms also strongly influences the coupling barrier. For example, the C–C coupling between the coordinated ethylene and μ-vinylidene in **3** proceeds with a higher energy barrier ($\Delta^{\neq}G^{\circ}_{298}$ = 24 kcal·mol^{-1}) than in **14** ($\Delta^{\neq}G^{\circ}_{298}$ = 20 kcal·mol^{-1}).

Our computational study shows that the mechanism originally proposed by Suzuki *et al*. needs some modifications, since the subsequent C–C coupling steps **3**→**4**→**5** turns out to proceed with a very high barrier.

A new, more favorable pathway has been found. The actual C–C coupling occurs in the vinyl-hydride complex **14**, which results from the C–H bond activation in μ-ethylidene in **3**. The ruthenacyclopentyl complex **16** is then formed as a result of two consecutive C–C coupling steps in this pathway. The following hydrogenation and rearrangement steps yield the ruthenacyclopentadiene complex **20** that corresponds to the experimentally isolated intermediate **B** in Scheme 1.

We have demonstrated that the intermediate **20** can be transformed to the final product **28** with an affordable free energy barrier (below 24 kcal·mol^{-1}). Thus, the presented computational results provide the evidence for the Suzuki *et al.*'s conclusion that conversion of the reactant **1** to the final product **28** occurs through the ruthenacyclopentadiene complex **20**.

In summary, the title reaction is a sophisticated multistep reaction with a large number of possible pathways.

4. This paper presents the computational study of the fluxional behavior of diruthenium bis(μ-silylene) complexes {CpRu(μ-H)}$_2$(μ-SiPhMe) (μ-SiMe$_2$) (**1**) and (CpRu)$_2$(μ-SiMe$_2$)(μ-CMe)(μ-H) (**2**). Two new pathways have been discovered for the site-exchange of hydrides in **1**. It was found that the hydride migration occurs without silyl internal rotation in the Path 1. The hydride exchange in the Path 2 occurs directly in the classical dihydride complexes **h2** and **h2a** without formation of a dihydrogen complex.

The conclusion about the favorable pathway of the hydride exchange in **1** hinges on the kinetical stability of the intermediate species. First, if one takes that all the intermediates are rather shallow minima, then the activation barrier of the Path 2 should be within 13–14 kcal/mol. In this case the described above Path 1 with the activation barrier of 7–9 kcal/mol is preferred.

From the other hand, one can consider at least those minima lying 2 kcal/mol below the corresponding transition state as deep enough to be stable kinetically. Then the activation barrier would be within 7–9 kcal/mol, like of Path 1, and both pathways become equivalent. Thus this process requires additional molecular dynamics simulations studies to resolve this dilemma.

The exchange of methyls in **1** proceeds as a result of the 1,2-shift of the μ–SiMe$_2$ (Path 2) in accordance with the Suzuki *et al.*'s original proposal. The Path 1 involving the isomerization to the terminal silylene was rejected for both, **1** and **2**, since no stationary point was located in this pathway.

The exchange of methyls in **2** occurs by the hydride transfer through the μ–SiMe$_2$ ligand (Path 2) with the free energy barrier of 17.2 kcal/mol. It is in a reasonable agreement with the experimentally determined value ($\Delta G^{\neq}_{333}$ = 15 kcal/mol). The migration of the hydride through the μ–CMe$_2$ requires a significantly higher $\Delta G^{\neq}_{333}$ barrier of 26 kcal/mol.

5. We have performed a detailed study of the dynamical behavior of the cation [C$_6$(SiMe$_2$)(SiHMe$_2$)$_5$]$^+$. The variable-temperature NMR experiments performed in the group

of Dr. Nikonov indicate that there are two processes taking place, both resulting in a shift of the Si–H–Si bridge position. The higher of the respective ΔG barriers is roughly estimated to be about 10 kcal·mol^{-1}.

The DFT calculations show that these processes are only possible when an internal rotation of a silyl group occurs. Either a β- or γ-silyl group can rotate, giving rise to two different hydride transfer mechanisms. The general picture of the hydride transfer obtained from the calculations is as follows. Rotating a β-silyl group forces the Si^{α}–H^{β} distances increase, which increases the electrophilicity of the corresponding α-silyl. The bridging H^{α} then moves toward the Si^{α}, which in turn makes the other α-silyl more electrophilic. As a consequence, the β-hydride moves too, turning to the bridging one. In the first mechanism, the complete shift of the bridging position occurs by a full 180° rotation of the β-silyl group. In the second mechanism, a full rotation of the γ-silyl group takes place, which due to steric effects causes some (but not complete) internal rotation of the β-silyl. Thus, two mechanisms with two different barriers can occur, which is in line with experiment. The static DFT calculations yield ΔE_e barriers of 7.9 kcal·mol^{-1} for γ-silyl rotation and about 11.5 kcal·mol^{-1} for β-silyl rotation, the latter value is in good accord with experimental estimates.

A more complete description of the hydride transfer process was obtained from a metadynamics study, with respective γ- and β-rotation dihedral angles as collective variables. These calculation yield the γ-silyl and β-silyl rotation barriers of 10 and 15 kcal·mol^{-1}, respectively, in acceptable agreement with the static DFT results.

We also attempted to estimate what proportion of the barrier is due to silyl internal rotation (which is of steric nature) and what is due to hydride transfer. These estimates indicate that the intrinsic hydrogen transfer barrier is between 0.5 and 2.5 kcal·mol^{-1}, while the remaining part of the barrier is due to the steric effects.

The analytic harmonic frequency analysis as well as vibrational dynamics reveals a clear difference between α-, β, and γ-vibrations. According to the vibrational dynamics results, the Si–H bond exhibits moderate anharmonicity. At 15 K the vibrations are rather localized, whereas at 161 K and 304 K there is a substantial, though incomplete, mixing of Si–H bonds, such that the β-silyls partly get an α-bridge character and vice versa.

Thus, the $[C_6(SiMe_2)(SiHMe_2)_5]^+$ cation is a rather labile and fascinating dynamic system.

11. Full list of publications

1. Tussupbayev S.N., Polatbekova G.P., Gabdrakipov V.Z. “Quantum chemical study of halide, aqua- and mixed unithiol complexes of Bi (III)” *Materials of National scientific and practical conference dedicated to 75th anniversary of E.A. Buketov*, Karaganda, **2000**, P.67–70.
2. Tussupbayev S.N., Polatbekova G.P. “Quantum chemical study of anionic, protonated, and hydrated forms of unithiol.” *Materials of International conference on analytic chemistry dedicated to 100 anniversary of O.A. Songina*, Almaty, **2001**, P.136–138.
3. Tussupbayev S.N., Polatbekova G.P. “Electronic, geometric and thermodynamic characteristics of protonated unithiol and its complexes with bismuth (III) halides” *Materials of the III International Beremzhan congress on chemistry and chemical technology*.- Ust-Kamenogorsk, **2001**, P.249–255.
4. Tussupbayev S.N., Polatbekova G.P. “Reactivity of bismuth (III) halides to form donor-acceptor complex: a quantum chemical study” *KazSU bulletin chem. series*, **2002**, *23*, P.316–320.
5. Zhusupova G., Tussupbayev S. “Quantum chemical studies of quercetin, myricetin and their derivatives” 3rd IUPAC International Conference on biodiversity (ICOB-3), Book of Abstracts, p.81, 2001.
6. Tussupbayev S.N., Zhusupova G.E. “Quantum chemical study of kaempferol, quercetin, myricetin and gossypol” *KazSU bulletin chem. series* **2001**, *22*, P.202–205.
7. Tussupbayev S.N., Polatbekova G.P. “Some characteristics of dimers of bismuth (III) halides and their ionization products” *KazSU bulletin chem. series*, **2002**, *23*, P.63–67.
8. Tussupbayev S.N., Polatbekova G.P., Kenzhaliev B.K. “Influence of solvatation on electronic structure of complex cyanide anions of metals of IB group” Complex utilization of mineral raw materials, nº 7, **2004**, P.18–23.
9. Tussupbayev S.N., Polatbekova G.P., Kenzhaliev B.K. “Influence of solvatation on electronic structure of complex cyanide anions of Fe, Co, Ni, Zn” Complex utilization of mineral raw materials, **2004**, P. 15-20.

The thesis is based on the next papers:

10. Tussupbayev S., Vyboishchikov S.F., "DFT study of the hydride exchange in binuclear ruthenium complex", *Organometallics* **2007**, *26*, 56–64.
11. Tussupbayev S., Vyboishchikov S.F., "Computational study of the C–H bond activation in ethylene on binuclear ruthenium complex", *Organometallics* **2008**, *27*, 3681–3692.
12. Tussupbayev S., Nikonov G.I., Vyboishchikov S.F."Dynamics of Si–H–Si bridges in agostically stabilized silylium ions", *J. Phys. Chem. A*, **2009**, *in press.*
13. Tussupbayev S., Vyboishchikov S.F., "Computational study of C–C coupling on diruthenium bis(μ-vinyl) ethylene π-complex", *J. Am. Chem. Soc.* **2009**, *submitted.*
14. Tussupbayev S. "DFT study of fluxional behavior of diruthenium μ-silylene complexes", *Organometallics* **2009**, *submitted.*

12. References

[1] Kubas, G. J.; Ryan, R. R.; Swanson, B. I.; Vergamini, P. J.; Wasserman, H. J. *J. Am. Chem. Soc*. **1984**, *106*, 451.

[2] Jessop, P. J.; Morris, R. H. *Coord. Chem. Rev.* **1992**, *121*, 155.

[3] (a) Kubas, G. J. *Acc. Chem. Res.*, **1988**, *21*, 120.

(b) Crabtree, R. H. *Acc. Chem. Res.*, **1990**, *23*, 95.

(c) Heinekey, D. M.; Oldham Jr., W. J. *Chem. Rev.*, **1993**, *93*, 913.

(d) Esteruelas, M. A.; Oro, L. A. *Chem. Rev.*, **1998**, *98*, 577.

(e) Kubas, G. J. *J. Organomet. Chem.* **2001**, *635*, 37.

[4] (a) Kjoshi, A. M.; MacFarlane, K. S.; James, B. R. *J. Organomet. Chem.* **1995**, *488*, 161;

(b) Jia, G.; Ng, W. S.; Lau, C. P. *Organometallics* **1998**, *17*, 4538.

[5] Darensburg, M. Y.; Lyon, E. J.; Smee, J. J. *Coord. Chem. Rev.* **2000**, *206–207*, 533.

[6] Maseras, F.; Lledós, A.; Clot, E.; Eisenstein, O. *Chem. Rev.*, **2000**, *100*, 601.

[7] McGrady, G. S. Guilera, G. *Chem. Soc. Rev*., **2003**, 32, 383.

[8] (a) Dewar, M. Bull. Soc. Chim. Fr. **1951**, 1 8 , C79.

(b) Chatt, J.; Duncanson, L. A. *J. Chem. Soc*., **1953**, 2939.

(c) Chatt, J.; Duncanson, L. A.; Venanzi, L. M. *J. Chem. Soc*., **1955**, 4456.

[9] Huber, K.P.; Herzberg, G. *Molecular Spectra and Molecular Structure. IV. Constants of Diatomic Molecules*, Van Nostrand Reinhold Co., **1979**

[10] Noyori, R. *Angew. Chem. Int. Ed*. **2002**, *41*, 2008.

[11] Liu, X.; Ibrahim, S. K.; Tard, C.; Pickett, C. J. *Coord. Chem. Rev*. **2005**, 1641.

[12] (a) Chaudret, B.; Poilblanc, R. *Organometallics* **1985**, *4*, 1722;

(b) Arliguie, T.; Chaudret, B.; Morris, R. H.; Sella, A. *Inorg. Chem*. **1988**, *27*, 598;

(c) Borowski, A. F.; Donnadieu, B.; Daran, J.-C.; Sabo-Etienne, S.; Chaudret, B. *Chem. Commun.* **2000**, 543;

(d) Grellier, M.; Vendier, L.; Chaudret, B.; Albinati, A.; Rizzato, S.; Mason, S.; Sabo-Etienne, S. *J. Am. Chem. Soc.* **2005**, *127*, 17592.

[13] Lin, Z.; Hall, M.B. *Organometallics*, **1992**, 11, 3801.

[14] Li, J.; Dickson, R. M.; Ziegler, T. *J. Am. Chem. Soc.* **1995,** *117*, 11482.

[15] Martinho Simoes, J. A.; Beauchamp, J. L. *Chem. Rev.* **1990**, *90*, 629.

[16] (a) Meakin, P.; Muetterties, E. L.; Jesson, J. P. *J. Am. Chem. Soc.* **1973**, *95*, 75.

(b) Darensbourg, D. J.; Graves, A. H. *Inorg. Chem*. **1979**, 18, 1257.

(c) Darensbourg, D. J.; Baldwin, B. J. *J. Am. Chem. Soc.* **1979**, *101*, 6447.

(d) Van-Catledge, F. A.; Ittel, S. D.; Jesson, J. P. *Organometallics* **1985**, *4*, 18.

(e) Tebbe, F. N.; Meakin, P.; Jesson, J. P.; Muetterties, E. L. *J. Am. Chem. Soc.* **1970**, *92*, 1068.

[17] Catti, M.; Gervasio, G.; Mason, S. A. *J. Chem. Soc., Dalton Trans.* **1977**, 2260.

[18] Bau, R.; Ho, N. N.; Schneider, J. J.; Mason, S. A.; McIntyre, G. J. *Inorg. Chem.* **2004**, *43*, 555.

[19] Bau, R.; Drabnis, M. H.; Garlaschelli, L.; Klooster, W. T.; Xie, Z. W.; Koetzle, T. F.; Martinengo, S. *Science* **1997**, *275*, 1099.

[20] Jackson, P. F.; Johnson, B. F. G.; Lewis, J.; Raithby, P. R.; McPartlin, M.; Nelson, W. J. H.; Rouse, K. D.; Allibon, J.; Mason, S. A. *J. Chem. Soc., Chem. Commun.* **1980**, 295.

[21] Hampton, C.; Cullen, W. R.; James, B. R.; Charland, J. P. *J. Am. Chem. Soc.* **1988**, *110*, 6918.

[22] Suzuki, H.; Omori, H.; Lee, D. H.; Yoshida, Y.; Moro-oka, Y. *Organometallics* **1988**, *7*, 2243.

[23] Y. Ohki, H. Suzuki, *Angew. Chem., Int. Ed*. **2000**, *39*, 3120.

[24] (a) Shima, T.; Suzuki, H. *Organometallics* **2005**, *24*, 3939.

(b) Gross, C. L.; Girolami, G. S. *Organometallics* **2007,** *26,* 160.

[25] Koga, N.; Morokuma, K. *J. Mol. Struct.* **1993**, *300*, 181.

[26] Hay, P. J.; Wadt, W. R. *J. Chem. Phys*., **1985**, *82*, 270.

[27] Binkley, J. S.; Pople, J. A.; Hehre, W. J. *J. Am. Chem. Soc*., **1980**, *102*, 939.

[28] Hehre, W. J.; Stewart, R. F.; Pople, J. A. *J. Chem. Phys*., **1969**, *51*, 2657.

[29] Fowe, E. P.; Therrien, B.; Süss-Fink, G.; Daul, C. *Inorg*. *Chem.*, **2008**, *47*, 42.

[30] Suzuki, H; Kakigano, T; Tada, K.; Igarashi, M.; Matsubara, K.; Inagaki, A.; Oshima, M.; Takao, T. *Bull. Chem. Soc. Jpn*. **2005**, *78*, 67.

[31] Kameo, H.; Suzuki, H. *Organometallics* **2008**, *27*, 4248

[32] Ohki, Y.; Uehara, N.; Suzuki, H. *Angew. Chem., Int. Ed*. **2002**, *41*, 4085.

[33] Ohki, Y; Uehara, N; Suzuki, H. *Organometallics* **2003**, *22*, 59.

[34] Shima, T.; Suzuki, H. *Organometallics* **2000**, *19*, 2420.

[35] (a) Via, J. C.; Jacobsen, G.; Dutta, T. K.; Fehlner, T. P. *J. Am. Chem. Soc*. **1985**, *107*, 5563.

(b) VanderVelde, D. G.; Holmgren, J. S.; Shapley, J. R. *Inorg. Chem*. **1987**, *26*, 3077.

[36] Riehl, J.F.; Koga, N.; Morokuma, K. *J. Am. Chem. Soc*. **1994**, *116*, 5414.

[37] For example, (a) Feng, J.; Garland, M. *Organometallics* **1999**, *18*, 417.

(b) Castiglioni, M.; Deabate, S.; Giordano, R.; King, P. J.; Knox, S. A. R.; Sappa, E. *J. Organomet. Chem*. **1998**, *571*, 251.

(c) Bazhenova, T. A. ; Bazhenova, M. A.; Mironova, S. A.; Petrova, G. N.; Shilova, A. K.; Shuvalova, N. I.; Shilov, A. E. *Inorg. Chem. Acta* **1998**, *270*, 221.

[38] (a) *Catalysis by Di- and Polynuclear Metal Cluster Complexes* Adams, R. A., Cotton, F. A., Eds.; Wiley-VCH: New York, 1998.

(b) E. K. Van der Beuken, B. L. Feringa *Tetrahedron* **1998**, *54*, 12985.

[39] Suzuki, H. *Eur. J. Inorg. Chem.* **2002**, 1009.

[40] Kameo, H; Nakajima, Y; Suzuki, H. *Eur. J. Inorg. Chem.* **2007**, *13*, 1793.

[41] (a) Suzuki, H.; Omori, H.; Moro-oka, Y. *Organometallics* **1988**, *7*, 2579.

(b) Suzuki, H.; Omori, H.; Lee, D. H.; Yoshida, Y.; Fukushima, M.; Tanaka, M.; Moro-oka, Y. *Organometallics* **1994**, *13*, 1129.

(c) Shima, T; Ichikawa, T; Suzuki, H. *Organometallics* **2007**, *26*, 6329.

[42] (a) Suzuki, H.; Takao, T.; Tanaka, M.; Moro-oka, Y. *J. Chem. Soc., Chem. Commun.* **1992**, 476.

(b) Takao, T.; Yoshida, S.; Suzki, H.; Tanaka, M. *Organometallics* **1995**, *14*, 3855.

(c) Y. Ohki, T. Kojima, M. Oshima, H. Suzuki, *Organometallics* **2001**, *20*, 2654.

(d) Takao, T.; Amako, M.; Suzuki, H. *Organometallics* **2001,** *20*, 3406.

(e) Takao, T.; Amako, M.; Suzuki, H. *Chem. Lett.* **2001,** 1100.

(f) Takao, T.; Amako, M.; Suzuki, H. *Organometallics* **2003,** *22*, 3855.

[43] (a) Takao, T; Inagaki, A; Murotani, E; Imamura, T.; Suzuki, H. *Organometallics* **2003,** *22*, 1361.

(b) Suzuki, H.; Takaya, Y.; Takemori, T. *J. Am. Chem. Soc.* **1994**, *116*, 10779.

[44] (a) Fryzuk, M. D.; Johnson, S. A.; Patrick, B. O.; Albinati, A.; Mason, S. A.; Koetzle, T. F. *J. Am. Chem. Soc.* **2001**, *123*, 3960.

(b) Shima, T; Suzuki, H. *Organometallics* **2005,** *24*, 1703.

[45] Matsubara, K.; Okamura, R.; Tanaka, M.; Suzuki, H. J. *Am. Chem. Soc.* **1998**, *120*, 1108.

[46] Kawashima, T; Takao, T; Suzuki, H. *Angew. Chem., Int. Ed*. **2006**, *45*, 7615.

[47] (a) Y. Nakajima, H. Suzuki, *Organometallics* **2003,** *22*, 959.

(b) Nakajima, Y; Inagaki, A; Suzuki, H. *Organometallics*, **2004,** *23*, 4040.

(c) Nakajima, Y.; Suzuki, H. *Organometallics*, **2005,** *24*, 1860.

(d) Nakajima, Y; Kameo, H; Suzuki, H. *Angew. Chem., Int. Ed*. **2006**, *45*, 950.

[48] T. Shima, H. Suzuki, *Organometallics* **2000**, *19*, 2420.

[49] Takao, T.; Suzuki, H.; Tanaka, M. *Organometallics* **1994**, *13*, 2554.

[50] (a) Suzuki, H.; Omori, H.; Lee, D. H.; Yoshida, Y.; Fukushima, M.; Tanaka, M.; Moro-oka, Y. *Organometallics* **1994**, *13*, 1129.

(b) Tada, K. Oishi, M.; Suzuki, H.; Tanaka, M. *Organometallics* **1996**, *15*, 2422.

(c) Kawashima, T; Takao, T; Suzuki, H. *J. Am. Chem. Soc.* **2007**, *129*, 11006.

(d) Takao, T.; Moriya, M.; Suzuki, H. *Organometallics* **2008,** *27*, 1044.

[51] Moriya, M; Takao, T; Suzuki, H. *Organometallics*, **2007,** *26*, 1650.

[52] (a) Ito, J; Shima, T; Suzuki, H. *Organometallics*, **2004,** *23*, 2447.

(b) Shima, T; Suzuki, H. *Organometallics*, **2005,** *24*, 3939.

(c) Ito, J; Shima, T; Suzuki, H. *Organometallics*, **2006,** *25*, 1333.

[53] Wells, A. F. In *Structural Inorganic Chemistry*, 3rd ed.; Oxford University Press: London, England, **1962**; p 696.

[54] Takemori, T.; Suzuki, H.; Tanaka, M. *Organometallics* **1996**, *15*, 4346.

[55] Inagaki, A.; Takaya, Y.; Takemori, T.; Suzuki, H.; Tanaka, M.; Haga, M. *J. Am. Chem. Soc.* **1997**, *119*, 625.

[56] Takemori, T.; Inagaki, A.; Suzuki, H. *J. Am. Chem. Soc.* **2001**, *123*, 1762.

[57] Inagaki, A.; Takemori, T.; Tanaka, M.; Suzuki, H. *Angew. Chem., Int. Ed.* **2000**, *39*, 404.

[58] Takao, T.; Takemori, T.; Moriya, M.; Suzuki, H. *Organometallics* **2002,** *21*, 5190

[59] Khoroshun, D. V.; Inagaki, A.; Suzuki, H.; Vyboishchikov, S. F.; Musaev, D. G.; Morokuma, K. *J. Am. Chem. Soc.* **2003**, *125*, 9910.

[60] Tsipis, A.C.; Kefalidis, C.E.; Tsipis, C.A. *J. Am. Chem. Soc*. **2007**, *129*, 13905.

[61] (a) Müller, T. *Adv. Organomet. Chem.* **2005**, *53*, 155.

(b) Reed, C. A. *Acc. Chem. Res.* **1998**, *31*, 325.

(c) Lambert, J. B.; Kania, L.; Zhang, S. *Chem. Rev.* **1995**, *95*, 1191.

(d) Lickiss, P. D. *J. Chem. Soc., Dalton Trans.* **1992**, 1333.

(e) Eaborn, C. *J. Organomet. Chem.* **1991**, *405*, 173.

[62] (a) Schleyer, P. von R. *Science* **1997**, *275*, 39.

(b) Gaspar, P. P. *Science* **2002**, *297*, 785.

a) Lambert, J. B.; McConnell, J. A.; Schulz Jr., W. J. *J. Am. Chem. Soc.* **1986**, *108*, 2482.

(b) Lambert, J. B.; McConnell, J. A.; Schilf, W.; Schulz, Jr., W. J. *J. Chem. Soc., Chem. Commun.* **1988**, 455.

(c) Prakash, G. K. S.; Keyaniyan, S. Aniszfeld, R.; Heiliger, L.; Olah, G. A.; Stevens, R. C.; Choi, H. K.; Bau, R. *J. Am. Chem. Soc.* **1987**, *109*, 5123.

(d) Xie, Z. Liston, D. J.; Jelinek, T.; Mitro, V.; Bau, R.; Reed, C. A. *J. Chem. Soc., Chem. Commun*. **1993**, 384.

(e) Kira, M. Hino, T. Sakurai, H. *Chem. Lett.* **1993**, 153.

(f) Bahr, S. R.; Boudjouk, P. *J. Am. Chem. Soc.* **1993**, *115*, 4514.

(g) Cremer, D.; Olsson, L.; Ottosson, C.-H. *J. Mol. Struct. (THEOCHEM)* **1994**, *313*, 91.

[64] a) Lambert, J. B.; Zhao, Y.; Zhang, S. M. *J. Phys. Org. Chem.* **2001**, *14*, 370.

(b) Reed, C. A.; Xie, Z.; Bau, R.; Benesi, A. *Science*, **1993**, *262*, 402.

(c) Xie, Z.; Manning, J. Reed, R. W.; Mathur, R.; Boyd, P. D. W.; Benesi, A.; Reed, C. A. *J. Am. Chem. Soc.* **1996**, *118*, 2922.

(d) Kira, M.; Hino, T.; Sakurai, H. *J. Am. Chem. Soc.* **1992**, *114*, 6697.

[65] a) Jutzi, P.; Bunte, A. E. *Angew. Chem., Int. Ed. Engl.* **1992**, *31*, 1605.

(b) Steinberger, H.-U.; Müller, T.; Auner, N.; Maerker, C.; Schleyer, P. v. R. *Angew. Chem., Int. Ed. Engl.* **1997**, *36*, 626.

(c) Schuppan, J.; Herrschaft, B.; Müller, T. *Organometallic* **2001**, *20*, 4584. d) Müller, T.; Bauch, C.; Ostermeier, M.; Bolte, M.; Auner, N. *J. Am. Chem. Soc.* **2003**, *125*, 2158.

[66] Müller, T.; Meyer, R.; Lennatz, D.; Siehl, H.-U. *Angew.Chem., Int. Ed. Engl.* **2000**, *39*, 3074.

[67] a) Lambert, J. B.; Zhang, S.; Stern, C.; Huffman, J. C. *Science* **1993**, *260*, 1917.

(b) Lambert, J. B.; Zhang, S. *Chem. Comm*. **1993**, 383.

(c) Schleyer, P. v. R.; Buzek, P.; Müller, T.; Apeloig, Y.; Siehl, H.-U. *Angew. Chem., Int. Ed. Engl*. **1993**, *32*, 1471.

(d) Olsson, L.; Cremer, D. *Chem. Phys. Lett*. **1993**, *215*, 433.

(e) Lambert, J. B.; Zhang, S. *Science* **1994**, *263*, 984. f) Pauling, L. *Science* **1994**, *263*, 983.

(g) Olah, G. A.; Rasul, G.; Buchholz, H. A.; Li, X.-Y.; Sandford, G.; Prakash, G. K. S. *Science* **1994**, *263*, 983.

(h) Reed, C. A.; Xie, Z. *Science* **1994**, *263*, 985.

(i) Arshadi, M.; Johnels, D.; Edlund, U.; Ottosson, C.-H.; D. Cremer, *J. Am. Chem. Soc.* **1996**, *118*, 5120.

[68] Ottosson, C.-H.; Cremer, D. *Organometallics* **1996**, *15*, 5309.

[69] (a) Ichinohe, M.; Igarashi, M.; Sanuki, K.; Sekiguchi, A. *J. Am. Chem. Soc.* **2005**, *127*, 9978.

(b) Sekiguchi, A.; Matsuno, T.; Ichinohe, M. *J. Am. Chem. Soc.* **2000**, *122*, 11250.

[70] Scott, V. J.; Celenligil-Cetin, R.; Ozerov, O. V. *J. Am. Chem. Soc.* **2005**, *127*, 2852.

[71] Douvris, C.; Ozerov, O.V. *Science* **2008**, *321*, 1188.

[72] Zhang, Y.; Huynh, K.; Manners, I.; Reed, C. A. *Chem. Commun.* **2008**, 494.

[73] (a) Lambert, J. B.; Zhao, Y. *Angew.Chem., Int. Ed. Engl.* **1997**, *36*, 400.

(b) Kim, K.-C.; Reed, C. A.; Elliott, D. W.; Mueller, L. J.; Tham, F.; Lin, L.; Lambert, J. B. *Science* **2002**, *297*, 825.

(c) Müller, T.; Zhao, Y.; Lambert, J. B. *Organometallics* **1998**, *17*, 278.

(d) Belzner, J. *Angew.Chem., Int. Ed. Engl.* **1997**, *36*, 1277.

[74] Driess, M.; Yao, S.; Brym, M.; van Wüllen, C. *Angew. Chem. Int. Ed.* **2006**, *45*, 6730.

[75] Kppers, T.; Bernhardt, E.; Eujen, R.; Willner, H.; Lehmann, C. W. *Angew. Chem. Int. Ed*. **2007**, *46*, 6346.

[76] Müller, T. *Angew. Chem., Int. Ed.* **2001**, *40*, 3033.

[77] Sekiguchi, A.; Muratami, A.; Fukaya, N.; Kabe, Y. *Chem. Lett.* **2004**, *33*, 530.

[78] Hoffmann, S. P.; Kato, T. Tham, F. S.; Reed, C. A. *Chem. Commun*. **2006**, 767.

[79] R. Panisch, M. Bolte, T. Mller, *J. Am. Chem. Soc*. **2006**, *128*, 9676.

[80] Khalimon, A.Y.; Lin, Z.; Simionescu, R.; Vyboishchikov, S.F.; Nikonov, G.I. *Angew. Chem.* **2007**, *46*, 4530–4533

[81] Szabo, A. Ostlund, N. S.. *Modern Quantum chemistry*. MacMillian, New York, **1982**.

[82] (a) Parr, R. G.; Yang, W. *Density Functional Theory of Atoms and Molecules*, Oxford University Press, New York, 1989.

(b) Koch, W. Holthausen, M.C. *A Chemist's Guide to Density Functional Theory*, Wiley-VCH, Weinheim, 2000.

[83] Thomas, L. H. Proc. *Camb. Phil. Soc*. **1927**, *23*, 542.

[84] Fermi, E. *Z. Physik*, **1928**, *48*, 73.

[85] Dirac, P. A. M. *Proc. Cambridge Phil. Soc.* **1930**, *26*, 376.

[86] Jones, R. O.; Gunnarsson. O. *Rev. Mod. Phys.* **1989**, *61*, 689.

[87] Hohenberg, P.; Kohn, W. *Phys. Rev. B* **1964**, *136*, 864.

[88] Kohn, W.; Sham, L. J. *Phys. Rev. A*, **1965**, *140*, 1133.

[89] Slater, J. C. *Phys. Rev*. **1951,** *81*, 385.

[90] Ceperley, D. M.; Alder, B. J. *Phys. Rev. Lett*. **1980**, *45*, 566.

[91] Herman, F.; Van Dyke, J.P.; Ortenburger, I.P. *Phys. Rev. Lett.***1969**, *22*, 807.

[92] Adamo, C.; di Matteo, A.; Barone, V. *Adv. Quant. Chem.*, **1999**, *36*, 45.

[93] Becke, A. D. *Phys. Rev. A*, **1988**, 38, 3098.

[94] (a) Perdew, J.P.; *Electronic Structure of Solids*, Ziesche, P.; Eschrig, H. (eds.), 1991, Akademie Verlag, Berlin.

(b) Burke, K.; Perdew, J.P.; Wang, Y. in *Electronic Density Functional Theory. Recent Progress and New Directions*, Dobson, J.F.; Vignale, G.; Das, M.P. (eds.), 1998, Plenum Press, New York.

[95] Laming, G.J.; Termath, V.; Handy, N.C. *J. Chem. Phys*., **1993**, *99*, 8765.

[96] Perdew, J. P. *Phys. Rev. B*, **1986**, *33*, 8822.

[97] Becke, A. D. *J. Chem. Phys*., **1986**, *84*, 4524.

[98] Lacks, D.J.; Gordon, R.G., *Phys Rev A,* **1993**, *47*, 8822.

[99] Perdew, J. P.; Burke, K.; Ernzerhof, M. *Phys. Rev. Lett.*, **19997**, *78*, 1396.

[100] Lee, C.; Yang, W.; Parr, R.G. *Phys. Rev. B*, **1988**, *37*, 785.

[101] Colle, R.; Salvetti, O. *Theor. Chim. Acta* **1975**, *37*, 329.

[102] Becke, A. D. *J.Chem. Phys*. **1993**, *98*, 1372.

[103] Becke, A. D. *J. Chem. Phys*. **1993**, *98*, 5648.

[104] Perdew, J. P.; Chevary, J. A.; Vosko, S. H.; Jackson, K. A.; Pederson, M. R.; Singh, D. J.; Fiolhais, C. *Phys. Rev. B* **1992**, *46*, 6671.

[105] Adamo, C.; Barone, V. *J. Chem. Phys*. **1999**, *110*, 6158.

[106] Gorling, A.; Levy, M. *Phys. Rev. B* **1993**, *47*, 13105.

[107] Baerends, E.J.; Ellis, D.E; Ros, P. *Chem. Phys.* **1973**, *2*, 41.

[108] Sambe, H.; Felton, R.H. *J. Chem. Phys.* **1975**, *62*, 1122.

[109] Ahlrichs, R.; Bär, M.; Häser, M.; Horn, H.; Kölmel, C. *Chem. Phys. Lett.* **1989**, *162*, 165.

[110] Gaussian 03, Revision C.02, M. J. Frisch, G. W. Trucks, H. B. Schlegel, G. E. Scuseria, M. A. Robb, J. R. Cheeseman, J. A. Montgomery, Jr., T. Vreven, K. N. Kudin, J. C. Burant, J. M. Millam, S. S. Iyengar, J. Tomasi, V. Barone, B. Mennucci, M. Cossi, G. Scalmani, N. Rega, G. A. Petersson, H. Nakatsuji, M. Hada, M. Ehara, K. Toyota, R. Fukuda, J. Hasegawa, M. Ishida, T. Nakajima, Y. Honda, O. Kitao, H. Nakai, M. Klene, X. Li, J. E. Knox, H. P. Hratchian, J. B. Cross, V. Bakken, C. Adamo, J. Jaramillo, R. Gomperts, R. E. Stratmann, O. Yazyev, A. J. Austin, R. Cammi, C. Pomelli, J. W. Ochterski, P. Y. Ayala, K. Morokuma, G. A. Voth, P. Salvador, J. J. Dannenberg, V. G. Zakrzewski, S. Dapprich, A. D. Daniels, M. C. Strain, O. Farkas, D. K. Malick, A. D. Rabuck, K. Raghavachari, J. B. Foresman, J. V. Ortiz, Q. Cui, A. G. Baboul, S. Clifford, J. Cioslowski, B. B. Stefanov, G. Liu, A. Liashenko, P. Piskorz, I. Komaromi, R. L. Martin, D. J. Fox, T. Keith, M. A. Al-Laham, C. Y. Peng, A. Nanayakkara, M. Challacombe, P. M. W. Gill, B. Johnson, W. Chen, M. W. Wong, C. Gonzalez, and J. A. Pople, Gaussian, Inc., Wallingford CT, 2004.

[111] *deMon2k*, Andreas M. Köster, Patrizia Calaminici, Mark E. Casida, Roberto Flores-Moreno, Gerald Geudtner, Annick Goursot, Thomas Heine, Andrei Ipatov, Florian Janetzko, Jorge M. del Campo, Serguei Patchkovskii, J. Ulises Reveles, Dennis R. Salahub, Alberto Vela, deMon developers, 2006.

[112] (a) te Velde, G.; Bickelhaupt, F.M.; van Gisbergen, S.J.A.; Fonseca Guerra, C.; Baerends, E.J.; Snijders, J.G.; Ziegler, T. *J. Comput. Chem.* **2001**, *22*, 931

(b) Fonseca Guerra, C.; Snijders, J.G.; te Velde, G.; Baerends, E.J. *Theor. Chem. Acc.* **1998**, *99*, 391.

(c) ADF2007.01, SCM, Theoretical Chemistry, Vrije Universiteit, Amsterdam, The Netherlands, http://www.scm.com

[113] Zener, C. *Phys. Rev*. **1930**, *36*, 51.

[114] Slater, J.C. *Phys. Rev.* **1930**, *36*, 57.

[115] Roothaan, C.C.J.; Bagus, P.S. *Methods in Computational Physics*, Academic Press, New York, **1963**, Vol. II.

[116] Boys, S.F. *Proc. R. Soc. London Ser. A* **1950**, *200*, 542.

[117] McWeeny, R. *Nature* **1950**, *166*, 21.

[118] K. Balasubramanian. In: P. R. Schleyer, N. L. Allinger, T. Clark, P. A. Kollman, H. F. Schaefer III, P. R. Scheiner (eds.). *Encyclopedia of Computational Chemistry*. Vol. 4. Chichester, UK: Wiley-VCH, 1998, pp. 2471–2480.

[119] P. J Hay, W. R. Wadt. *J. Chem. Phys.*, **1985**, *82*, 299.

[120] W. J. Stevens, M. Krauss, H. Basch, G. Jasien. *Can. J. Chem.* **1992**, *70*, 612.

[121] (a) M. Dolg, U. Wedig, H. Stoll, H. Preuss. *J. Chem. Phys.* **1987**, *86*, 866.

(b) D. Andrae, U. Häussermann, M. Dolg, H. Stoll, H. Preuss. *Theor. Chim. Acta.* **1990**, *77*, 123.

[122] (a) L. F. Pacios, P. A. Christiansen. *J. Chem. Phys*. **1985**, *82*, 2664.

(b) M. M. Hurley, L. F. Pacios, P. A. Christiansen, R. B. Ross, W. C. Ermler. *J. Chem. Phys.* **1986**, *84*, 6840.

(c) L. A. LaJohn, P. A. Christiansen, R. B. Ross, T. Atashroo, W. C. Ermler. *J. Chem. Phys.* **1987**, *87*, 2812.

(d) R. B. Ross, J. M. Powers, T. Atashroo, W. C. Ermler, L. A. LaJohn, P. A. Christiansen. *J. Chem. Phys.* **1990**, *93*, 6654.

[123] (a) P Pyykkö. *Chem. Rev.* **1988**, *88*, 563.

(b) J Almlöf, O. Gropen. Rev. Comput. Chem. **1996**, *8*, 203.

[124] (a) L. A. Barnes, M. Rosi, C. W. Bauschlicher. *J. Chem. Phys.* **1990**, *93*, 609.

(b) I. Antes, G. Frenking. *Organometallics* **1995**, *14*, 4263.

[125] (a) Frenkel, D.; Smit, B. *Understanding Molecular Simulation – From Algorithms to Applications*, Academic Press, San Diego, **1996**.

(b) Allen, M. P. Tildesley, D. J. *Computer Simulations of Liquids*, Claredon Press, Oxford, **1987**.

[126] (a) Swope, W. C.; Andersen, H. C.; Berens, P. H.; Wilson, K. R. *J. Chem. Phys*. **1982**, *76*, 637.

(b) Andersen, H. C. *J. Comput. Phys*. **1983**, *52*, 24.

[127] Marx, D.; Hutter, J. in *Modern Methods and Algorithms of Quantum Chemistry*, J. Grotendorst, Ed. (NIC, FZ Jülich, Germany, 2000), pp. 301-449.

(a) Carter, E. A.; Ciccotti, G.; Hynes, J. T.; Kapral, R. *Chem. Phys. Lett.* **1989**, *156*, 472.

(b) Sprik, M.; Ciccotti, G. *J. Chem. Phys.* **1998**, *109*, 7737.

(c) Torrie, G. M.; Valleau, J. P. *J. Chem. Phys*. **1977**, *66*, 1402.

(d) VandeVondele, J.; Rothlisberger, U. *J. Chem. Phys.* **2000**, *113*, 4863.

(e) Rahman, J. A.; Tully, J. C. *J. Chem. Phys.* **2002**, *116*, 8750.

(f) VandeVondele, J.; Rothlisberger, U. *J. Am. Chem. Soc*. **2002**, *124*, 8163.

(g) Passerone, D.; Parrinello, M. *Phys. Rev. Lett.* **2001**, *87*, 108302.

[129] Iannuzzi, M; Laio, A; Parrinello, M. *Phys. Rev. Lett.* **2003**, *90*, 238302.

[130] (a) Car, R.; Parrinello, M. *Phys. Rev. Lett.* **1985**, *55*, 2471.

(b) Andersen, H.C. *J. Chem. Phys.* **1980**, *72*, 2384.

(c) Nose, S. *Mol. Phys.***1984**, *52*, 255.

[131] Laio, A.; Parrinello, M. *Proc. Natl. Acad. Sci. U.S.A.* **2002**, *99*, 12562.